Answers to Anonymous Reviewer #1

"Near East Desertification: Impact of Dead Sea drying on convective rainfall" by Khodayar and Hoerner submitted to Atmospheric Chemistry and Physics

Dear Reviewer1:
Thanks for your comments and suggestions. We have considered all of them and improved the manuscript accordingly. In the following you can find a detail answer to all your general and specific comments.
Kind regards
Samiro Khodayar

General Comments:

1. I do not think that you can say that you investigate the impact of drying on convective rainfall. You use only daily model output, while convective events are short-term and local events, and can thus be lost in daily output. I would thus recommend to analyse the hourly output for the entire 10-year period, and not only for two events. However, as I understand from the manuscript you have saved daily output only for that simulation so analysis of hourly events across decade-long simulations would not be possible without rerunning the simulation. I wonder if you should then at least change the title into something like "Near East Desertification: Impact of Dead Sea drying on the water cycle" or "Near East Desertification: Impact of Dead Sea drying on the water budget" or "Near East Desertification: Impact of Dead Sea drying on the local climate".

We agree with the reviewer that the ideal approach would have been to analyse the hourly output for the entire 10-year period. Unfortunately, as specified in the manuscript we initially only saved daily output because of the storage capacity since our initial purpose was to assess the impact of a drying Dead sea on the climatology of the region. However, after careful inspection of our results we found interesting impacts on the precipitation field, particularly on severe events mainly of convective nature (which are rare but relevant in the area) and even more interesting results when analysing the underlying mechanisms. Even though only daily precipitation was available for the entire 10-year long simulation, the convective nature of the investigated cases was clear due to the isolated situation of the events investigated as well as their characteristics such as high local convective available potential energy. Following the need for higher temporal information new simulations with hourly outputs were performed. The approach as well as some of the results obtained is novel, therefore, we believed in the relevance of publishing this study.
In a follow-up publication covering a 20-year period, hourly outputs are being saved for the entire simulation. This will allow us to come back to the points raised by the reviewer. Indeed, in this follow-up publication we will investigate in more detail the impacts on the local climate. Therefore, regarding a change in the title and following the reviewer suggestion we propose the following
Near East Desertification: impact of Dead Sea drying on the local conditions leading to convection.

A comment has been included in the manuscript to clarify that the daily output supposes a limitation.

2. Why do you use high-resolution convection-permitting simulation since you analyse only daily output on decadal time-scales and daily statistics is already well represented with the coarser resolution model? The studies that you cite show that the largest benefit of using such a high resolution is at the sub-daily time scale.

Even when using daily outputs the use of high-resolution convection-permitting simulations is beneficial for a better representation of model characteristics and atmospheric processes leading to convective precipitation, such as topography, secondary wind circulations etc

Although the main benefit of high-resolution convection-permitting simulations versus parameterized convection simulations is at sub-daily time scales, particularly for summer period, as adequately pointed out by the reviewer, daily precipitation has also been seen to be affected and improved, particularly in winter time (Fosser et al. 2014).

Fosser, G. & Khodayar, S. & Berg, P.. (2014). Benefit of convection permitting climate model simulations in the representation of convective precipitation. Climate Dynamics. 44. 45-60. 10.1007/s00382-014-2242-1.

Moreover, high-resolution convection-permitting simulations on shorter time scales with hourly output are used for further investigation of underlying mechanisms leading to heavy precipitation in the area of investigation. This allows the consistency between the simulation of the events at both simulation schemes.

We agree with the reviewer that this is a relevant point, so we included a comment with respect to this point in the manuscript.

3. The manuscript would further benefit from a better explanation of the domain that you simulate. I do not see how many grid points you have in x and y direction, and how large is the relaxation zone which you should take out from the analysis. How many grid points do you have at the end for the analysis? My rough estimate leads to a smaller number, so the influence of the domain size has to be discussed.

In Figure 1a, the simulation domains at 7 km and at 2.8km km as well as the investigation domain or study area are shown, to complement this information further details such as the number of grid points in x and y direction have been included in the manuscript as suggested by the reviewer.

The 7 km run covers a box of 250 x 250 grid points, the 2.8 km run covers a 150 x 150 grid points box, 22500 in total, and the study area, 72 x 92 grid points, leaving between 20-40 grid points as relaxation zone in the north-south-east-west direction.

The influence of the domain size on the simulation and analysis has been already pointed out in literature for different regions. In this study we have discussed with experts in the region and considered past studies in the area to make sure that our larger domain is well located and large enough to have into consideration all possible relevant synoptic situations as well as the Mediterranean sea impact relevant for the development of extreme phenomena in the study area. This explanation has been included in the manuscript.

4. Since you are doing the sensitivity experiment, I wonder if you really need a 10- year long period and if you could already address the problem with 1-5 years long simulations. With reducing the number of simulated years, you could use a larger domain.

In our sensitivity experiment we have seen that at least 1 to 2 years spin-up time are needed. After this consideration we agree that shorter time periods could be beneficial when particular situations/periods/events have to be investigated, particularly regarding the computational time and costs of the study. After discussion with experts in the modelization of the area regarding the size of the larger domain no benefit has been found in doing so. However, the time period considered is highly beneficial for the climatic aspects considered in this analysis, which provides a novel perspective of the conditions in the area.

5. How is the model performing over that region? You do not show any validation of the results for the reference simulation, so why should we trust the model? You even state on page 4, line 101-102 that this is the first attempt i.e., a convection-permitting model is for the first time applied in that region, so the manuscript should for sure present some evaluation results. You already mention some papers with the observations, so maybe these can be used. Or in the absence of high-resolution observations, EOBS observations can be used as well. Of course, one should be aware of and take into account the uncertainties for different regions and fields.

In general, the observations in the area are scarce in time and space. We performed some initial comparisons with the CMORPH satellite precipitation product; however, no comparisons were included in the manuscript due to some strange values over the Dead Sea region. No validation of this satellite product has been attempted in the region to the authors knowledge.
Following the reviewer suggestion, we performed comparisons with EOBS data set despite the coarse resolution of the later, 0.1º, and the indication by experts in the region of the bad performance of this product in the area.

*2.8km CTRL model_*
mean over the 2004-2013 period

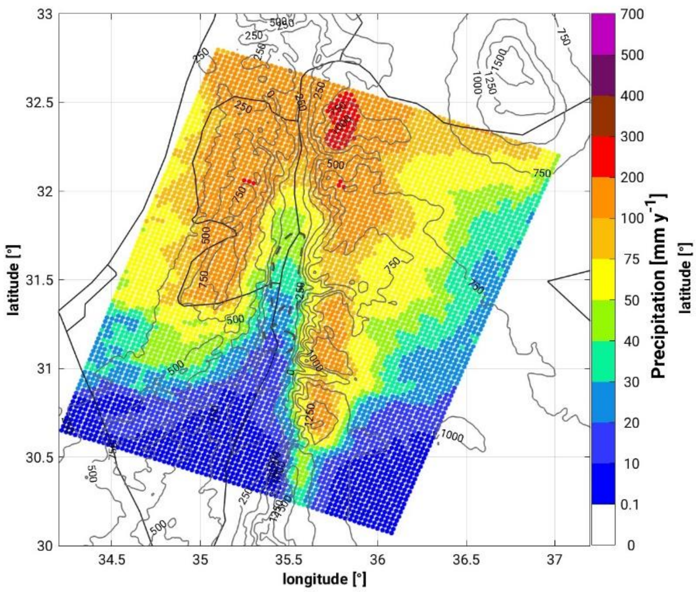

EOBS_data set
Same period

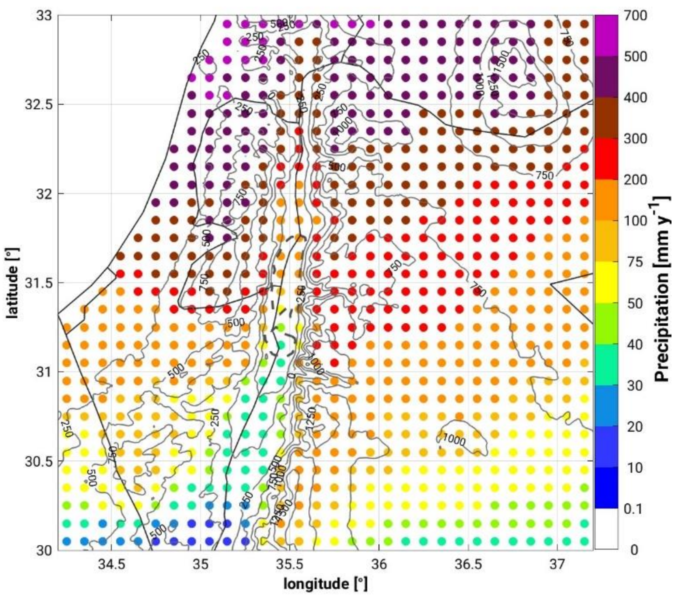

This comparison points out a general underestimation of precipitation in the north and particularly near the Mediterranean shoreline, but correctly captures the north-south gradient in the area.
This suggests that the model well simulates the orographic effect, while the general effect of distance from sea on precipitation is not well captured. Both the 7 km and the 2.8 km runs exhibit the same performance, thus, discarding a relationship of the biases with the grid spacing. Nevertheless, one may notice an improvement in the finer model resolution, particularly over topographic areas.

An additional comparison has been performed with the APHRODITE's (Asian Precipitation - Highly-Resolved Observational Data Integration Towards Evaluation) daily gridded precipitation which is the only long-term continental-scale daily product that contains a dense network of daily rain-gauge data for Asia. It has a resolution of 0.25º and is available for 1980-2007. The advantage is that it includes more rain gauge stations and it is a product widely used for validation purposes in this region of the globe. We compared the data from 2004-2007 with the respective data from the 2.8km simulation and EOBS. Please be aware of the different colormap scale between the EOBS/APHRODITE and the model simulation precipitation fields.

The Aphrodite data shows lower precipitation values than EOBS, but still higher than our simulation particularly close to the northern Mediterranean shoreline, over coastal-flat terrain, whereas the best agreement is again at areas dominated by complex terrain. This agrees with previous high-resolution modelling activities in the region with different models such as Rostkier-Edelstein et al. (2014) using WRF at 2 km. They suggest in this publication that inaccuracies in the gridded SST dataset used in the simulations could be responsible for the observed bias pointing out the strong sensitivity of precipitation in the Mediterranean basin to very small differences in the SST (Miglietta et al. 2011). Contrary to these results, Hochmann et al. (2018) showed with the COSMO-CLM model at 8 km resolution and driven by CMCC-CM against APHRODITE, a west-east pattern of overestimations in the coastal plains and underestimations in the mountainous regions in the seasonal precipitation, especially in the winter months (DJF).

EOBS

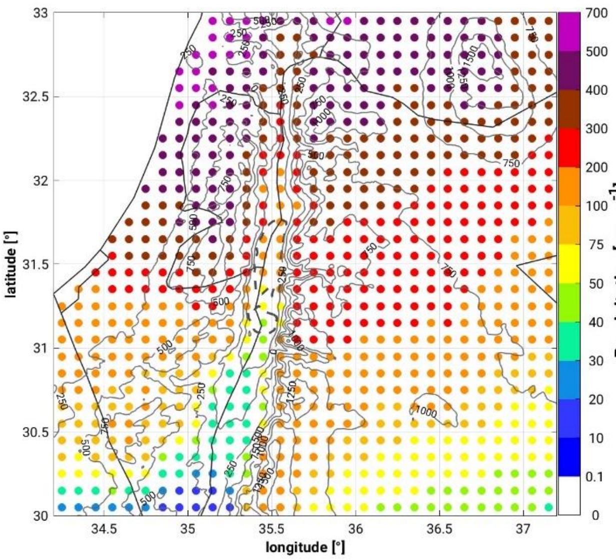

APHRODITE

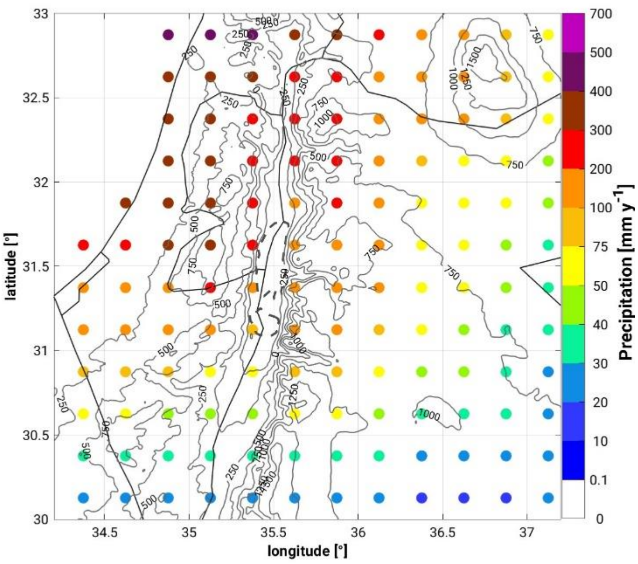

2.8km-CTRLsimulation-IFS forcing

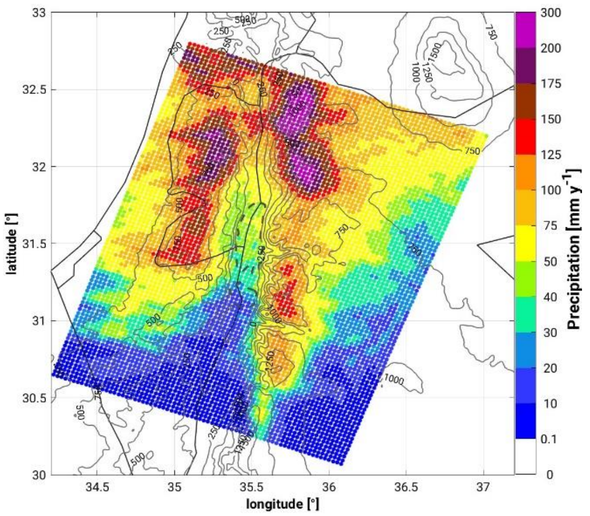

We performed an additional comparison for the year 2007, between the 2.8km-CTRL simulation-IFS forcing from the present study and the new simulations we are performing for the region, with hourly outputs covering the 2006-2018 period and forced by the newly available hourly ERA-5 data, also with a larger *simulation domain for the 2.8 km simulation. Our intention was to assess the possible impact of using different forcing data and/or domain of simulation. Our results show quite similar results between both simulations and similar biases with respect to the APHRODITA dataset, particularly at the Mediterranean shoreline, although a small improvement is shown in this area in the new model realization.*

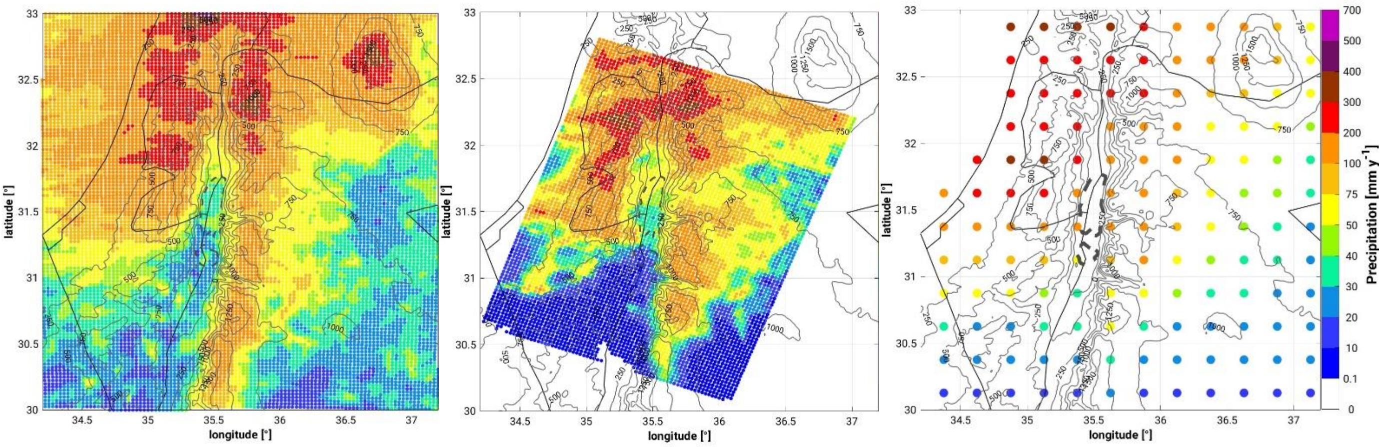

The comparison of the temporal evolution and the yearly sum for the year 2007 shows that in general the COSMO-CLM model both at 7 km and 2.8 km, quite well represents the precipitation events in the region.

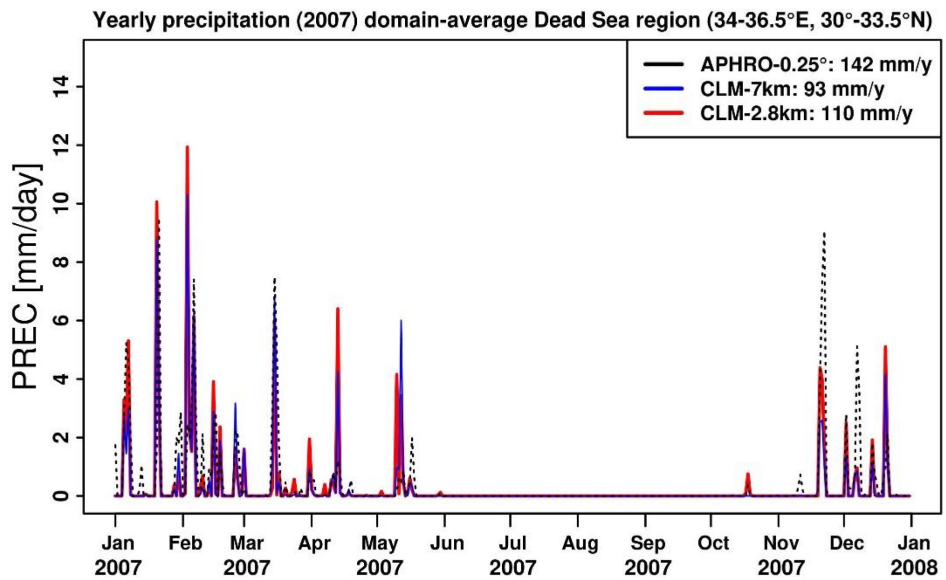

We will discuss this in the paper and additionally indicate in the conclusions that further improvement/refinement in the model simulations in the region is needed despite the improvement seen by using higher resolution convection permitting model simulations.

6. Throughout the manuscript, you use the difference between the REF and SEN experiments, and you calculate it as REF-SEN, which is a bit strange since it is common to use the reference simulation, in your case REF, as a subtrahend. This would make a discussion and figures easier to follow.

This has been changed throughout all the manuscript. Changes include Figure 2, 3, 4 5 and 7.

7. I do not think that the heavy precipitation events that you analyze are well chosen. You take two events that have the same synoptic patterns, while in the introduction you mention that heavy precipitation events are associated with the three main synoptic patterns. The two chosen events are only a few days apart and their connection is not discussed. It would be more interesting to choose 1-2 events for each type and then analyze them. These would lead to more meaningful results.

We agree with the reviewer that the selection of events could attend different motivations, for example different events associated to different synoptic patterns. However, in this case it was not our motivation or purpose to investigate convective situations under different synoptic patterns, but rather cases in which the mechanisms leading to the observed differences in the precipitation field between the reference and the sensitivity experiment are noticeable different at the local-to-mesoscale. As indicated in section 3.1 and Figure 6, the selected situations where those showing a larger deviation regarding SAL (Structure-Amplitude-Location) components between both simulations. Nevertheless, we generally investigated all cases listed in table 1 to have a general idea of the mechanisms leading to the differences; however, it was out of the scope of this paper to analyse all in detail.
A relevant point indeed is the possible connection between both events, thanks for pointing out this. We did not discuss this in the text, but we did investigate this point during the analysis of the cases finding out that in the period in between both events no atmospheric differences could be found between the simulations. This information has been included in the text.

8. Some plots are really difficult to read in the printed version, especially in Figure 3. In addition, not all that is shown on the plots is explained in the captions (for example in Figure 4). Please do a better caption and work on the visibility of the plots.

We have improved the quality and size of most figures to improve their visibility. Additionally, we have carefully examined all captions to include relevant information that was missing.

Specific comments:

1. Page 2, line 5-6: “Perturbation simulations. . .” I would call them “Sensitivity simulations. . .”

Changed

2. Page 2, line 13-14: You only look into the sensitivity on the presence of the lake, not really the future warmer climate. For that, you would need to modify your experiment.

I would thus suggest here to explain only the influence of the lake presence, and in the final line, you can explain what would that mean for the future warmer climate.
We agree with the reviewer that we are not simulating the future, however, literature agrees that the future climate in the region includes a drier Dead Sea. In this sense, the expected ongoing lake level is expected to have the described consequences on the local climate. To clarify this point and avoid any misunderstanding we rewrote the paragraph following the reviewer’s suggestion.

3. Page 2, line 15-16: I do not think that you show that.

This is not explicitly shown in the manuscript, mainly because the differences are not significant. Therefore, following the reviewer's suggestion regarding this point we removed this information from the abstract.

4. Page 2, line 21-23: Why on many occasions, if you find/show that for only one event?

Even though we just show as example a more detailed analysis of two selected cases, we did investigate for all other events listed in Table 1, which were the main mechanisms leading to the differences between both simulations. This was also to evidence that the cases examined were not unique. This information has been included in the manuscript.

5. Page 3, line 39-40: A bit strange line. Please rewrite. Also, if the influence of Dead sea on local climate is already known, why do we need another study on it.

The paragraph has been rewritten.
Even though the influence of the Dead Sea on local climate has been evidenced in several publications starting in 1939, Ashbel et al., the advances in the last decade regarding observational and computational capacities allow us to better understand the consequences of the sea level decline, which is furthermore a continuous process rather than a static change.

6. Page 3, line 61-65: I have the feeling that these two lines are describing the same but still say different. Please synchronize it, or if the different studies say different things, please mention it to be clearer.

Modified

7. Page 4, line 78: by ". . .these events. . ." you mean ". . .these heavy events. . ."

Included

8. Page 4, line 88: As already mentioned above, you look into the sensitivity of climate the presence of the lake and not the climate change.

Modified

9. Page 5, line 120-122: This part needs a better explanation of the model setup. The 7km and 2.8 km domains are different (as shown in Figure 1). How many grid points do you use for each of them? How does 7 km and 2.8 km model differ in model physics? Do you use the parameterization of convection in 7 km or not?

A paragraph is included extending the information regarding the 7 and 2.8 km runs.

10. Page 5, line 122-125: Here you say that you are using ECMWF IFS as a driving data for 7 km model, and later on page 6 (line 148-150) you say that the reanalysis is used. Please clarify.

This has been corrected.

11. Page 6, line 136: The more appropriate reference for the delta-two-stream approach is Ritter and Geleyn (1992). [Ritter, B., and J.-F. Geleyn, 1992. A comprehensive radiation scheme for numerical weather prediction models with potential applications in climate simulations. Mon. Wea. Rev., 120, 303–325.]

We agree with the reviewer, thanks for pointing out this.

12. Page 6, line 142: Please note that the event of 14.11.2011 is not listed in Table 1.

Thanks for noticing this has been correctly indicated.

13. Page 5-6: If you are already running the 7km simulation, maybe you should consider to use the output and compare it to 2.8 km simulation to assess the benefit of high-resolution (and or switching off convection parametrization) simulations for that region.

The 7 km simulation has been run only in reference mode (CTRL). The benefit of the CCLM-2.8 km high-resolution convection permitting simulations versus CCLM-7 km with parameterized convection has been already investigated in detail in the past e.g. in Fosser et al. (2014). We additionally performed some comparisons, please see answer to comment number 5.

14. Page 6, line 153: To what soil texture do you put it? Which soil type from page 5 line 130?

The soil types are histosols, clay and loamy clay, visible in Figure 1 as they are bordering the Dead Sea.

15. Page 6, line 166-167: Can we talk about the trends in 10-yearlong simulations?

Modified

16. Page 7, line 173: This is how you should do the differences, but note that you do them with respect to the sensitivity simulation. See general comment 6.

Thank you for pointing out this, as previously explained we modified all calculations in the manuscript.

17. Page 7, line 196-199: I do not understand this paragraph.

This corresponds to the classification in Table 1, which has been clarified now in the text.

18. Page 5-8: I do not find any explanation on how do you define heavy events that you list in Table 1 or how do you classify them as localized or widespread.

The events were selected with an area mean difference in precipitation larger than 0.1 mm/d. localised or widespread nature of the vents was assessed visually for each case. Due to the low temporal resolution of the simulation it was not possible to use any predefined index such as tau, which requires more frequent outputs.

19. Page 9, line 251: For consistency, please use only one name for the sensitivity experiment.

Changed

20. Page 9, line 254: I still do not understand how do you define heavy precipitation events.

Please see 18

21. Page 9, line 256-257: You do not show that results, but could you at least mention how much is that difference? If it is not that significant or large, I do not see why you mention in the abstract that there is that difference.

Initially we included a table specifying the number of dry and wet days as well as the differences between simulations. However, since the differences where almost negligible, just a few days as described in the text, we considered this table was not relevant enough to be included in the final version. We agree with the reviewer that the differences are not significant, therefore we removed this information from the abstract.

22. Page 9, line 264: I do not see reduced precipitation in the SENCLIM experiment.

For each event the percentage of precipitation change has been calculated and included in the table. Additionally, the total percentage of change for the whole period, which corresponds to a reduction of about 0.5 % in the SEN simulation has been calculated and all this information has been included in the manuscript.

23. Page 10, line 280-281: How do you define these regions? This should be explained in the methods.

This information has been included in the methodology as suggested by the reviewer.

24. Page 10, line 289-295: Do you always use only land points or just for Figure 3? If just for Figure 3, explain why do you do it. How is that contributing to the overall analysis?

- *Figure 2: all GP for all calculations are considered. In the following the example of evaporation including all GP(left) and only land points (right) is shown.*

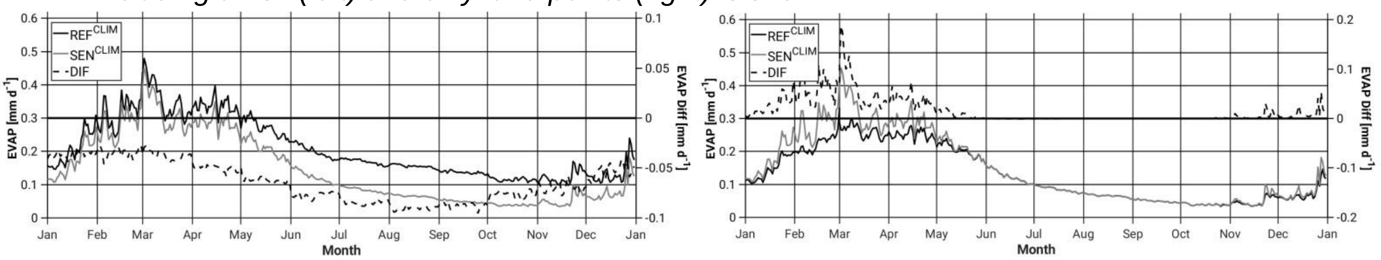

- *Figure 3: Only land points for evap and all GP for the rest*

  The Dead Sea grids have very high evaporation in the REF simulation and very low evaporation in SEN simulation, this difficult the interpretation of the results, thus we removed this effect in Figure 3 for evaporation, also because of the separation in 4 subdomains. In the following the example of evaporation including all GP(left) and only land points (right) for Area 1 is shown.

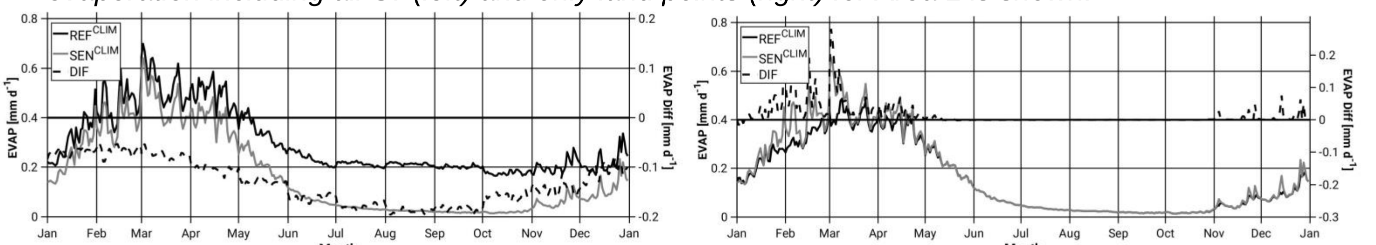

25. Page 13, line 381-383: What is the relation between these two events? Are not they too close? Why only these two are chosen from the same period and with the same synoptic situation?

These two events where those showing the larger difference between the REF and SEN simulations (FIG SAL), the synop situation and the fact that they were close in time were no relevant factors for our analysis *rather the mechanisms responsible for the differences observed between both simulations. Even though the two cases were close in time and a connection was to be expected between the first and the second periods, after analysing atmospheric conditions between these two periods similar atmospheric conditions were found.*

26. Page 13, line 393: Caption below Figure 7 says that this is mean precipitation and not accumulated.

This has been corrected

27. Page 17, line 522-524: This is the third time that you mention these results, so it adds on their importance but still you do not show them in the manuscript. Either just mention it in the discussion, but if you want to discuss them in the abstract and conclusion you should consider adding these plots to the manuscript. Please note also that these differences could be larger for the hourly precipitation events i.e., more local convective events which would depend on the local evaporation sources.

As previously discussed, we agree with the reviewer, therefore we removed this in the abstract, and in the conclusion just mentioned that number of dry/wet days is not largely affected, suggesting that these differences could be larger for hourly precipitation events to point out the limitation in this study and a possible future aspect to be studied.

Answers to Anonymous Reviewer #2

"Near East Desertification: Impact of Dead Sea drying on convective rainfall" by Khodayar and Hoerner submitted to Atmospheric Chemistry and Physics

Dear Reviewer2:

We have corrected this manuscript following all your comments and suggestions. In the following you can find a detail answer to all your general and specific comments.

Kind regards

Samiro Khodayar

General Comments:

Major comments:

1) Modeled mean annual precipitation: The mean annual precipitation computed by the model (Figure 5b) is quite different from observations, both in absolute magnitude and in gradients. At this region, the mean annual rain near the Mediterranean shoreline is in the range of 400-600 mm/year while over the higher topography west of the lake it can reach 500-700 mm. In the simulations presented in Figure 5b the range is from <75 mm/year at a close distance to the Mediterranean shore to 125-300 mm/year at the high topography west to the Dead Sea. The model presents much drier conditions and much larger gradients and seems not to represent well the typical more intense rain near the shore. The general effect of distance from sea on precipitation is not captured, while the orographic effect is probably well simulated. Although this paper is not focused on the effect of the Mediterranean Sea, still, as the main source of moisture to precipitation in the region, including in the study area, it is of concern that total amounts and gradients of precipitations are not represented well. The authors do not refer to this important deviation at all, not to mention explain why is it so high and why is it not harming the validity of the results and conclusions.

We have performed an extensive analysis/validation of the precipitation field using EOBS and APHRODITE information, the results show in agreement with other modelling efforts in the region a general underestimation with particular focus on the near-coast flat areas and better results over the complex areas. We have demonstrated that neither the simulations domain, the forcing data or the grid spacing used are the main reason for this bias. Indeed, closer results are obtained for the finer resolution simulations. Revising past simulation and validation exercises in the region in past publications we found out that similar biases have been identified in the past, also with different model schemes. In these publications it is pointed out inaccuracies in the SST as the reason for the biases in the precipitation field in the Mediterranean coastal area. Generally, relevant inaccuracies are identified in the SST field forcing our simulations, which have been demonstrated in the past to have a significant impact in the simulation of precipitation in the region. It is out of the scope of this paper to demonstrate this relevance, but we do agree with the reviewer that this is a relevant point to be discussed and to be investigated. Therefore, we *have included this discussion in the manuscript and proposed in the conclusions the need to investigate, for example though sensitivity experiments the relevance of SST to obtain a more accurate precipitation field.*

2) Dead Sea representation in the model: the lake form shown in Figure 1b is very noisy and different from the real lake shape and coverage. I understand this is how the lake is seen in the global data set of land use but the authors still could manually apply the actual lake shape. Furthermore, it is not stated anywhere in the paper if the salinity of the water was account for. The very high salinity reduces substantially evaporation rate compared to fresh water. Another important aspect is water temperature. What was used? This also can affect substantially evaporation and it is very different from the Mediterranean Sea temperature. All these features – lake shape, water salinity and temperature must be addressed as this is the most important feature in the simulation. The authors should note there are publications on the Dead Sea evaporation rate (e.g., Hamdani et al., 2018), so the simulated lake evaporation in the REF run can be verified.

We agree with the reviewer that differences exist between the reality and the modelled Dead Sea, whose characteristics are given by the global data set. It was out of the scope of this article to improve this representation in our model simulations, but we agree with the reviewer that this is a relevant point. Therefore, we will investigate this point and the sensitivity of our simulations to this in the new simulations we are performing in the area as indicated in the conclusions. The salinity is not considered in the Dead Sea simulations. Nevertheless, in the PhD thesis of Jutta Metzger/Vüllers, and the corresponding paper,

Wind Systems and Energy Balance in the Dead Sea Valley, 2017 | dissertation-thesis, DOI: 10.5445/KSP/1000072084

Dead Sea evaporation by eddy covariance measurements vs. aerodynamic, energy budget, Priestley–Taylor, and Penman estimates. Hydrology and Earth System Sciences. 2018-02-09 | journal-article, DOI: 10.5194/hess-22-1135-2018

it has been demonstrated that wind speed and vapour pressure deficit (humidity) are governing factors for evaporation in the Dead Sea valley, being the influence of salinity low as assessed by measurements and calculations. During the measurement campaign of the DESERVE project evaporation measurements were performed for a period of one year, which have been used in this publication as reference. We have included in the conclusions some sentences pointing out these issues raised by the reviewer, which we agree have to be considered but were out of the scope of this study.

3) Dead Sea abundance simulation: for the sensitivity analysis simulations the authors replace the lake with a soil at an elevation of 405 m below mean sea level, stating that this is the depth of the Dead Sea in the external data set, GLOBE. I find this quite strange as presently the lake level is at ~430 m below sea level; the lake's bathymetry is characterized by steep slopes and wide, flat lake floor at 720 m below mean sea level (see for example Sirota et al., 2017 among many other publications about the lake). So it is not clear what does the height of 405 m represent; if the Dead Sea will dry out, most probably the surface will be at a much lower height. Furthermore, the high gradient slopes exposed as a result of this drying can possibly affect precipitation, which is presently not considered in the paper. Also, please note, some studies claim it will not dry out but will get to a new (possibly much lower) steady state level (Yechieli et al., 1998).

The remaining flat floor of the lake at some level above 720 m will be much smaller than the actual lake area. The dry level will be higher than 720 m because of the huge amount of NaCl in the valley. We agree with the reviewer that there is discussion about the possibility of the lake never drying out, they indeed point out that a wet swamp of semi-crystalline salt would remain, even if there is no more inflow of fresh water in the valley. It was out of the scope of this paper to explore or discuss this or further possibilities. However, we agree with the reviewer about the relevance of this point, for that reason in the new set of simulations *we are performing (follow-up article) we are considering "intermediate condition/situation of the Dead sea" in addition to the more extreme condition, totally dry, investigated in this publication.*

4) Dead Sea moisture transport and winds: it could be very helpful to give some background on the prevailing winds in the region and, if possible, on tracks of Dead Sea-originated moisture, possibly by backward moisture tracking analyses. For example, as the western component is mostly positive in wind direction, changes in precipitation patterns associated with Dead Sea absence are expected to be much stronger east to the lake than at its west side. This aspect is mentioned for the two case study analyzed but not in the climatologically sense.

The article from Metzger et al. (2017) investigates in detail the climatology of the winds in the region. This information and corresponding reference is included in the article. It is not possible to recalculate backward moisture trajectories over the simulations performed given the resolution of our output and the impossibility of reproducing the simulations. External Lagrangian schemes could be used such as the freely available HYSPLIT software; however, this uses different model information that the one in this publication and validation will be needed to demonstrate the consistency of the results. We intend to include these calculations in the follow-up simulations we are performing in the region to complement this information.

5) Separating real effects from noise: it is hard to tell what of the effects presented in the paper are real and what are part of a noise or random error. Although the two model runs receive the exact same lateral and initial conditions, still, some differences could result from small numerical effects, not related to the Dead Sea absence. Especially, if one considers the argument in 4, above, it is not expected to have symmetrical differences on the west-east axis; however, Figure 5b (right) looks very noisy and the noise seems to have a similar pattern west and east to the lake. Could it be this noisy field of precipitation differences between the two simulations is random errors? one way to check this is to build the distribution of random differences by repeating the reference simulation few times and then consider only differences between the SEN and the REF simulations that are out of the 0.95 quantile.

Unfortunately, it is not possible to repeat the reference simulation since the computation system in which we run this simulations is not available anymore. However, we can confirm that at the moment of realization of these simulations we did run the same simulation in two different machines and we obtained the same results. Also the fact that we observe the same results in the 10-year long simulations and in the events simulated for several days, furthermore in many different events confirms that the effects presented in this paper are not random errors or noise.

Specific comments:

6) In some of the figures (e.g., Figure 2) evaporation is computed over land and lake areas and such results are hard to interpret. Obviously, the lake pixels have very high evaporation in the REF simulation and very low evaporation in SEN simulation. Could it be that this is the main control of the total volume difference between the two simulations? or, alternatively, it is just a small fraction of the total volume difference? if computation is done on land pixels only, it would be more informative in my opinion.

Evaporation is only computed over land in Figure 3 to facilitate the interpretation of the results.

Figure 2: all GP for all calculations are considered. In the following the example of evaporation including all GP(left) and only land points (right) is shown.

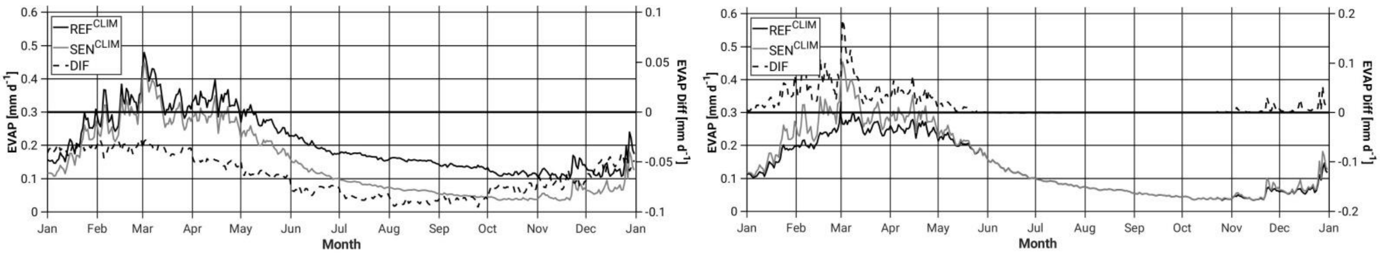

Figure 3: Only land points for evap and all GP for the rest

The Dead Sea grids have very high evaporation in the REF simulation and very low evaporation in SEN simulation, this difficult the interpretation of the results, thus we removed this effect in Figure 3 for evaporation, also because of the separation in 4 subdomains. In the following the example of evaporation including all GP(left) and only land points (right) for Area 1 is shown.

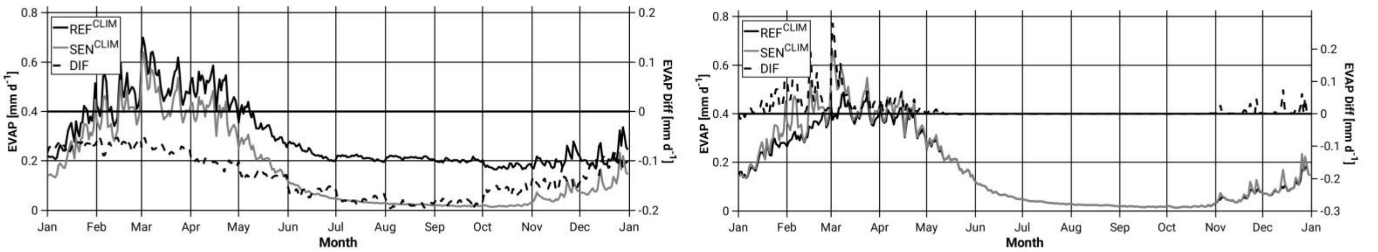

7) The authors describe in the introduction the lake level decline, which is presently > 1 m/year, but they do not state clearly that this decline is due to the massive water consumption at its upstream. One may get the impression that this substantial lake level decrease is due to climate change; this is wrong. It is possible of course that climate changes have a contribution to the lake level decrease during the last decades but it can explain much smaller decline rates comparing to the effect of water use (Lensky and Dente 2015).

This information has been included in the manuscript as we agree with the reviewer this is relevant for the readers.

8) The model spatial resolution is high, 2.8 km, and at this resolution convection can be resolved directly. However, not sure this is also true for shallow convective. Can you provide some info how was shallow convection handled? Another question is whether 2.8 km is small enough for small-scale convective typical to the Dead Sea manifested for example in the small convective rain cell size (e.g., Belachsen et al., 2017).

This information has been included in the description of the model.

9) *L101: Note that high resolution modelling in the region was performed by few studies, including: Hochman et al. (2018), Rostkier-Edelstein et al. (2014), Kunin et al. (2019) and possibly others.*

This information has been included in the text.

10) L290: “…almost no difference…”. I may have misunderstood the sentence, but it seems to me there are large differences in simulated evaporation in REF and SEN for A1 and A2 (Figure 3b). Also, it seems as there is more evaporation in the absence of the Dead Sea. Could it be because of the higher 2mT? Maybe there is also a change in the wind regime that could contribute to this?

Evaporation difference is negligible in the May to November period.

11) L351: can you explain the differences in 500 hPa geopotential height?

Differences in the near-surface conditions impact surface pressure as well as wind circulations, this information is transported upwards in the atmosphere locally and remotely, which results in the weak changes in the upper-atmospheric levels in this case the 500 hPa geopotential height.

12) *L358-359: how many instances does a probability of 1^e-6 represents? Could it be a single occurrence, possibly by chance?*

A probability of 1^e-6 represents approximately 22 instances. The total number of instances is 21759840, so one instance would be represented with a probability of approximately 5^e-8.

13) L439: how MSB is differentiated from the cyclone-related wind? Does ground temperatures in this day hotter or colder than SST? Could the decreased wind near the Dead Sea be related to the higher friction caused by the change in land use? Wouldn't this differ if the ground was set to 700 m below mean sea level rather than 405 m?

The timing, characteristics and evolution of the horizontal and vertical air flow helped us identify the MSB. Ground temperature in this day varies between 18° and 31°, whereas temperature over the Dead Sea varies only slightly between 25-26°.The temperature difference between the cooler maritime air mass and the warmer valley in REF result in the downward penetration of the MSB.

To give an accurate answer to the last two questions we believe it would be necessary to perform some sensitivity experiments to demonstrate these hypothesis. However, we believe that the change in land use is a contributing factor to the decrease wind, but not the only one, and the depth of the Dead Sea in the SEN simulation would not have changed the observed dynamics. It would have rather enhanced the behaviour to more marked temperature differences.

14) L456: This is a good point. However, what is the temperature of the Dead Sea surface in the REF simulation? Isn’t the opposite effect expected, since the Dead Sea surface temperature in November is ~25 oC (e.g., Hamdani et al., 2018)?

The ground temperature in SEN is higher than the surface temperature in REF between 8UTC and 13UTC. At point B, the mean surface temperature on the 18.11.2011 in REF is about 26°, whereas the mean ground temperature in SEN is about 19°.

Minor comments

15) L183: The statement about L (from SAL) is not accurate. It measures the distance of the center of mass of precipitation from the modelled one, and the average distance of each object from the center of mass.

Corrected

16) L286: north-west instead of north-east for A1

Corrected

17) L307: mm per day?

mm per month, as indicated in the caption of figure 4 monthly mean values calculated using daily mean values are presented. This has been corrected.

18) L330: a better citation for lake evaporation would be Hamdani et al., 2018

This reference has been included

19) L332: evaporation is probably correlated with rainfall which in turn correlated with topography. Also, soil type is often correlated with topography and rainfall.

Yes, we agree.

20) L368: correct zero 0.

Corrected

21) L406: gradient units should not be per km?

Corrected

22) L457-458: it is hard to see the "near-surface" temperature in Figure 11, since it is plotted from 1000 hPa, while the Dead Sea is at ~1060 hPa.

Unfortunately, this is the lowest level available as pressure level.

23) Figure 7 caption: please check. left and right of 7a are not the REF and REF-SEN.

Corrected

24) Some of the figure units should be corrected. For example, mm to mm d^-1.

This has been corrected.

References:

Belachsen, I., Marra, F., Peleg, N., Morin, E. 2017. Convective rainfall in a dry climate: relations with synoptic systems and flash-flood generation in the Dead Sea region. Hydrology and Earth System Sciences, 21, 5165-5180. doi:10.5194/hess-21-5165-2017.

Hamdani, I., Assouline, S., Tanny, J., Lensky, I.M., Gertman, I., Mor, Z. and Lensky, N.G., 2018. Seasonal and diurnal evaporation from a deep hypersaline lake: The Dead Sea as a case study. Journal of hydrology, 562, pp.155-167.

Hochman, A., Mercogliano, P., Alpert, P., Saaroni, H. and Bucchignani, E., 2018. High‐resolution projection of climate change and extremity over Israel using COSMO‐CLM. International Journal of Climatology, 38(14), pp.5095-5106.

Kunin, P., Alpert, P. and Rostkier-Edelstein, D., 2019. Investigation of sea-breeze/foehn in the Dead Sea valley employing high resolution WRF and observations. Atmospheric Research.

Lensky, N. and Dente, E., 2015. The hydrological proecesses driving the accelerated Dead Sea level decline in the past decades. Geological Survey of Israel Report.

Rostkier‐Edelstein, D., Liu, Y., Wu, W., Kunin, P., Givati, A. and Ge, M., 2014. Towards a high‐resolution climatography of seasonal precipitation over Israel. International Journal of Climatology, 34(6), pp.1964-1979.

Sirota, I., Enzel, Y. and Lensky, N.G., 2017. Temperature seasonality control on modern halite layers in the Dead Sea: In situ observations. Bulletin, 129(9-10), pp.1181-1194.

Yechieli, Y., Gavrieli, I., Berkowitz, B. and Ronen, D., 1998. Will the Dead Sea die?. Geology, 26(8), pp.755-758.

~~**Near East Desertification: impact of Dead Sea drying on convective rainfall**~~

Near East Desertification: impact of Dead Sea drying on the local conditions leading to convection

Samiro Khodayar[1,2] and Johannes Hoerner[2]

[1]Institute of Meteorology and Climate Research (IMK-TRO), Karlsruhe Institute of Technology (KIT), Karlsruhe, Germany

[2]Mediterranean Centre for Environmental Studies (CEAM), Valencia, Spain

Submitted to Atmospheric Chemistry and Physics

(HyMeX Inter-journal SI)

* Corresponding author. E-mail address: Khodayar_sam@gva.es (S. Khodayar)

Mediterranean Centre for Environmental Studies (CEAM),

Technological Park, Charles R. Darwin Street, 14 46980 - Paterna - Valencia - Spain

Abstract

The Dead Sea desertification-threatened region is affected by continual lake level decline and occasional, but life-endangering flash-floods. Climate change has aggravated such issues in the past decades. In this study, the impact of the Dead Sea drying on the severe convection generating heavy precipitation in the region is investigated. Perturbation Sensitivity simulations with the high-resolution convection-permitting regional climate model COSMO-CLM and several numerical weather prediction (NWP) runs on an event time scale are performed over the Dead Sea area. A reference simulation covering the 2003 to 2013 period and a twin sensitivity experiment, in which the Dead Sea is dried out and set to bare soil, are compared. NWP simulations focus on heavy precipitation events exhibiting relevant differences between the reference and the sensitivity decadal realization to assess the impact on the underlying convection-related processes.

On a decadal scale, the difference between the simulations points out that in future regional climate, under ongoing lake level decline, a decrease in evaporation, higher air temperatures and less precipitation is to expect. Particularly, an increase in the number of dry days and in the intensity of heavy precipitation is foreseen. The drying of the Dead Sea is seen to affect the atmospheric conditions leading to convection in two ways: (a) the local decrease in evaporation reduces moisture availability in the lower boundary layer locally and in the neighbouring, directly affecting atmospheric stability. Weaker updrafts characterize the drier and more stable atmosphere of the simulations where the Dead Sea has been dried out. (b) Thermally driven wind system circulations and resulting divergence/convergence fields are altered preventing in many occasions convection initiation because of the omission of convergence lines. On a decadal scale, the difference between the simulations points outsuggests that in future regional climate, under ongoing lake level decline, a decrease in evaporation, higher air temperatures and less precipitation is tomay be expected. Particularly, an increase in the number of dry days and in the intensity of heavy precipitation is foreseen.

Key Words: Dead Sea drying, climate change, convection, heavy precipitation, boundary layer, wind systems, *high-resolution modelling*

1. Introduction

The Eastern Mediterranean and the Middle East is a sensitive climate change area (Smiatek et al. 2011). The anticipated warming in the 21st century combined with the general drying tendency, suggest important regional impacts of climate change, which should be investigated to assess and mitigate local effects on society and ecosystems. The Dead Sea basin is~~,~~ dominated by semi-arid and arid climates except by the north-western part that is governed by Mediterranean climate (Greenbaum et al. 2006). It~~,~~ is an ideal area to study climate variation in the Near East. It was already discussed by Ashbel (1939) the influence of the Dead Sea on the climate of its neighbouring regions. The change in the climate of the Dead Sea basin caused by the drying of the Dead Sea has also been evidenced in the last decades (Alpert et al. 1997; Cohen and Stanhill 1996; Stanhill 1994). The Dead Sea is the lowest body of water in the world (~ -430 m) surrounded by the Judean Mountains (up to ~ 1 km amsl) to the west and to the east by the Maob Mountains (up to ~ 3 km amsl). The area in between is rocky desert. The complex topography of the area favours the combined occurrence of several wind regimes in addition to the general synoptic systems, namely valley and slope winds, Mediterranean breezes and local lake breezes (e.g. Shafir and Alpert 2011). These wind systems are of great importance for the living conditions in the region since they influence the visibility and the air quality (e.g. Kalthoff et al. 2000; Corsmeier et al. 2005) as well as the atmospheric temperature and humidity. Since the Dead Sea is a terminal lake of the Dead Sea Valley, no natural outflow exists, being evaporation the main loss of water, being the wind velocity and vapour pressure deficit identified as the main governing factors of evaporation throughout the year (Metzger et al. 2017). Through the high evaporation the lake level declines and results in a desertification of the shoreline and a changing fraction of water and land surface in the valley. The documented Dead Sea water level drop of about 1 m/y in the last decades (Gavrieli et al. 2005) is mainly due to the massive water consumption at its upstream having climate changes a small contribution to the lake level decrease (Lensky and Dente 2015). This situation ~~-~~severely affects agriculture, industry and the environmental conditions in the area, thus, leading to substantial economic losses (Arkin and Gilat 2000).

The Jordan River catchment and Dead Sea ~~-~~exhibit in the north, annual precipitation in the order of 600-800 mm, whereas in the south, there is an all year arid climate with an

Con formato: Fuente: (Predeterminado) Arial annual precipitation of <150 mm (Schaedler and Sasse 2006). Rain occurs between October and May and can be localized or widespread (Dayan and Sharon 1980) ~~with annual variations of the same order of magnitude as the rainfall itself~~ (Sharon and Kutiel 1986). Rainfall varies seasonally and annually, and it is often concentrated in intense showers (Greenbaum et al. 2006)~~. The Dead Sea basin is prone to flash flooding~~ caused mainly by severe convection ~~generating heavy precipitation~~ (Dayan and Morin 2006). Flash floods are among the most dangerous meteorological hazards affecting the Mediterranean countries (Llasat et al 2010), thus, knowledge about the processes shaping these events is of high value. This is particularly relevant in arid climates, where rainfall is scarce, and often, local and highly variable. In flood-producing rainstorms, atmospheric processes often act in concert at several scales. Synoptic-scale processes transport and redistribute the excess sensible and latent heat accumulated over the region and subsynoptic scale processes determine initiation of severe convection and the resulting spatio-temporal rainfall characteristics. The main responsible synoptic weather patterns leading to heavy rainfall in the region are in general well known and described in previous publications (e.g. Belachsen et al. 2017; Dayan and Morin 2006). Belachsen et al. (2017) pointed out that three main synoptic patterns are associated to these heavy rain events: Cyprus low accounting for 30% of the events, Low to the east of the study region for 44%, and Active Read Sea Trough for 26%. The first two originate from the Mediterranean Sea, while the third is an extension of the Africa monsoon. Houze (2012) showed that orographic effects lead to enhanced rainfall generation; rain cells are larger where topography is higher. Sub-synoptic scale processes play a decisive role in deep convection generation in the region. Convection generated by static instability seems to play a more important role than synoptic-scale vertical motions (Dayan and Morin 2006). The moisture for developing intensive convection over the Dead Sea region can be originated from the adjacent Mediterranean Sea (Alpert und Shay-EL 1994) and from distant upwind sources (Dayan and Morin 2006).

In this study, ~~the climatic change at~~ the drying of the~~the~~ Dead Sea ~~region caused by its drying~~ is investigated focusing on the impact on atmospheric conditions leading to heavy precipitating convection in the region. The relevance of the Dead Sea as a local source of moisture for precipitating convection as well as the impact of the energy balance partitioning changes and related processes caused by the drying of the Dead Sea are investigated. With this purpose, a sensitivity experiment with the high-resolution regional climate model COSMO-CLM [Consortium for Small scale Modelling model (COSMO)-in Climate Mode (CLM); Böhm et al. 2006] is conducted. The high horizontal grid spacing used (~ 2.8 km) resolves relevant orographic and small-scale features of the Dead Sea basin, which is not the case when coarser resolution simulations are performed. Moreover, at this resolution convection is explicitly resolved instead of being parametrized, which has been already extensively demonstrated to be highly beneficial for the simulation of heavy precipitation and convection-related processes. The benefit of employing high-resolution convection permitting simulations is mainly in sub-daily time-scales, ~~-~~(e.g., Prein et al., 2013; Fosser et al., 2014; Ban et al., 2014), however, daily precipitation is also positively affected, particularly in winter time (Fosser et al., 2014). ~~This effort, to the knowledge of the authors, has not been previously attempted in the region~~Previous studies in the area applying high-resolution modelling agree with the benefitial impact of finer resolution against coarser ones (e.g. *Rostkier-Edelstein et al. 2014; Hochman et al. 2018; Kunin et al. 2019*).

Con formato: Fuente: (Predeterminado) Arial

The impact of completely drying the Dead Sea on the regional atmospheric conditions and precipitating convection is discussed. A decadal simulation and several event-based Numerical Weather Prediction (NWP) runs covering the eastern Mediterranean are carried out. A process understanding methodology is applied to improve our knowledge about how sub-synoptic scale processes leading to severe convection are affected by the drying of the Dead Sea. The article is organized as follows. Section 2 provides an overview of the data and the methodology used. Then, in section 3, the climatology of the region based on the high-resolution convection-permitting decadal simulation is presented and the impact of drying the Dead Sea is examined across scales. Finally, conclusions are discussed in section 4.

2. Data and methodology

2.1 The COSMO-CLM model

In this investigation, the regional climate model (RCM) of the non-hydrostatic COSMO model, COSMO-CLM (CCLM), is used (Version 5.0.1). It has been developed by the Consortium for Small-scale modeling (COSMO) and the Climate Limited-area Modeling Community (CLM) (Böhm et al., 2006). It uses a rotated geographical grid and a terrain-following vertical coordinate. The model domain covers the southern half of the Levant, ~~centered~~centred around the Dead Sea, with a horizontal resolution of 7 km and 2.8 km, 60 vertical levels and a time step of 60 and 20 seconds, respectively. Using ~~The driving data for the 7 km with a horizontal resolution of 0.25° is derived from the~~ IFS (Integrated Forecasting System) analysis, the spectral weather model of ECMWF

(European Centre for Medium-Range Weather Forecast) as driving data for the simulations, a double nesting procedure was employed. The coarsest nest at 0.0625º resolution (about 7 km) covers 250 grid points in x direction and 250 grid points in y direction. The size and location of the 7 km domain has been considered large enough to have into consideration all possible synoptic situations relevant for the development of extreme phenomena in the study area as well as the influence of the Mediterranean Sea. The finest nest at 0.025º (circa 2.8 km) covers 150 x 150 grid points, thus a total area of 22500 grid points and includes the study area (72 grid point in x direction and 92 in y direction) centred around the Dead Sea.

A Tiedtke (1989) mass-flux scheme is used for moist convection in the 7 km, and reduced Tiedke mass-flux scheme for shallow convection. Contrary to the CCLM-7 km simulation, where convection is parameterized, in the CCLM-2.8 km convection is explicitly resolved (Doms and Baldauf, 2015), so only the reduced Tiedke mass-flux scheme is used for shallow convection. ~~Additionally, orography data from GLOBE (Global Land One-km Base Elevation Project) of NOAA (National Oceanic and Atmospheric Administration) and soil data from HWSD (Harmonized Worlds Soil Database) TERRA is used. HWSD is a global harmonization of multiple regional soil data sets with a spatial resolution of 0.008° (FAO, 2009), resulting in 9 different soil types in the model, namely 'ice and glacier', 'rock / lithosols', 'sand', 'sandy loam', 'loam', 'loamy clay', 'clay', 'histosols', and 'water'.~~

~~With a horizontal resolution below 3 km, convection can be resolved directly (Doms and Baldauf, 2015).~~ The model physics includes a cloud physics parameterization with 5 types of hydrometeors (water vapor, cloud water, precipitation water, cloud ice, precipitation ice), a radiative transfer scheme based on a delta-two-stream solution (~~Doms et al., 2011~~Ritter and Geleyn, 1992) and a roughness-length dependent surface flux formulation based on modified Businger relations (Businger et al., 1971).

~~Additionally, o~~Orography data from GLOBE (Global Land One-km Base Elevation Project) of NOAA (National Oceanic and Atmospheric Administration) and soil data from HWSD (Harmonized Worlds Soil Database) TERRA is used. HWSD is a global harmonization of multiple regional soil data sets with a spatial resolution of 0.008° (FAO, 2009), resulting in 9 different soil types in the model, namely 'ice and glacier', 'rock / lithosols', 'sand', 'sandy loam', 'loam', 'loamy clay', 'clay', 'histosols', and 'water'.

Con formato: Sin Resaltar

Con formato: Sin Resaltar

Con formato: Sin Resaltar

Con formato: Sin Resaltar

Con formato: Fuente: (Predeterminado) Arial

Multiple model runs have been performed. A 7 km run from 2003 to 2013 with daily output is used as nesting for two 2.8 km runs over the same time span. The Dead Sea is dried out and replaced with soil types from the surrounding area in one of them (SEN), the other one is used as reference (CLIM). For the detailed investigation of convective events on 14.11.2011 and 19.11.2011, sub-seasonal simulations have been performed with the same settings as the decadal simulation, but with hourly outputs due to the limitations imposed by the daily output.

2.2 Methodology

In order to assess the impact of the drying of the Dead Sea on the atmospheric conditions leading to severe convection in the region, a set of sensitivity experiments was performed. A decadal simulation covering the 2003 to 2013 time period was carried out with the convection permitting 2.8 km COSMO-CLM model. Lateral boundary conditions and initial conditions are derived from the European Centre for Medium-Range Weather Forecasts (ECMWF) reanalysisdata. The COSMO-CLM 7 km is used as nesting step in between the forcing data and the 2.8 km run. This reference simulation will be hereafter referred to as REF^{CLIM} simulation. Parallel to this, a sensitivity experiment (hereafter SEN^{CLIM}) is carried out in which the Dead Sea is dried out and set to bare soil on -405 m level (depth of the Dead Sea in the external data set, GLOBE (Hastings and Dunbar, 1999)). After examination of the results, the first year of simulations is considered spin-up time, thus, our analysis covers the 2004-2013 period.

The precipitation field has been validated using the EOBS dataset (Haylock et al. 2008) with a resolution of 0.1° and available for the period 1980-2011, and the APHRODITE's (Asian Precipitation - Highly-Resolved Observational Data Integration Towards Evaluation: Yatagai et al. 2008, 2012) daily gridded precipitation which is the only long-term continental-scale daily product that contains a dense network of daily rain-gauge data for Asia. It has a resolution of 0.25º and is available for 1980-2007. The APHRODITE data shows generalized lower precipitation values than EOBS, but still higher than our simulation particularly close to the northern Mediterranean shoreline, over coastal-flat terrain, whereas the best agreement is at areas dominated by complex terrain. This agrees with previous high-resolution modelling activities in the region such as Rostkier-Edelstein et al. (2014) using WRF at 2 km. They suggest in this publication that inaccuracies in the gridded SST dataset used in the simulations could be responsible for the observed bias highlighting the strong sensitivity of precipitation in the Mediterranean basin to very small differences in the SST (Miglietta et al. 2011). Despite these biases the comparison of the temporal areal-mean of the model

Con formato: Fuente: Sin Negrita

Con formato: Fuente: Sin Negrita

Con formato: Fuente: Sin Negrita

Con formato: Fuente: Sin Negrita

Con formato: Fuente: Sin Negrita

Con formato: Fuente: Sin Negrita

Con formato: Fuente: Sin Negrita, Sin Resaltar simulations at 7 km and 2.8 km and the APHRODITE dataset demonstrates that in general the model quiete well captures the precipitation events. An improvement is seen at the finer resolution.

Regional dry and wet periods are identified and quantified in the simulations by means of the Effective Drought Index (EDI; Byun and Wilhite 1999; Byun and Kim 2010). The EDI is an intensive measure that considers daily water accumulations with a weighting function for time passage normalizing accumulated precipitation. The values are accumulated at different time scales and converted to standard deviations with respect to the average values. Here we use an accumulation period of 365 days. EDI dry and wet periods are categorized as follows: moderate dry periods -1.5 <EDI<-1, severe dry periods -2<EDI<-1.5, and extreme dry periods EDI<-2. Normal periods are revealed by -1<EDI<1 values.

Based on daily mean values, precipitation and evapotranspiration distribution and possible ~~trends~~ tendencies in the 10-year period are assessed. To further asses the most affected areas in our ~~The~~ study area, this is divided in four subdomains surrounding the Dead Sea and trying to respect the orographic pattern in the area (Figure 3). Annual cycles are thus separately investigated to take into consideration the relevant differences in orography, soil types, and distance to the coast among others (Figure1), which are known to have a significant impact in the precipitation distribution in the region (e.g. Belachsen 2017; Houze 2012). ~~centred at the Dead Sea to examine dependencies in relation to the regional patterns (Figure 1).~~ Differences in the annual cycle and temporal evolution of precipitation and evapotranspiration between the REF^{CLIM} and SEN^{CLIM} are discussed. Also, differences in the near-surface and boundary layer conditions and geopotential height patterns are examined. Geographical patterns of mean evapotranspiration and precipitation and differences with respect to the reference simulation are assessed. Probability distribution functions (PDFs), and the Structure, Amplitude and Location (SAL: Wernli et al. 2008) analysis methodologies are used to illustrate differences in the mean and extreme precipitation between the reference and the sensitivity experiments. The SAL is an object-based rainfall verification method. This index provides a quality measure for the verification of quantitative precipitation forecasts considering three relevant aspects of precipitation pattern: the structure (S), the amplitude (A), and the location (L). The A component measures the relative deviation of the domain-averaged rainfall; positive values indicate an overestimation of total precipitation, negative values an underestimation. The component L ~~provides an estimation of the 'accuracy of location', comparing the proportion of high and low rainfall totals within each object~~ measures the distance of

Con formato: No ajustar espacio entre texto latino y asiático, No ajustar espacio entre texto asiático y números

Con formato: Fuente: 11 pto, Inglés (Reino Unido)

Con formato: Fuente: 11 pto, Inglés (Reino Unido)

Con formato: Fuente: 11 pto, Inglés (Reino Unido)

Con formato: Fuente: 11 pto, Inglés (Reino Unido)

Con formato: Fuente: 11 pto, Inglés (Reino Unido)

Con formato: Fuente: 11 pto, Inglés (Reino Unido)

Con formato: Fuente: Sin Cursiva

the center of mass of precipitation from the modelled one, and the average distance of each object from the center of mass. The component S is constructed in such a way that positive values occur if precipitation objects are too large and/or too flat and negative values if the objects are too small and/or too peaked, quantifying the physical distance between the centres of mass of the two rainfall fields to be compared. Perfect agreement between prediction and reference are characterized by zero values for all components of SAL. Values for the amplitude and structure are in the range (−2, 2), where ±0.66 represents a factor of 2 error. The location component ranges from 0 to 2, where larger values indicate a greater separation between centres of mass of the two rainfall fields. This is done by selecting a threshold value of 1/15 of the maximum rainfall accumulation in the domain (following Wernli et al. 2008). The structure and location components are thus independent of the total rainfall in the domain.

Con formato: Fuente: (Predeterminado) Arial

Differences in the temporal evolution of precipitation between the REF^{CLIM} and SEN^{CLIM} are identified. In Table 1, tThose events in which an area-mean (study area, Figure 1) difference between both simulations higher than ±0.1 mm/d exists are selected as potential heavy precipitation events and classified attending to their synoptic scale environment, and atmospheric stability conditions (Table 1).

Although Dayan and Morin (2006) discuss that in general large-scale vertical motions do not provide the sufficient lifting necessary to initiate convection, it was demonstrated by Dayan and Sharon (1980) that a relationship exists between the synoptic-scale weather systems and deep moist convection, being those systems responsible for the moisturizing and destabilization of the atmosphere prior to convective initiation. They pointed out that indices of instability proved the most efficient determinants of the environment characterizing each rainfall type in the region. Thus, two indicators of the atmospheric degree of stability/instability, namely the Convective Available Potential Energy (CAPE; Moncrieff and Miller 1976) and the KO-index (Andersson et al. 1989), are examined in this study. The CAPE is a widely known index indicating the degree of conditional instability. Whereas, the KO-index, which is estimated based on the equivalent potential temperature at 500, 700, 850 and 1000 hPa (following the recommendations by Bolton 1980), describes the potential of deep convection to occur as a consequence of large-scale forcing (Andersson et al. 1989; Khodayar et al. 2013). Generally, regions with KO-index < 2 K and large-scale lifting are identified as favourable for deep convection. Parcel theory (50 hPa ML (Mixed Layer) parcel) and virtual temperature correction (Doswell and Rasmussen 1994) are applied to these calculations.

Based on the above criteria, a separation was made between events with widespread rainfall and those more localized. Among the latter, we selected two events to illustrate the local impacts on the boundary layer conducive to deep moist convection. Particularly, differences in the amount, structure and location of precipitation are assessed by examining the spatial patterns and the SAL verification method. The two selected events for detail analysis in this study are those showing the larger SAL deviations. Those two cases occur close in time. Carefull inspection of the atmospheric conditions after the first event shows no significant differences between simulations suggesting no connetion between both events. Even though a more detail analysis is provided for the two selected cases, all convective-events listed in Table 1 have been examined to assess the main impacts on the mechanisms leading to convection. High-resolution simulations with the NWP COSMO 2.8 km model are performed with hourly output temporal resolution and covering a 3-day period (including 48-h prior to the day of the event, from 00 UTC) to capture atmospheric pre-conditions conducive to deep moist convection. For this, a reference simulation, REF^{NWP}, and a sensitivity experiment, SEN^{NWP}, are carried out for each event.

Con formato: Fuente: (Predeterminado) Arial

3. Results and discussion

3.1 Climatology of the Dead Sea region

Annual cycle

To assess the climatology of the study region (Figure 1) the annual evaporation and precipitation cycles based on daily means of the respective quantities are investigated (Figure 2). Additionally, we examine the evolution of specific humidity (Qv_{2m}) and temperature at 2 m (T_{2m}) as well as total column integrated water vapour (IWV) and low-boundary layer (< 900 hPa) equivalent potential temperature (Θ_e). Possible changes in the atmospheric stability conditions are evaluated by examination of the CAPE and KO-index. In Figure 2, all grid points over the study region (Figure 1) and the time period 2004-2013 are considered. Differences between the REF^{CLIM} and the SEN^{CLIM} simulations are also discussed.

The annual cycle of evaporation shows minimum values in the autumn season (around October, ~ 0.1 mm/d) and maximum evaporation in spring (around March, ~ 0.4 mm/d). The dependency with the precipitation cycle is clear with maximum values of the latter around March and rain occurring between October and May (Figure 2a) in agreement with observations in the area (Dayan and Sharon 1980). The difference between the evaporation in the REF^{CLIM} and the SEN^{CLIM} simulations indicates a mean decrease in the order of 0.02 (February) to ~ 0.1 (August) mm/d in the absence of the Dead Sea water (SEN^{CLIM}). The largest difference is in the dry period (May to October) when water availability is less dependent on precipitation, and evaporation is higher over the Dead Sea in contrast to the minimum values over land (Metzger et al. 2017). In general, there is a decrease of about 0.5 % in precipitation in the ~~“non-Sea” simulation,~~ SEN^{CLIM} simulation. In contrast to the differences in evaporation, precipitation differences between the reference and the sensitivity experiment occur in both directions during the rain period, from October to May. Examining the total number over the whole decadal simulation it is seen that the number of dry or wet days (> 0.1 mm/d) or heavy precipitation events is not largely affected in the sensitivity experiment. In general, the number of dry days increases (fewer wet days) in the SEN^{CLIM} simulation, whereas the number of high intensity events show almost no variation. For each simulation, the difference between precipitation and evaporation is negative mainly in spring and summer contributing to the dryness in the region. Furthermore, the negative difference between the REF^{CLIM} and SEN^{CLIM} simulations indicates that the PREC-EVAP difference is higher in the SEN^{CLIM} simulation probably in relation to the reduced evaporation over the dry sea area and the general decrease in the precipitation amount in the region.

Con formato: Sin Superíndice / Subíndice

In addition to the reduced evaporation and precipitation (about 0.5 %) in the whole domain in the SEN^{CLIM} simulation a drier and warmer lower-troposphere is identified (Figure 2b) in agreement with the observational assessment by Metzger et al. (2017) of the cooling effect of evaporation on air temperature in the region. The annual cycle of IWV and $\Theta_{e<900hPa}$ in Figure 2c show that the impact of the dry Dead Sea resulting evaporation is less pronounced when a deeper atmospheric layer is considered. Indeed, $\Theta_{e<900hPa}$ evolution evidences that the warming effect due to the decreased evaporation in the SEN^{CLIM} simulation is restricted to the near surface.

In Figure 2d, the annual cycle of areal mean CAPE displays larger values in the period from August to November, being this the period more favourable for convection. Positive CAPE differences between the REF^{CLIM} and the SEN^{CLIM} simulations are presumably in relation to the identified distinct lower-atmospheric conditions, being these more favourable and consequently CAPE values higher in the REF^{CLIM} simulation. In the same period, the KO-index indicates a more potentially unstable atmosphere, i.e. prone to deep convection because of large-scale forcing, and larger differences between simulations.

~~To further assess the most affected areas in our investigation domain, the study region is divided in four subdomains surrounding the Dead Sea (Figure 3). Annual cycles are separately investigated to take into consideration the relevant differences in orography, soil types, and distance to the coast among others (Figure1), which are known to have a significant impact in the precipitation distribution in the region (e.g. Belachsen 2017; Houze 2012).~~ In agreement with the well-known precipitation distribution in the region most of the events occur in A1 (north-~~east~~west) and A2 (north-east). Also, in these subdomains larger differences between the REF^{CLIM} and SEN^{CLIM} simulations are identified pointing out the relevance of the Dead Sea evaporation in the pre-convective environment for rainfall episodes over the study area (Figure3a). Considering only land grid points almost no difference between simulations is found in the evaporation annual cycle of A1 and A2 (Figure3b) suggesting the distinct amount of moisture advected towards A1 and A2 from the Dead Sea in REF^{CLIM} and SEN^{CLIM} as responsible for the differences in the boundary layer conditions conducive to convection. Also, in these subdomains the dryer and warmer lower boundary layer and the reduced instability in the SEN^{CLIM} are recognized

Inter-annual variability

In Figures 4 we discuss the inter-annual variability (based on monthly-daily areal mean values) of evaporation, precipitation as well as drought evolution.

The reduced evaporation in the annual cycle of the SEN^{CLIM} simulation for the whole investigation domain, resulting from the drying of the Dead Sea and affected evaporation, remains from year to year (Figure 4a). Larger differences between the simulations occur in the May to November months in agreement with the annual cycle in Figure 2a. This, and the time period of the maximum/minimum is constant over the years. A tendency towards lower evaporation at each simulation and higher differences between both at the end of the period are identified. An inter-annual fluctuation is observed in both REF^{CLIM} and SEN^{CLIM} simulations. The yearly rate of evaporation shows, for example, in REF^{CLIM} maximum values of about 7 mm in 2011 and around 17 mm in 2012. This is in agreement with the positive correlation expected between precipitation and evaporation, a trend towards decreased precipitation and a correspondence between drier years such as the 2011-2012 period and lower annual evaporation are seen in Figure 4b. Year to year EDI calculations in Figure 4c help us identify the regional extreme dry and wet periods. The EDI range of variation from about -1 to 2 for the whole period of simulation indicates that the dry condition is the common environment in the area, while the wet periods, EDI up to 6, could be identified as extreme wet periods (relative to the area), in this case in the form of heavy precipitation events. Maximum positive EDI values are in the first months of the year in agreement with the precipitation annual cycle in Figure 2, whereas minimal EDI values occur in summer and autumn indicative of the dry conditions in these periods. Differences in the EDI calculations from both simulations reveal distinct precipitation evolutions and denote timing differences in the occurrence of the precipitation events. When the regional climate evolution is examined in combination with the impact on the number of heavy precipitation events (Table 1) the impact is stronger in the dry period of 2011 (Figure 4a). About six events show relevant differences in this period, contrary to the average 3 episodes per year.

Spatial distribution

The geographical patterns of evaporation and precipitation are presented in Figure 5. Over the Dead Sea, the simulated average annual evaporation for the period under consideration is in the order of 1500-1800 mm/y, in contrast to the values in the deserts east and south, where the evaporation is less than 20 mm/y. Observed annual evaporation of this lake is known to be about 1500 mm and to vary with the salinity at the surface of the lake and freshening by the water inflow (Dayan and Morin 2006; Hamdani et al. 2018). Over land, higher evaporation is seen over the Judean Mountains and the Jordanian Highlands. High correlation with the orography and soil types is seen (Figure 1). Evaporation is probably correlated with rainfall which in turn is correlated with topography. Particularly, in the Jordanian Highlands where maximum evaporation is around 200 mm/y, the complex topography coincides with sandy loam soils, whereas most of the soil in study region is defined as loamy clay or clay (Figure 1). The evaporative difference field between simulations in Figure 5a shows a highly inhomogeneous patchiness not evidencing any relationship with orography or soil type, but rather with changes in the precipitation pattern in the SEN^{CLIM} simulation as seen in Figure 5b.

In agreement with the temporal series of areal mean precipitation in Figure 3 higher annual precipitation are in the north-west and -east, with respect to the southern regions. Topographic features exert a large impact on precipitation distribution with maxima of about 175 to 300 mm/y over the Judean Mountains and the Jordanian Highlands. To the northern end of the Dead Sea valley, the largest precipitation difference between the REF^{CLIM} and the SEN^{CLIM} simulations is identified, rather than directly over the Dead Sea area noting the importance of advected moisture from the Dead Sea evaporative flux upslope and along the Dead Sea valley as well as the

Con formato: Fuente: Sin Cursiva

Con formato: Fuente: Sin Cursiva

Con formato: Fuente: (Predeterminado) Arial, indirect effects of a different spatial distribution of low-tropospheric water vapour in the occurrence of precipitating convection.

Regarding the impact on the large-scale conditions, differences in the spatial pattern and strength of the 500 hPa geopotential height field are identified over the Dead Sea (not shown). In the 10-year mean, differences up to 0.002gpdm higher in SEN than in REF are observed. Around the Dead Sea area, the differences are smaller and more irregular. Generally, the differences are higher in the east of the Dead Sea than in the west.

Precipitation probability distribution function

While the probability for lower intensity precipitation is very similar in the REF^{CLIM} and the SEN^{CLIM} simulations differences are recognized in the higher precipitation intensities, from about 150 mm/d (Figure 6a). Particularly, above 180 mm/d extreme precipitation values occur less frequent at the SEN^{CLIM} simulation where a drier, warmer and more stable atmosphere is identified (Figure 2).

SAL

The use of the SAL method in this study differs from the approach frequently presented in literature since it is here not our purpose to examine differences between the simulated field and observations (adequate observations for this comparison are not available in the area), but to compare changes regarding the structure, amount and location of the precipitation field between our reference and sensitivity experiments. Figure 6b shows that when the mean precipitation over the whole simulation period is considered all three SAL components are close to zero ~~0~~, meaning that very small differences are found. However, when single precipitation events in the REF^{CLIM} simulation are compared with the same period at the SEN^{CLIM} simulation, larger differences regarding structure, amount and location of rainfall events are found. For further examination of this issue two exemplary heavy precipitation events (indicated by boxes in Figure 6b) are analysed in detail. In both cases, a negative A-component is recognized, that is, less precipitation falls in the SEN^{CLIM} simulation. The S-component also evidences the change in the structure of the convective cells. The L-component is low meaning that the convective location does not change significantly in the SEN^{CLIM} simulation, in contrast to the intensity and structure of the cells.

3.2 Sensitivity of atmospheric conditions to the Dead Sea drying: episodic investigation

Among those events exhibiting differences in the precipitation field between both simulations (Table 1 and Figure 6b) two situations occurring in the time period of the 14 to 19 November 2011 are investigated in the following.

In this term, the synoptic situation is characterized by a Cyprus low and its frontal system located over the Dead Sea at about 00 UTC on the 15 November 2011 and at 12 UTC on the 18 November 2011. The low-pressure system and its frontal system induced strong south-westerly to westerly winds with mean wind velocities up to 15 m/s.

In the first situation (hereafter CASE1), in association with the western movement of the cold front a convective system develops over the Jordanian Highlands with precipitation starting at about 21 UTC on the 14 November 2011. This convective system is of high interest because of the large difference in its development between the REF$^{14.11}$ and the SEN$^{14.11}$ simulations.

In Figure 7a the 24-h accumulated precipitation, from 14.11 09 UTC to 15.11 08 UTC, in the investigation area is shown for the REF$^{14.11}$ and the SEN$^{14.11}$ simulations. Two precipitation areas are seen, on the north-western and north-eastern of the Dead Sea. Larger difference between models is on the north-eastern region (24-h accumulated precipitation > 100 mm/d in REF$^{14.11}$, while < 50 mm/d in SEN$^{14.11}$), which is the focus of our analysis.

The REF$^{14.11}$ simulation shows that in the 6 hours period prior to the initiation of convection the pre-convective atmosphere and more specifically the lower boundary layer exhibit a moist (IWV ~ 24-30 mm, qvPBLmax ~ 7-10 g/kg) and unstable (CAPE ~ 1100 J/kg; KO-index ~ -8 K; not shown) air mass on the western side of the investigation area, particularly close to the western Mediterranean coast, and drier (IWV~ 8-16; qvPBLmax ~ 4-6 g/kg) and more stable conditions (CAPE< 200 J/kg; KO-index ~ 0-2 K) on the eastern side of the domain (Figure 7b). A maximum ~~gradient~~ difference of about 5 g/kg from west to east is established in the lower boundary layer. Main differences between both simulations are over the Dead Sea (IWV difference up to 2 mm and qvPBL up to 1.5 g/kg) and north and north-east of it, but almost similar conditions everywhere else. In our target area (subdomain of investigation where the convection episode takes place (red box in Figure 7)), north-east of the Dead Sea, a drier and a more stable atmosphere is identified at the SEN$^{14.11}$ simulation.

The evolution of the wind circulation systems in the area is similar in both simulations (Figure 7c). The 700 hPa, 850 and 950 hPa winds dominantly blow from the south south-west during the pre-convective environment advecting the moist unstable air mass towards the Dead Sea valley and north-east of it, directly affecting the atmospheric conditions at the target area (for a comparison with a climatology of the wind conditions in the region please see Metzger et al. 2017). In both simulations, the passage of the cold front over the Dead Sea establishes a strong southerly wind from about 10 UTC on the 14 November 2011.

Prior to this time, dry air was advected below about 850 hPa towards the target area from the east. The turning of the low-level winds and the resulting moistening of the atmosphere is well and equally captured by both simulations (Figure 8a). Furthermore, at the near-surface, from about 16 UTC, ~ 5 h prior to convection initiation in the target area, a near-surface convergence line forms at the foothills of the northern part of the Jordanian Highlands, which is also well and equally captured by both simulations (Figure 8b). The lifting provided by the convergence line triggers convection in the area. However, the drier and more stable atmosphere in the $SEN^{14.11}$simulation results in less intense convection, weaker updrafts, and reduced precipitation at the eastern slope of the valley.

In the second case, CASE2, we address an episode of localized convection taking place on the north-western edge of the Dead Sea in the REF simulation, whereas no convection develops in the SEN simulation. The isolated convection in the REF simulation left about 50 mm rain in 3 h starting at about 03 UTC on the 19 November 2011 (Figure 9).

In contrast to CASE1, the modification of the pre-convective environment relevant for convective initiation is in this case dominated by dynamical changes in the mesoscale circulations. Differences in the evolution and strength of the Mediterranean Sea Breeze (MSB), the Dead Sea breeze and orographic winds influence atmospheric conditions in the target area leading to the assistance to or to the absence of convection. The most significant difference observed between the simulations is in the development of a strong near-surface convergence line in the REF simulation (which is not present in the SEN simulation hindering convection in the area), which forms about 2 h before convective initiation (Figure 10).

Even in the first hours of the 18 November 2011 differences in the speed and direction of the near-surface winds over the Dead Sea and on the eastern flank of the Jordanian

Highlands could be identified. A fundamental difference between simulations occurs from about 17 UTC when strong westerly winds indicating the arrival of the MSB reach the western shore of the Dead Sea. One hour later, in the $REF^{19.11}$ run the MSB strongly penetrates the Dead Sea valley reaching as far as the eastern coast in the centre to south areas. However, in the $SEN^{19.11}$ simulation the MSB does not penetrate downward, instead strong northerly winds flow along the valley (Figure 10a). Numerous observational and numerical studies carried out to investigate the dynamics of the MSB (e.g. Naor et al. 2017; Vuellers et al. 2018) showed that the downward penetration of the MSB results from temperature differences between the valley air mass, which is warmer than the maritime air mass. An examination of temperature differences along a near-surface north-south valley transect (positions in Figure 10a) indicates a decrease of about 4 ºC at the near-surface over the dried Dead Sea area in contrast to negligible changes on a parallel transect inland, on the western coast of the Dead Sea. These evidences the notorious impact of the absence of water in the valley temperature, thus, gradients in the region. The colder valley temperatures do not favour the downward penetration of the MSB, which strongly affects the atmospheric conditions in the valley. Moreover, a north-easterly land breeze is visible from about 20 UTC on the eastern shore of the Dead Sea in the $REF^{19.11}$ simulation, but not in the $SEN^{19.11}$ simulation (Figure 10b). This situation reflects an interesting case different from the ones generally presented in former investigations in the area (e.g. Alpert et al. 1997 ; and Alpert et al. 2006b) in which due to the recent weakening of the Dead-Sea breeze, mainly because of the drying and shrinking of the Sea, the Mediterranean breeze penetrates stronger and earlier into the Dead-Sea Valley increasing the evaporation because of the strong, hot and dry wind.

Mountain downslope winds develop in both simulations from about 22 UTC. One hour later, strong northerly valley flow in the northern part of the Dead Sea contrasts with the westerly flow in the $SEN^{19.11}$ simulation (Figure 10c). As the valley cools down during night time in the SEN simulation, T2m decreases about 1 K from 20 UTC to 03 UTC in contrast with the 0.1 K decrease of the Dead Sea in the REF simulation, the temperature gradient weakens and the northerly valley flow present in the REF simulation is absent in the SEN simulation. During the night, the synoptic conditions gain more influence than the local wind systems governing the conditions in the valley during day time. South-easterly winds prevail in the valley in both simulations. Much stronger wind velocities are reached in the REF simulation, confirming the sensitivity of large-scale dynamics to near-surface climate change-induced impacts.

The encounter of the north north-westerly and south south-easterly winds over the Dead Sea area in the $REF^{19.11}$ simulation induces the formation of a convergence zone, which intensifies and extends offshore over the next hours and determines the location of convective initiation. Meanwhile, homogeneous south-easterly winds are observed in the SEN simulation (Figure 10d).

The differences in the wind circulations contribute to a different distribution of the atmospheric conditions in the target area, particularly, low-tropospheric water vapour as seen in the vertical cross sections in Figure 11. The evolution of the atmospheric conditions in the 3-h period prior to convective initiation evidences the deeper and wetter boundary layer in the $REF^{19.11}$ simulation at the north-western foothills of the ridge at the Jordanian Highlands. Differences of IWV up to 2 mm, and of instability (CAPE) close to 200 J/kg are found in this area (not shown). This is the location of the convergence line where convective updrafts, which start close to the ground, are triggered reaching a maximum vertical velocity of about 5 m/s above the convergence zone in the $REF^{19.11}$ simulation.

4. Conclusions

The drying and shrinking of the Dead Sea has been extensively investigated in the last decades from different points of view. This process has been related to significant local climate changes which affect the Dead Sea valley and neighboring regions. The climate of the Dead Sea is very hot and dry. But occasionally the Dead Sea basin is affected by severe convection generating heavy precipitation, which could lead to devastating flash floods.

In this study, high-resolution COSMO model simulations are used to assess the impact of the Dead Sea on the occurrence of convective precipitation in the region. A set of high-resolution, ~ 2.8 km, climate simulations covering the period 2003 to 2013, and several numerical weather prediction (NWP) runs on an event time scale (~ 48-36 h) are performed over the Dead Sea area. On a decadal time scale, two simulations are carried out. The first “reference” run with the Dead Sea area, and a second run “sensitivity” in which the Dead Sea is dried out and set to bare soil. The NWP simulations focus on two heavy precipitation events exhibiting relevant differences between the reference and the sensitivity decadal runs. A total of four simulations are performed in this case.

As the energy balance partitioning of the Earth's surface changes due to the drying of the Dead Sea, relevant impacts could be identified in the region. From a climatological point of view, in a future regional climate under ongoing Dead Sea level decline, less evaporation, higher air temperatures and less precipitation is to expect. Reduced evaporation over the Dead Sea occurs from May to October. The cooling effect of evaporation in the neighboring areas results in an increase of T-2m in the absence of the Dead Sea. Atmospheric conditions, such as air temperature and humidity, are mostly affected in the lower-tropospheric levels, which in turn influence atmospheric stability conditions, hence, precipitating convection. ~~The number of dry days is reduced, but i~~In ~~general~~general, the number of dry/wet days is not largely affected by the drying of the Dead Sea, although these differences could be larger for hourly precipitation; rather the structure and intensity of the heavier precipitation events is changed. While a general and homogeneous decrease in evaporation is seen at the SEN^{CLIM} simulation, precipitation deviations occur in both directions, which could suggest and impact on the timing of the events. A relevant year to year variability is observed in evaporation-precipitation which indicates the need of long time series of observations to understand local conditions and to validate model simulations.

The detailed analysis of two heavy precipitation events allowed us to further assess the possible causes and the processes involved regarding the decrease in precipitation intensity or the total omission of convection with respect to the reference simulation in the absence of the Dead Sea water. Two main components, strongly affected by the drying of the Dead Sea, are found to be highly relevant for the understanding of the environmental processes in the Dead Sea region.

(a) First, the lower-atmospheric boundary layer conditions. Changes in the energy balance affect the atmosphere through the heat exchange and moisture supply. The drying of the Dead Sea in the SEN simulations and the resulting decrease in local evaporation, impact the Dead Sea Basin conditions and the neighbouring areas. A reduction in boundary layer humidity and an increase in temperature result in a general decrease of atmospheric instability and weaker updrafts indicating reduced deep-convective activity. Main differences on the atmospheric conditions are directly over the Dead Sea, but these conditions are frequently advected to neighbouring areas by the thermally driven wind systems in the region which play a key role for the redistribution of these conditions and the initiation of convection.

(b) Secondly, wind systems in the valley. In the arid region of the Dead Sea Basin with varied topography, thermally and dynamically driven wind systems are key features of the local climate. Three different scales of climatic phenomena coexist: The Mediterranean Sea Breeze (MSB), the Dead Sea breeze and the orographic winds, valley-, and slope-winds, which are known to temper the climate in the Dead Sea valley (Shafir and Alpert, 2011). The drying of the Dead Sea in the SEN simulation disturbs the Dead Sea thermally driven wind circulations. The Dead Sea breezes are missing, weaker wind speeds characterize the region and along valley winds are consequently affected. Furthermore, the dynamics of the Mediterranean breeze penetration into the Jordan Valley are affected.

Consequently, the impacts on convection initiation and development are twofold:
(i) Distinct redistribution of atmospheric conditions, locally or remotely, which yields to different atmospheric conditions that in the absence of the Dead Sea result in a reduced moisture availability in the lower atmospheric levels and increased stability hindering convection or reducing the intensity of the events.
(ii) Modification of the divergence/convergence field. The absence of the Dead Sea substantially modifies the wind circulation systems over the Dead Sea valley, which leads to the omission of convergence lines which act as triggering mechanism for convection.

We can conclude that in general the lack of sufficient low-atmospheric moisture in relation to the drying of the Dead Sea, the increase of atmospheric stability in addition to an absence or reduction in the intensity of the convergence zones, works against initiation or intensification of precipitating convection in the area. The relevance of the small-scale variability of moisture and the correct definition and location of convergence lines for an accurate representation of convective initiation illustrates the limitation and the lack of adequate observational networks in the area and the need for high-resolution model simulations of boundary layer processes to predict intense and localised convection in the region.

These results contribute to gain a better understanding of expected conditions in the Dead Sea valley and neighbouring areas under continual lake level decline. Energy balance partitioning and wind circulation systems are determinant for local climatic conditions, e.g. temperature and humidity fields as well as aerosol redistribution, therefore, any change should be well understood and properly represented in model simulations of the region. Our results point out, in agreement with past modelling activities in the region, the need to further improve the representation of precipitation fields in the area, particularly close to the Mediterranean coastline. More accurate

Mediterranean SST input fields have been suggested as relevant to reduce the model inaccuracies. Furthermore, a more realistic representation of the lake shape, water salinity and temperature, as well as Dead Sea abundance must be addressed to accurately describe the impact on the simulation results.

In a further step, the authors will ~~assess~~investigate some of these issues peforming sensitivity experiments, and will assess the impact of model grid resolution on the horizontal and vertical flow field in the region across scales, including the impact on large-scale dynamics. We will also put emphasis in trying to better understand the dynamics of the MSB under lake level decline using high-resolution modelling, especially the contrasting behaviour pointed out in this study. Fine resolution simulations up to 100 m will be performed for this purpose. Furthermore, we will provide a verification of the complex chain of processes in the area using unique measurements in the framework of the interdisciplinary virtual institute Dead Sea Research VEnue (DESERVE; Kottmeier et al., 2016).

Con formato: Sangría: Izquierda: 0 cm, Sangría francesa: 1,27 cm

Author contribution

SK wrote the manuscript, analysed the data, interpreted the results and supervised the work. JH carried out data analysis, interpretation of results and prepared all the figures.

Acknowledgements

The first author’s research was supported by the Bundesministerium für Bildung und Forschung (BMBF; German Federal Ministry of Education and Research). The authors acknowledge the colleagues at the Karlsruhe Institute of Technology (KIT) involved in the interdisciplinary virtual institute Dead Sea Research VEnue (DESERVE) for their support and interesting discussions. We acknowledge Sebastian Helgert and Alberto Caldas Alvarez for their assistance in the preparation of the simulations. This article is a contribution to the HyMeX program.

References

Alpert, P., and Shay-EL, Y.,: The Moisture Source for the Winter Cyclones in the Eastern Mediterranean. Israel Meteorological Research Papers, 5, 20-27, 1994.

Alpert, P., and Coauthors: Relations between climate variability in the Mediterranean region and the tropics: ENSO, South Asian and African monsoons, hurricanes and Saharan dust. Developments in Earth and Environmental Sciences, 4, 149-177, https://doi.org/10.1016/S1571-9197(06)80005-4, 2006.

Alpert, P., Shafir, H., and Issahary, D.,: Recent Changes in the Climate At the Dead Sea – a Preliminary Study. Climatic Change, 37(3), 513-537, https://doi.org/10.1023/A:1005330908974, 1997.

Andersson, T., Andersson, M., Jacobsson, C., Nilsson, S.: Thermodynamic indices for forecasting thunderstorms in southern Sweden. Meteorol. Mag. 116, 141-146, 1989.

Arkin, Y., and Gilat, A.: Dead Sea sinkholes - an ever-developing hazard. Environmental Geology, 39(7), 711-722, https://doi.org/10.1007/s002540050485, 2000.

Ashbel, D., and Brooks, C.: The influence of the dead sea on the climate of its neighbourhood. Quarterly Journal of the Royal Meteorological Society, 65(280), 185-194, https://doi.org/10.1002/qj.49706528005, 1939.

Ban, N., Schmidli, J., and Schär, C.: Evaluation of the convection-resolving regional climate modeling approach in decade-long simulations, J. Geophys.

Res. Atmos., 119, 7889– 7907, https://doi.org/10.1002/2014JD021478, 2014.

Belachsen, I., Marra, F., Peleg, N., and Morin, E.: Convective rainfall in dry climate: relations with synoptic systems and flash-flood generation in the Dead Sea region. Hydrology and Earth System Sciences Discussions, 21, 5165-5180, https://doi.org/10.5194/hess-21-5165-2017, 2017.

Böhm, U., and Coauthors: The Climate Version of LM: Brief Description and Long-Term Applications. COSMO Newsletter, 6, 225-235, 2006.

Businger, J., Wyngaard, J., Izumi, Y., and Bradley, E.: Flux-Profile Relationships in the Atmospheric Surface Layer. Journal of the Atmospheric Sciences, 28(2), 181-189, https://doi.org/10.1175/1520-0469(1971)028<0181:FPRITA>2.0.CO;2, 1971.

Byun, H., and Kim, D.: Comparing the Effective Drought Index and the Standardized Precipitation Index. Options Méditerranéennes. Séries A. Mediterranean Seminars, 95, 85-89, 2010.

Byun, H., and Wilhite, D.: Objective quantification of drought severity and duration. J. Climate, 12(9), 2747-2756, https://doi.org/10.1175/1520-0442(1999)012<2747:OQODSA>2.0.CO;2, 1999.

Cohen, S., and Stanhill, G.: Contemporary Climate Change in the Jordan Valley. J. Appl. Meteor., 35(7), 1051-1058, https://doi.org/10.1175/1520-0450(1996)035<1051:CCCITJ>2.0.CO;2, 1996.

Corsmeier, U., Behrendt, R., Drobinski, P., Kottmeier, C.: The mistral and its effect on air pollution transport and vertical mixing, Atmos. Res., 74, 275–302, https://doi.org/https://doi.org/10.1016/j.atmosres.2004.04.010, 2005.

Dayan, U., and Morin, E.: Flash flood – producing rainstorms over the Dead Sea: A review. Geological Society of America, 401(4), 53-62, https://doi.org/10.1130/2006.2401(04) , 2006.

Dayan, U., and Sharon, D.: Meteorological parameters for discriminating between widespread and spotty storms in the Negev. Israel Journal of Earth Sciences, 29(4), 253-256, 1980.

Dayan, U., Ziv, B., Margalit, A., Morin, E., and Sharon, D.: A severe autumn storm over the middle-east: synoptic and mesoscale convection analysis. Theoretical and

Código de campo cambiado

Applied Climatology, 69(1-2), 103-122, https://doi.org/10.1007/s007040170038, 2001.

Doms, G., and Baldauf, M.: A Description of the Nonhydrostatic Regional COSMO-Model. Part I: Dynamics and Numerics. Deutscher Wetterdienst, 2015.

~~Doms, G., and Coauthors: A Description of the Nonhydrostatic Regional COSMO Model Part II : Physical Parameterization. Deutscher Wetterdienst, 2011.~~

Doswell, C., and Rasmussen, E.: The Effect of Neglecting the Virtual Temperature Correction on CAPE Calculations. Weather and Forecasting, 9(4), 625-629, https://doi.org/10.1175/1520-0434(1994)009<0625:TEONTV>2.0.CO;2, 1994.

FAO/IIASA/ISRIC/ISSCAS/JRC.: Harmonized World Soil Database (version 1.2). FAO, Rome, Italy and IIASA, Laxenburg, Austria, (accessed 01.02.2017) , 2009.

Fosser, G., Khodayar, S., and Berg, P., 2014: Benefit of convection permitting climate model simulations in the representation of convective precipitation, Clim. Dyn., 44(1– 2), 45– 60.

Gavrieli, I., Bein, A., and Oren, A., 2005: The expected impact of the “Peace Conduit” project (the Red Sea - Dead Sea pipeline) on the Dead Sea. Mitigation and Adaptation Strategies for Global Change, 10(4), 759-777, https://doi.org/10.1007/s11027-005-5144-z.

European Commission, Joint Research Centre, 2003: Global Land Cover 2000 database, (accessed 01.02.2017).

GLOBE National Geophysical Data Center, 1999: Global Land One-kilometer Base Elevation (GLOBE) v.1. Hastings, D. and P.K. Dunbar. National Geophysical Data Center, NOAA, (accessed 01.02.2017).

Greenbaum, N., Ben-Zvi, A., Haviv, I., and Enzel, Y., 2006: The hydrology and paleohydrology of the Dead Sea tributaries. Geological Society of America, 401(4), 63-93, https://doi.org/10.1130/2006.2401(05).

Haylock, M.R., Hofstra, N., Klein Tank, A.M.G., Klok, E.J., Jones, P.D. and New, M. (2008) A European daily high-resolution gridded dataset of surface temperature and precipitation. Journal of Geophysical Research: Atmospheres, 113, D20119. https://doi.org/10.1029/2008JD10201.

Con formato: Fuente: (Predeterminado) Arial, 11 pto, Alemán (Alemania)

Con formato: Normal, Sangría: Izquierda: 0 cm, Primera línea: 0 cm, No ajustar espacio entre texto latino y asiático, No ajustar espacio entre texto asiático y números

Con formato: Fuente: (Predeterminado) Arial, 11 pto, Inglés (Reino Unido)

Con formato: Fuente: (Predeterminado) Arial, 11 pto, Inglés (Reino Unido)

Con formato: Fuente: (Predeterminado) Arial, 11 pto, Inglés (Reino Unido)

Con formato: Alemán (Alemania)

Con formato: Default, Sangría: Izquierda: 0 cm, Primera línea: 0 cm

Hochman, A., Mercogliano, P., Alpert, P., Saaroni, H. and Bucchignani, E., 2018. High-resolution projection of climate change and extremity over Israel using COSMO-CLM. International Journal of Climatology, 38(14), pp.5095-5106.

Houze, R., 2012: Orographic effects on precipitating clouds. Reviews of Geophysics, 50(1), https://doi.org/10.1029/2011RG000365.

Kalthoff, N., Horlacher, V., Corsmeier, U., Volz-Thomas, A., Kolahgar, B., Geiß, H., Möllmann-Coers, M., and Knaps, A. 2000: Influence of valley winds on transport and dispersion of airborne pollutants in the Freiburg-Schauinsland area, J. Geophys. Res. Atmos, 105, 1585–1597, https://doi.org/10.1029/1999jd900999.

Khodayar, S., Kalthoff, N., and Schaedler, G., 2013: The impact of soil moisture variability on seasonal convective precipitation simulations. Part I: validation, feedbacks, and realistic initialisation. Meteorologische Zeitschrift, 22(4), 489-505, https://doi.org/10.1127/0941-2948/2013/0403.

Kunin, P., Alpert, P. and Rostkier-Edelstein, D., 2019. Investigation of sea-breeze/foehn in the Dead Sea valley employing high resolution WRF and observations. Atmospheric Research.

Lensky, N. and Dente, E., 2015. The hydrological proecesses driving the accelerated Dead Sea level decline in the past decades. Geological Survey of Israel Report.

Llasat, M., and Coauthors, 2010: High-impact floods and flash floods in Mediterranean countries: the FLASH preliminary database. Advances in Geosciences, 23, 47-55, https://doi.org/10.5194/adgeo-23-47-2010.

Metzger, J., Nied, M., Corsmeier, U., Kleffmann, J., and Kottmeier, C., 2017: Dead Sea evaporation by eddy covariance measurements versus aerodynamic, energy budget, Priestley-Taylor, and Penman estimates. Hydrology and Earth System Sciences Discussions, 22(2), 1135-1155, https://doi.org/10.5194/hess-2017-187.

Miglietta MM, Conte D, Mannarini G, Lacorata G, Rotunno R. 2011. Numerical analysis of a Mediterranean 'hurricane' over south-eastern Italy: sensitivity experiments to sea surface temperature. *Atmos. Res.* **101**: 412–426.

Con formato: Fuente: 11 pto, Sin Cursiva

Con formato: Inglés (Reino Unido), Revisar la ortografía y la gramática

Con formato: Sangría: Izquierda: 0 cm, Primera línea: 0 cm

Con formato: Fuente: Sin Cursiva

Con formato: Fuente: 11 pto, Sin Cursiva

Con formato: Default, Sangría: Izquierda: 0 cm, Primera línea: 0 cm

Con formato: Fuente: Sin Cursiva

Con formato: Fuente: Cursiva, Inglés (Reino Unido), Revisar la ortografía y la gramática

Con formato: Fuente: (Predeterminado) Arial, 11 pto, Inglés (Reino Unido)

Con formato: Normal, Sangría: Izquierda: 0 cm, Primera línea: 0 cm, No ajustar espacio entre texto latino y asiático, No ajustar espacio entre texto asiático y números

Con formato: Fuente: (Predeterminado) Arial, 11 pto, Inglés (Reino Unido)

Con formato: Fuente: (Predeterminado) Arial, 11 pto, Inglés (Reino Unido)

Con formato: Fuente: (Predeterminado) Arial, 11 pto, Inglés (Reino Unido)

Con formato: Color de fuente: Color personalizado(RGB(35;31;32)), Revisar la ortografía y la gramática

Moncrieff, M., and Miller, M., 1976: The dynamics and simulation of tropical cumulonimbus and squall lines. Quarterly Journal of the Royal Meteorological Society, 102(432), 373-394, https://doi.org/10.1002/qj.49710243208, 2014.

Naor, R., Potchter, O., Shafir, H., and Alpert, P.: An observational study of the summer Mediterranean Sea breeze front penetration into the complex topography of the Jordan Rift Valley, Theor. Appl. Climatol., 127, 275–284, https://doi.org/10.1007/s00704-015-1635-3, 2017.

Prein, A., Gobiet, A., Suklitsch, M., Truhetz, H., Awan, N., Keuler, K., and Georgievski, G. : Added value of convection permitting seasonal simulations, Clim. Dyn., 41(9– 10), 2655– 2677, 2013.

Ritter, B., and J.-F. Geleyn, 1992. A comprehensive radiation scheme for numerical weather prediction models with potential applications in climate simulations. Mon. Wea. Rev., 120, 303–325.

Rostkier-Edelstein, D., Liu, Y., Wu, W., Kunin, P., Givati, A. and Ge, M., 2014. Towards a high-resolution climatography of seasonal precipitation over Israel. International Journal of Climatology, 34(6), pp.1964-1979.

Schaedler, G., and Sasse, R.: Analysis of the connection between precipitation and synoptic scale processes in the Eastern Mediterranean using self-organizing maps. Meteorologische Zeitschrift, 15(3), 273-278, https://doi.org/10.1127/0941-2948/2006/0105, 2006.

Shafir, H., and Alpert, P.: Regional and local climatic effects on the Dead-Sea evaporation. Climatic Change, 105(3-4), 455-468, https://doi.org/10.1007/s10584-010-9892-8, 2011.

Sharon, D., and Kutiel, H.: The distribution of rainfall intensity in Israel, its regional and seasonal variations and its climatological evaluation. International Journal of Climatology, 6(3), 277-291, https://doi.org/10.1002/joc.3370060304, 1986.

Smiatek, G., Kunstmann, H., and Heckl, A.: High-resolution climate change simulations for the Jordan River area. Journal of Geophysical Research, 116(D16), https://doi.org/10.1029/2010JD015313, 2011.

Con formato: Fuente: Sin Cursiva

Con formato: Interlineado: 1,5 líneas

Con formato: Fuente: Sin Cursiva

Con formato: Inglés (Reino Unido)

Con formato: Fuente: Sin Cursiva

Con formato: Sangría: Izquierda: 0 cm, Primera línea: 0 cm

Stanhill, G.: Changes in the rate of evaporation from the dead sea. International Journal of Climatology, 14(4), 465-471, https://doi.org/10.1002/joc.3370140409,1994.

Vicente-Serrano, S., Beguería, S., López-Moreno, J.: A Multiscalar Drought Index Sensitive to Global Warming: The Standardized Precipitation Evapotranspiration Index. J. Climate, 23(7), 1696-1718, https://doi.org/10.1175/2009JCLI2909.1, 2010.

Vüllers, J., Mayr, G. J., Corsmeier, U., and Kottmeier, C.: Characteristics and evolution of diurnal foehn events in the Dead Sea valley. Atmos. Chem. Phys., 18, 18169-18186, https://doi.org/10.5194/acp-18-18169-2018, 20, 2018.

Wernli H, Paulat M, Hagen M, Frei C. SAL – a novel quality measure for the verification of quantitative precipitation forecasts. Mon. Weather Rev. 136: 4470–4487, 2008.

Yatagai, A., Alpert, P. and Xie, P. (2008) Development of a daily gridded precipitation data set for the Middle East. Advances in Geosciences, 12, 1–6.

Yatagai, A., Kamiguchi, K., Arakawa, O., Hamada, A., Yasutomi, N. and Kitoh, A., 2012: APHRODITE: constructing a long-term daily gridded precipitation dataset for Asia based on a dense network of rain gauges. Bulletin of the American Meteorological Society, 93, 1401–1415.

Tables

	PREC diffmn	REF PMX	SEN PMX	PREC relative diff [%]	Synoptic Situation	REF CAPEmx	SEN CAPEmx	REF KOmn	SEN KOmn	Localis Widesp (Subar...

Con formato: Fuente: 11 pto, Inglés (Reino Unido)
Con formato: Justificado, Interlineado: 1,5 líneas
Con formato: Fuente: 11 pto, Inglés (Reino Unido)
Con formato: Espacio Después: 0 pto, No ajustar espacio entre texto latino y asiático, No ajustar espacio entre texto asiático y números
Con formato: Fuente: 11 pto, Inglés (Reino Unido)
Con formato: Fuente: (Predeterminado) Arial, 11 pto, Inglés (Reino Unido)
Con formato: Justificado, Interlineado: 1,5 líneas
Con formato: Fuente: (Predeterminado) Arial, 11 pto
Con formato: Fuente: (Predeterminado) Arial, 11 pto, Inglés (Reino Unido)
Con formato: Espacio Después: 0 pto, No ajustar espacio entre texto latino y asiático, No ajustar espacio entre texto asiático y números
Con formato: Inglés (Reino Unido)
Con formato: Fuente: (Predeterminado) Arial, 11 pto, Inglés (Reino Unido)
Con formato: Fuente: (Predeterminado) Arial, 11 pto, Inglés (Reino Unido)
Con formato: Fuente: (Predeterminado) Arial, 11 pto, Inglés (Reino Unido)
Con formato: Sangría: Izquierda: 0 cm, Sangría francesa: 1,27 cm
Tabla con formato
Con formato: Fuente: 9 pto
Con formato: Fuente: 9 pto

										affected)
089.12.2004	-0,10	30,09	31,31	2,76	ARST	1	1	4,85	4,85	W (A1, A2)
134.01.2006	-0,11	45,64	54,64	-4,26	Cyprus Low	239	225	6,57	6,54	L/W (A1, A3)
167.04.2006	-0,11	57,41	56,09	4,89	Syrian Low	43	47	1,97	1,94	L (A1, A4)
101.04.2007	-0,29	42,61	70,20	30,78	Cyprus Low	686	679	-4,77	-4,70	L (A2, A4)
134.04.2007	-0,12	134,36	127,79	1,62	Cyprus Low	573	576	-1,95	-1,92	L (A1, A2, A3, A4)
123.05.2007	-0,16	41,82	47,90	-8,24	Syrian Low	436	81	-5,30	-5,29	L (A1, A2)
278.01.2008	-0,14	23,11	17,24	-17,25	Syrian Low	7	7	5,12	5,12	W (A1, A3)
256.10.2008	-0,23	139,01	125,73	-16,52	ARST	1274	1361	-5,50	-4,08	L (A3)
134.11.2008	-0,30	40,83	45,55	25,68	ARST	25	7	1,37	1,38	L (A2, A4)
145.05.2009	-0,39	59,28	68,84	-8,49	Syrian Low	433	429	-3,90	-3,91	L (A1, A2, A3, A4)
156.05.2009	-0,20	49,23	42,28	13,50	Syrian Low	208	203	-2,30	-2,36	L (A1, A2, A3)
3101.101.2009	-0,19	166,21	111,79	-7,65	Cyprus Low	435	445	-5,03	-4,46	L (A1, A2)
156.01.2011	-0,11	73,02	72,03	3,74	Syrian Low	49	37	7,82	7,83	L/W (A1, A4)
289.05.2011	-0,24	44,51	32,73	-14,33	Cyprus Low	158	170	-10,27	-10,26	W (A2)
156.11.2011	-0,11	42,65	9,34	-65,90	Cyprus Low	2	0	-7,14	-7,12	L (A1, A2)
178.11.2011	-0,11	90,07	93,04	4,76	Cyprus Low	386	304	-9,14	-9,16	L (A1)
189.11.2011	-0,11	28,68	34,69	-8,67	Cyprus Low	356	378	-8,61	-8,65	L (A1)
1920.11.2011	-0,03	58,11	12,36	4,09	Cyprus Low	133	81	-7,60	-7,46	L (A2, A4)
223.10.2012	-0,20	29,88	41,64	51,21	ARST	2068	2097	-5,83	-5,59	L (A1, A2)
1009.11.2012	-0,11	27,20	22,56	-18,29	Cyprus Low	218	215	3,97	3,98	W (A1)
234.11.2012	-0,21	155,77	117,81	-10,17	ARST	189	286	-2,18	-1,95	L (A1, A2, A3)
256.11.2012	-0,11	41,48	54,33	-7,87	ARST	354	332	4,19	4,37	L (A3, A4)

Table 1: Classification of heavy precipitation cases in the decadal simulation covering the period 2004 to 2013. The areal-mean (study area, Figure 1) difference ($PREC_{diffmn}$) and maximum grid precipitation in the reference (REF_{PMX}) and sensitivity (SEN_{PMX}) realizations, the synoptic situation, and the stability conditions illustrated by maximum grid point CAPE (CAPEmx) and minimum grid point KO-index (KOmn) are summarized. Additionally, the nature of the precipitation, localized (L) or widespread (W) and the main subarea affected (following division in Figure 1; A1, A2, A3, A4) are listed.

Figures

(a)

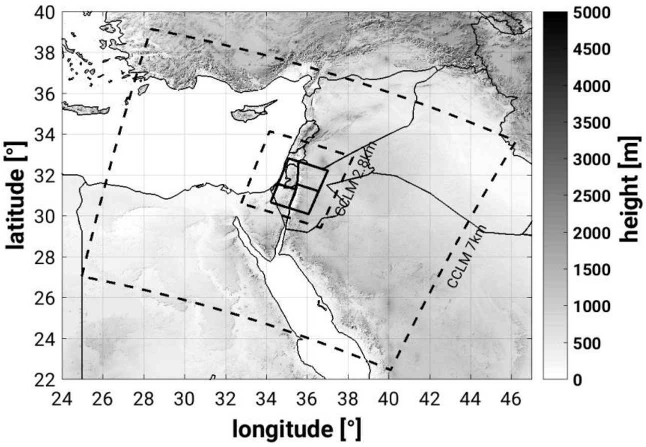
latitude [°]
longitude [°]
height [m]
CCLM 7km
CCLM 2.8km
0
500
1000
1500
2000
2500
3000
3500
4000
4500
5000

(b)

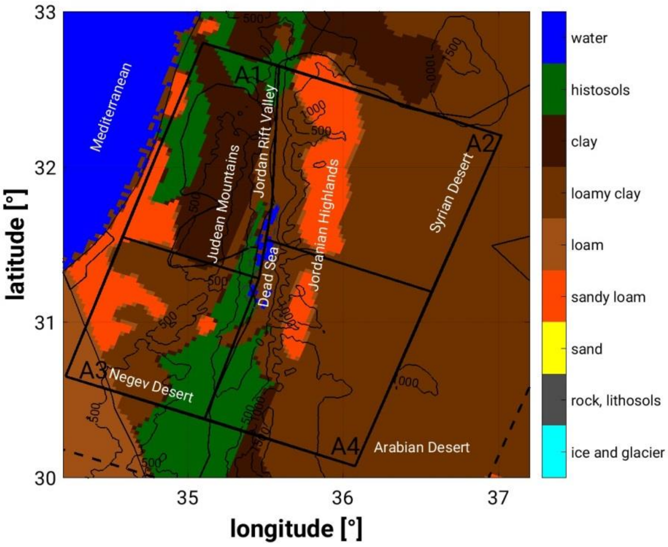
latitude [°]
longitude [°]
Mediterranean
Judean Mountains
Jordan Rift Valley
Jordanian Highlands
Syrian Desert
Dead Sea
Negev Desert
Arabian Desert
A1
A2
A3
A4
water
histosols
clay
loamy clay
loam
sandy loam
sand
rock, lithosols
ice and glacier

Figure 1: (a) Topography (m above msl), simulation domains (dashed lines, CCLM7km and CCLM2.8km) and study area (bold line). (b) Model soil types (colour scale), topography (black isolines) and study area (black bold line) including the 4 subdomains to be examined, A1-4 (Area 1-4).

(a)

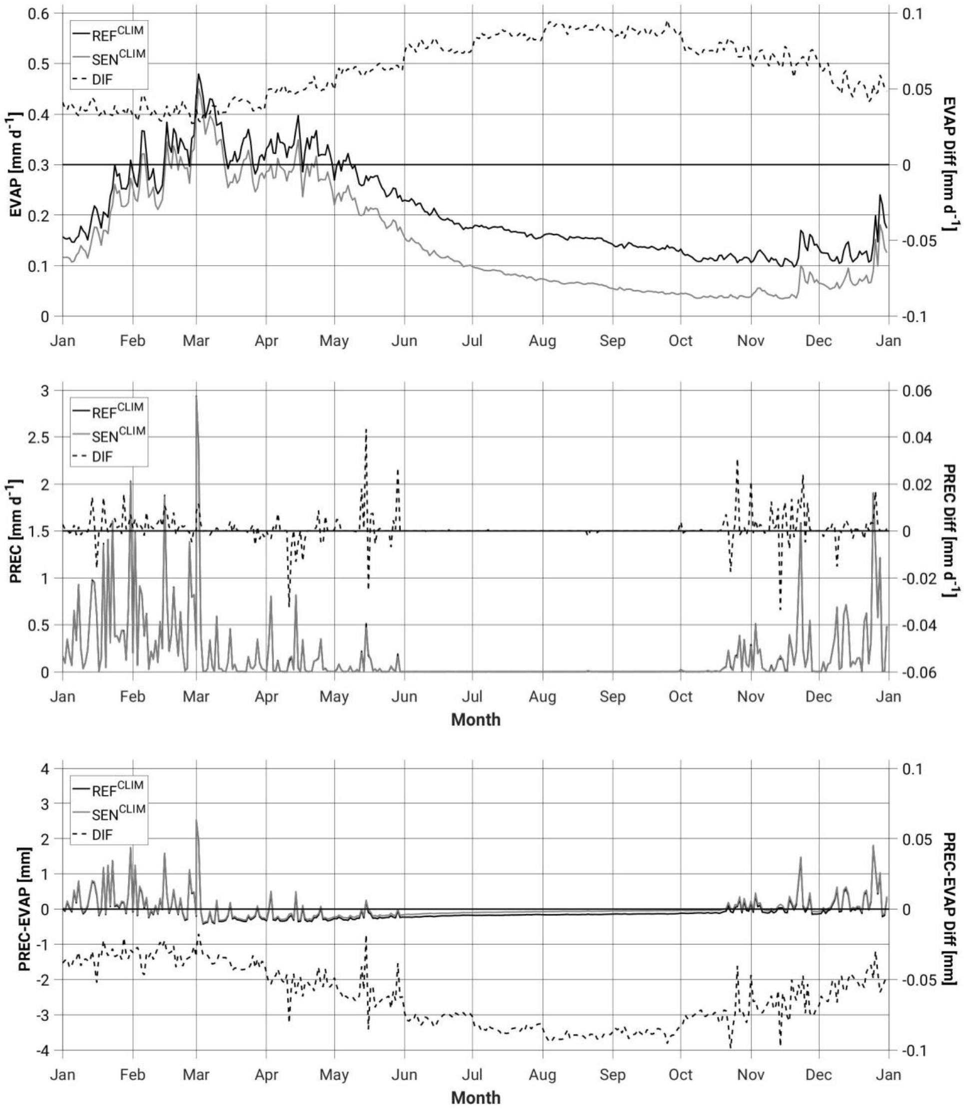

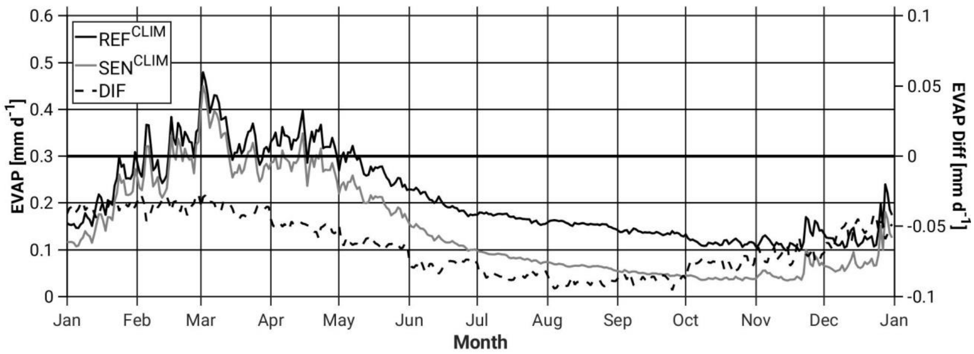
REF^CLIM
SEN^CLIM
-DIF
EVAP [mm d-1]
EVAP Diff [mm d-1]
Month
Jan Feb Mar Apr May Jun Jul Aug Sep Oct Nov Dec Jan
0 0.1 0.2 0.3 0.4 0.5 0.6
-0.1 -0.05 0 0.05 0.1

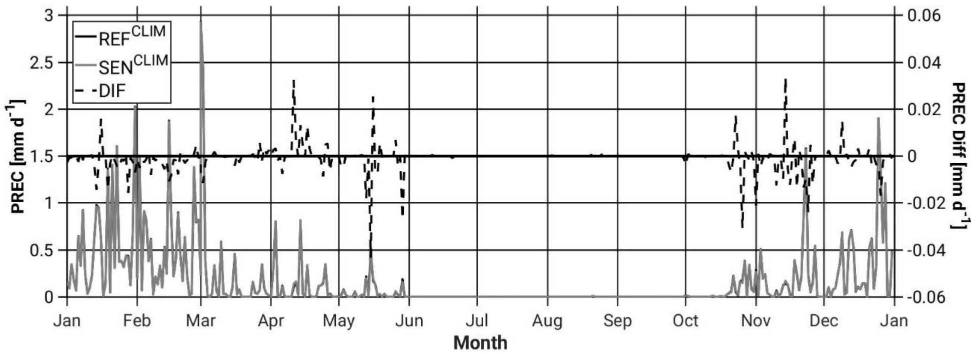
REF^CLIM
SEN^CLIM
-DIF
PREC [mm d-1]
PREC Diff [mm d-1]
Month
Jan Feb Mar Apr May Jun Jul Aug Sep Oct Nov Dec Jan
0 0.5 1 1.5 2 2.5 3
-0.06 -0.04 -0.02 0 0.02 0.04 0.06

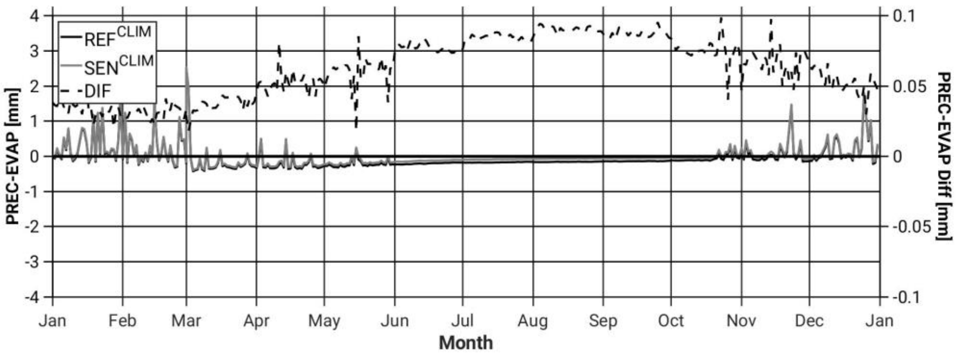
REF^CLIM
SEN^CLIM
DIF
PREC-EVAP [mm]
PREC-EVAP Diff [mm]
Month
Jan
Feb
Mar
Apr
May
Jun
Jul
Aug
Sep
Oct
Nov
Dec
Jan

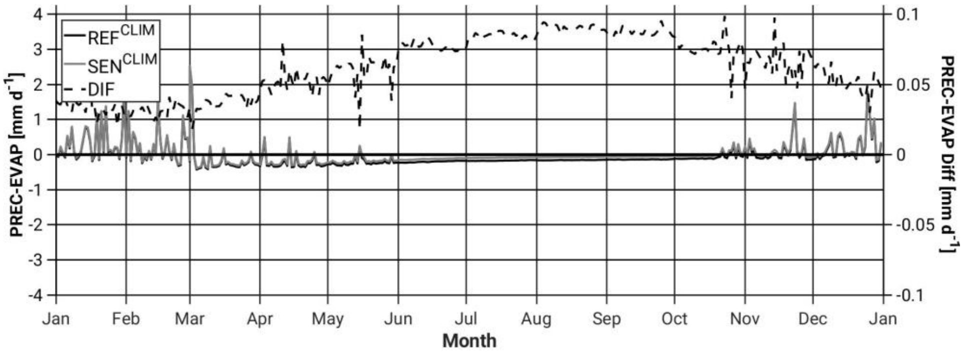
REF^CLIM
SEN^CLIM
DIF
PREC-EVAP [mm d^-1]
PREC-EVAP Diff [mm d^-1]
Month
Jan
Feb
Mar
Apr
May
Jun
Jul
Aug
Sep
Oct
Nov
Dec
Jan

(b)

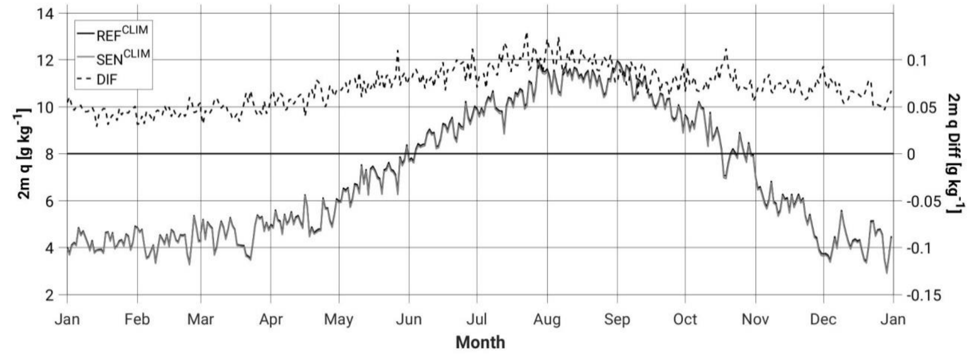
REF^CLIM
SEN^CLIM
DIF
2m q [g kg-1]
2m q Diff [g kg-1]
Month
Jan Feb Mar Apr May Jun Jul Aug Sep Oct Nov Dec Jan

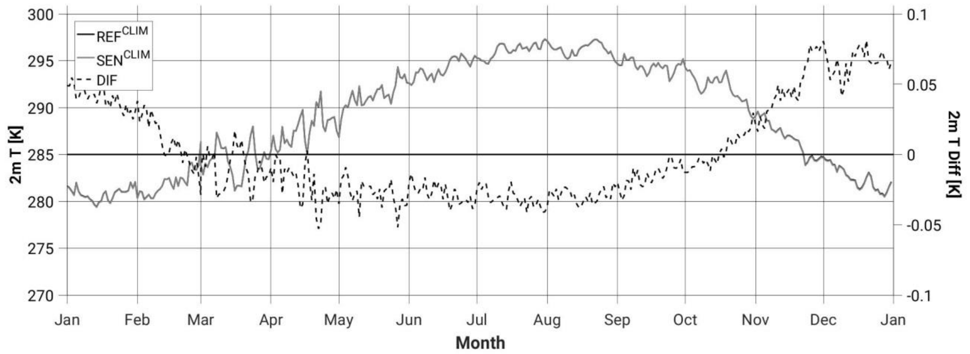
REF^CLIM
SEN^CLIM
DIF
2m T [K]
2m T Diff [K]
Month
Jan Feb Mar Apr May Jun Jul Aug Sep Oct Nov Dec Jan

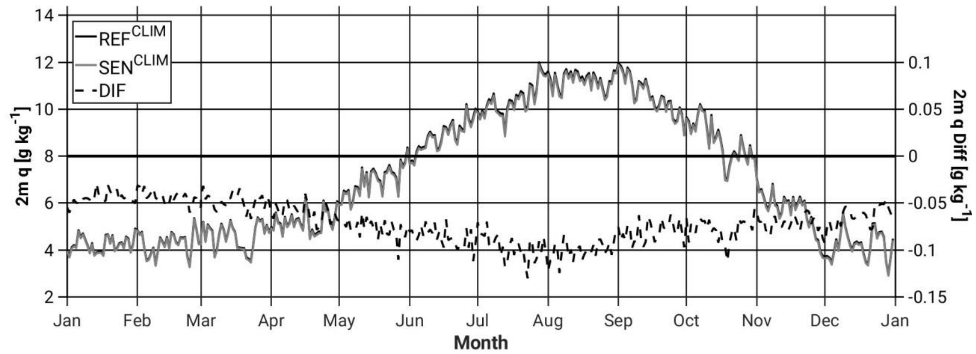
REF^CLIM
SEN^CLIM
DIF
2m q [g kg-1]
2m q Diff [g kg-1]
Month
Jan Feb Mar Apr May Jun Jul Aug Sep Oct Nov Dec Jan

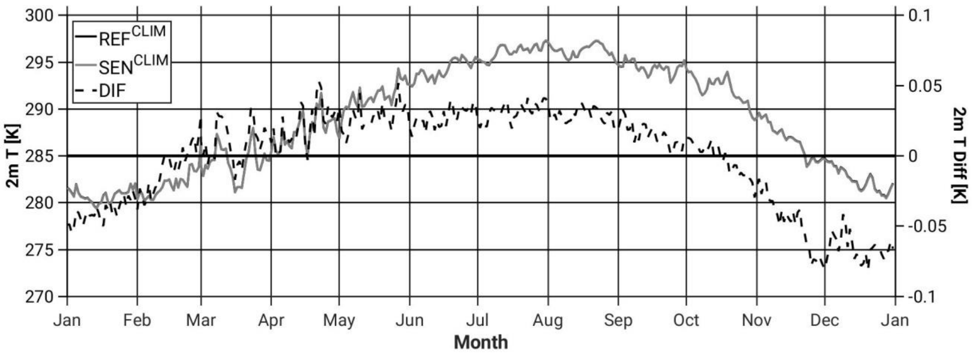
REF^CLIM
SEN^CLIM
DIF
2m T [K]
2m T Diff [K]
Month
Jan Feb Mar Apr May Jun Jul Aug Sep Oct Nov Dec Jan

(c)

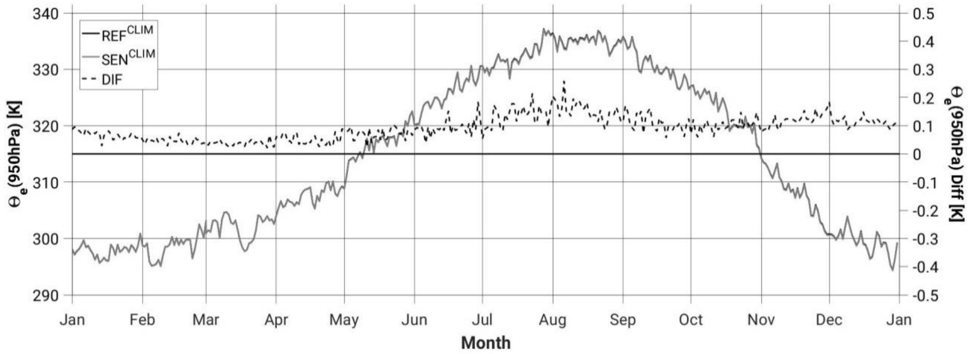
REF^CLIM
SEN^CLIM
DIF
Θe(950hPa) [K]
Θe(950hPa) Diff [K]
Jan Feb Mar Apr May Jun Jul Aug Sep Oct Nov Dec Jan
Month

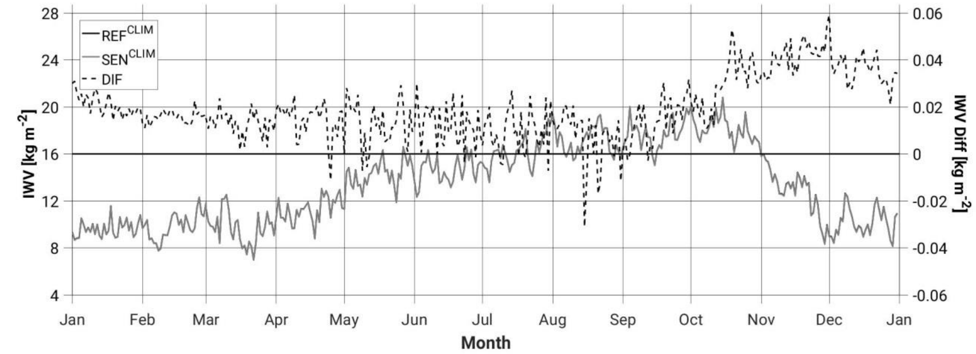
REF^CLIM
SEN^CLIM
DIF
IWV [kg m-2]
IWV Diff [kg m-2]
Jan Feb Mar Apr May Jun Jul Aug Sep Oct Nov Dec Jan
Month

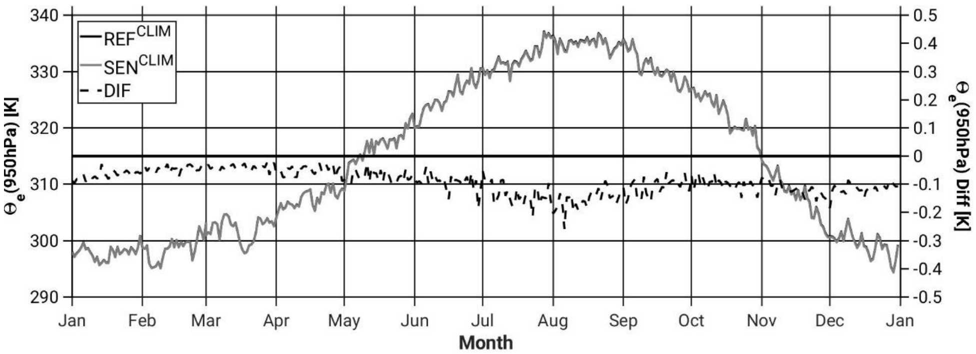
REF^CLIM
SEN^CLIM
-DIF
Θe(950hPa) [K]
Θe(950hPa) Diff [K]
Jan Feb Mar Apr May Jun Jul Aug Sep Oct Nov Dec Jan
Month

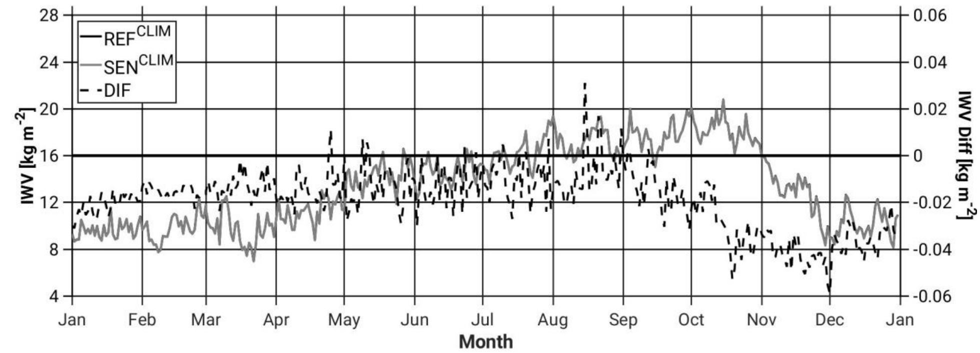
REF^CLIM
SEN^CLIM
-DIF
IWV [kg m-2]
IWV Diff [kg m-2]
Jan Feb Mar Apr May Jun Jul Aug Sep Oct Nov Dec Jan
Month

(d)

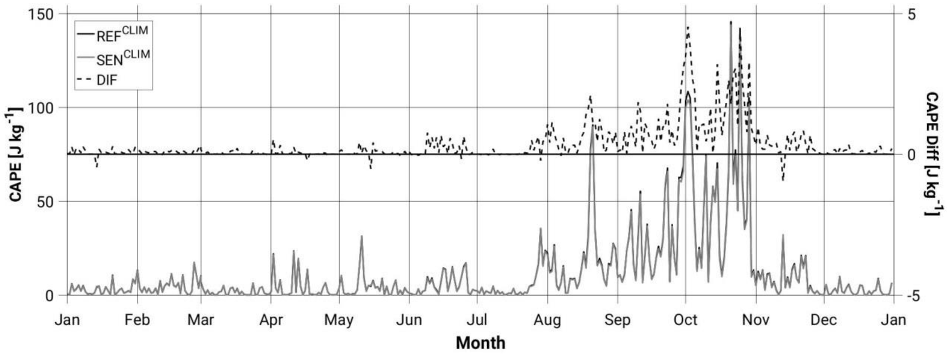
REF^CLIM
SEN^CLIM
DIF
CAPE [J kg^-1]
CAPE Diff [J kg^-1]
Month
Jan Feb Mar Apr May Jun Jul Aug Sep Oct Nov Dec Jan

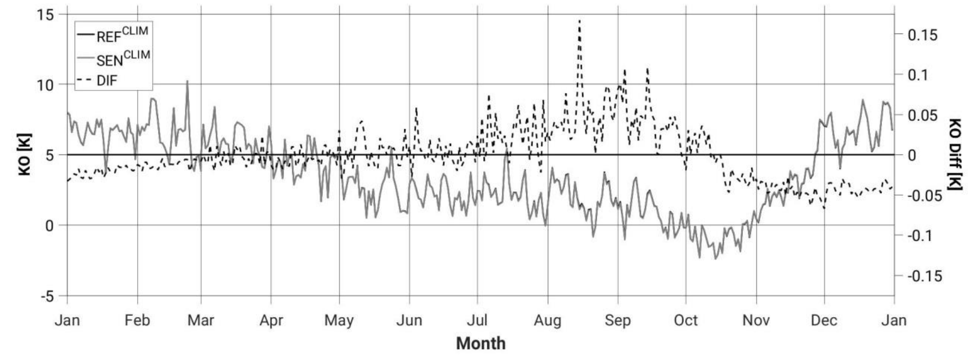
REF^CLIM
SEN^CLIM
DIF
KO [K]
KO Diff [K]
Month
Jan Feb Mar Apr May Jun Jul Aug Sep Oct Nov Dec Jan

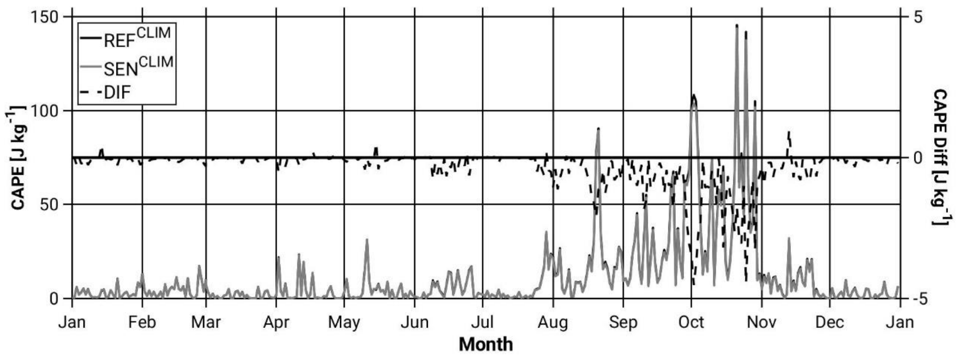
REF^CLIM
SEN^CLIM
DIF
CAPE [J kg^-1]
CAPE Diff [J kg^-1]
Month
Jan Feb Mar Apr May Jun Jul Aug Sep Oct Nov Dec Jan

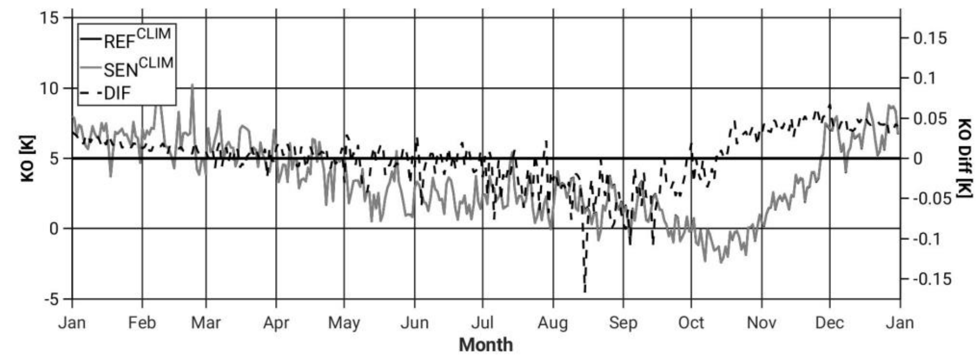
REF^CLIM
SEN^CLIM
DIF
KO [K]
KO Diff [K]
Month
Jan Feb Mar Apr May Jun Jul Aug Sep Oct Nov Dec Jan

Figure 2: Annual cycle of the areal-daily averaged (and differences (black dashed line; SEN-REF)) of (a) evaporation, precipitation, and precipitation minus evaporation (b) specific humidity and temperature at 2-m, and (c) Θ_e below 950 hPa and IWV, and (d) CAPE and KO-index, from the REF^{CLIM} (full black line) and the SEN^{CLIM} (full grey line) simulations. All grid points in the ~~investigation domain~~study area (Figure 1) and the period 2004 to 2013 are considered.

(a)

Area1 (NW) Area2 (NE)

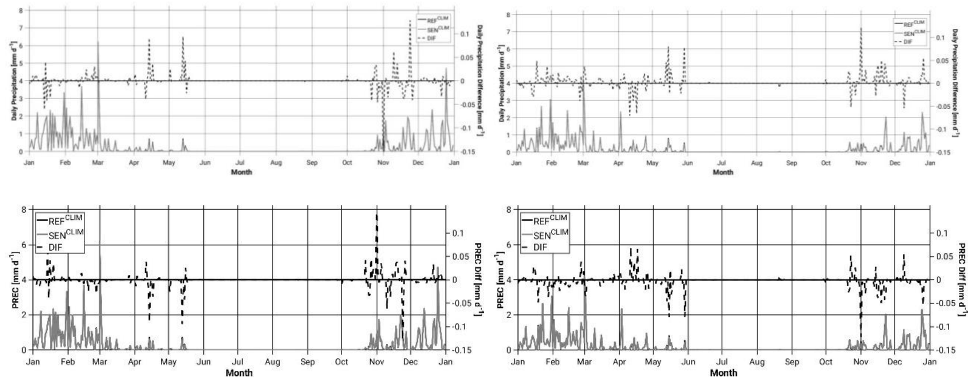

Area3 (SW) Area4 (SE)

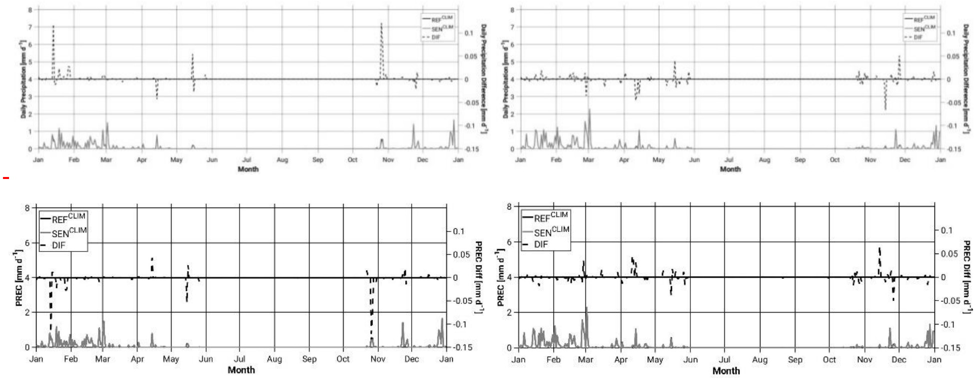

(b)

Area1 (NW) Area2 (NE)

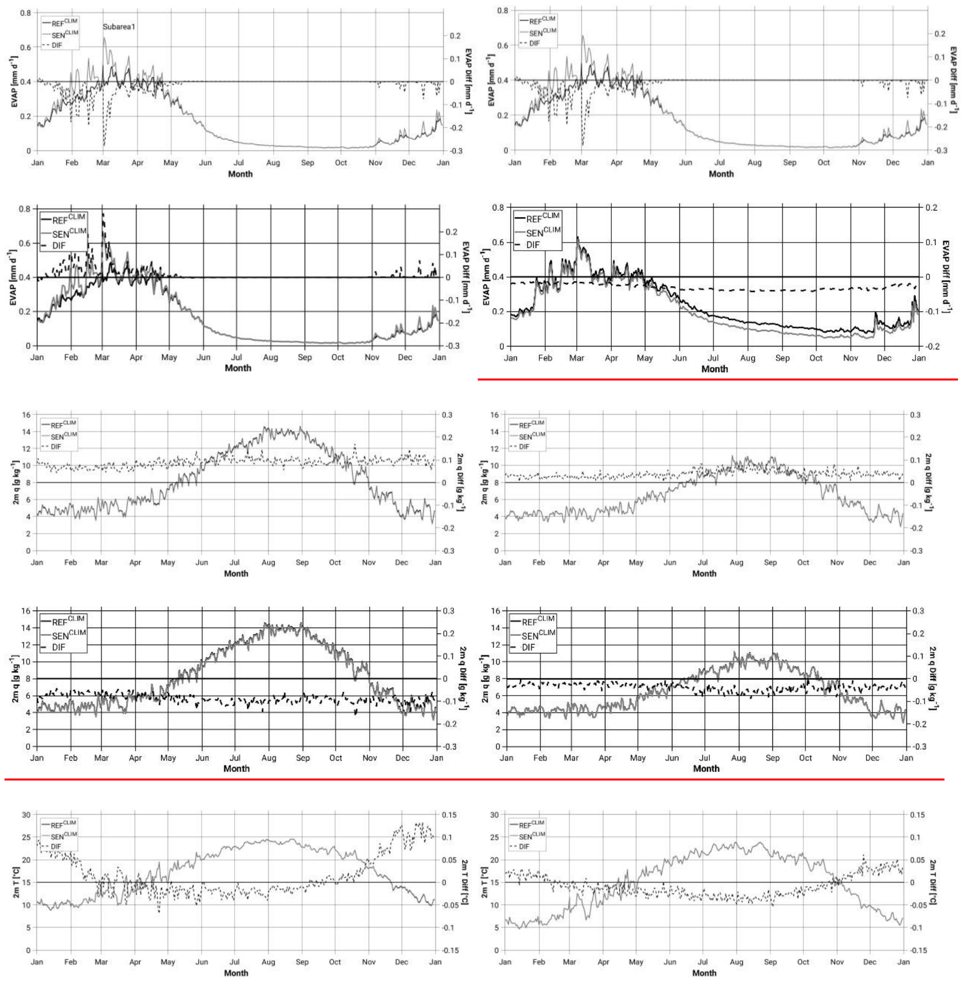

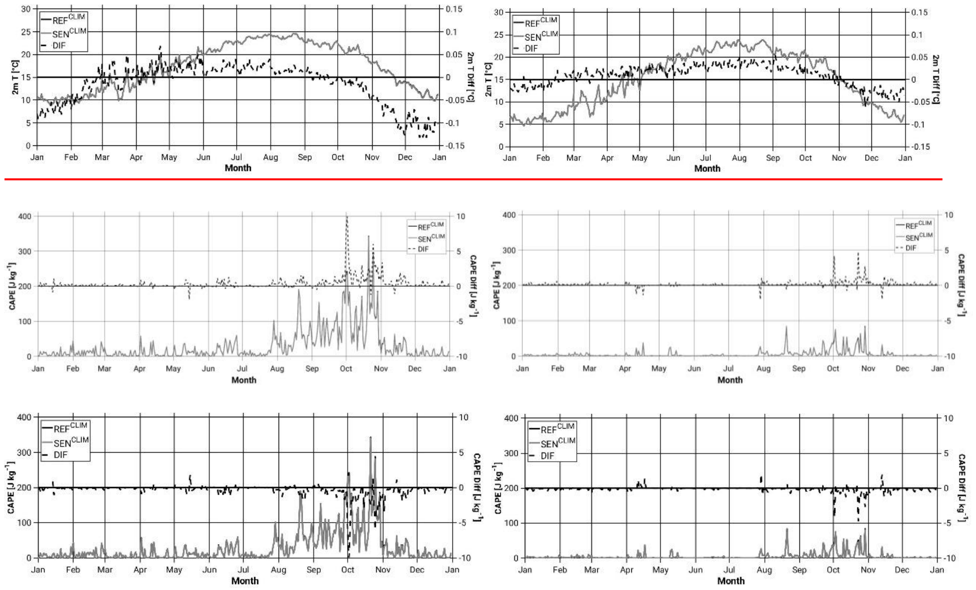

Figure 3: Annual cycle of the areal-daily averaged (and differences (black dashed line; SEN-REF)) of (a) precipitation for areas A1, A2, A3, A4 (see Figure 1b), and (b) evaporation, specific humidity and temperature at 2-m, and CAPE for areas A1 and A2, from the REF^{CLIM} (full black line) and the SEN^{CLIM} (full grey line) simulations. Only land points in the ~~investigation domain~~study area (Figure 1) for evaporation, and all grid points for the rest of variables and the period 2004 to 2013 are considered.

(a)

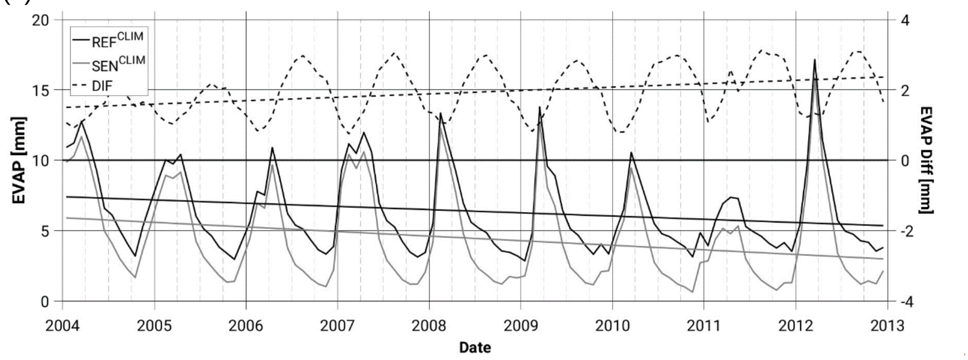

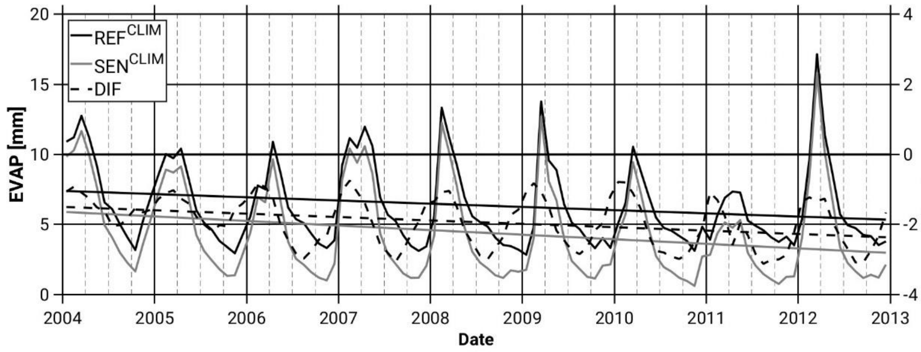
REF^CLIM
SEN^CLIM
DIF
EVAP [mm]
EVAP Diff [mm]
Date

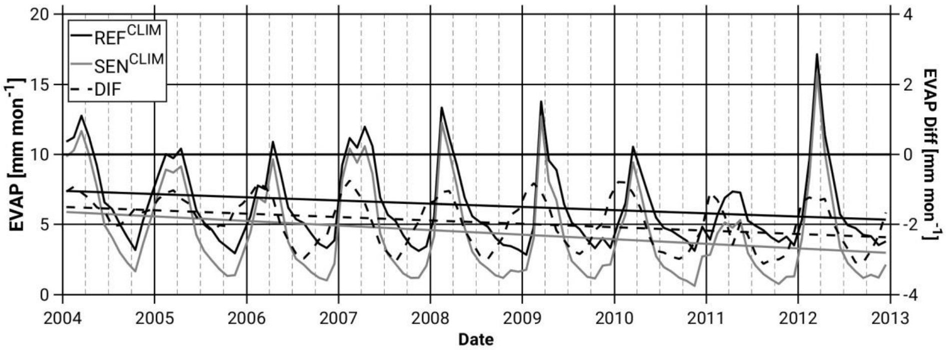
REF^CLIM
SEN^CLIM
DIF
EVAP [mm mon^-1]
EVAP Diff [mm mon^-1]
Date

(b)

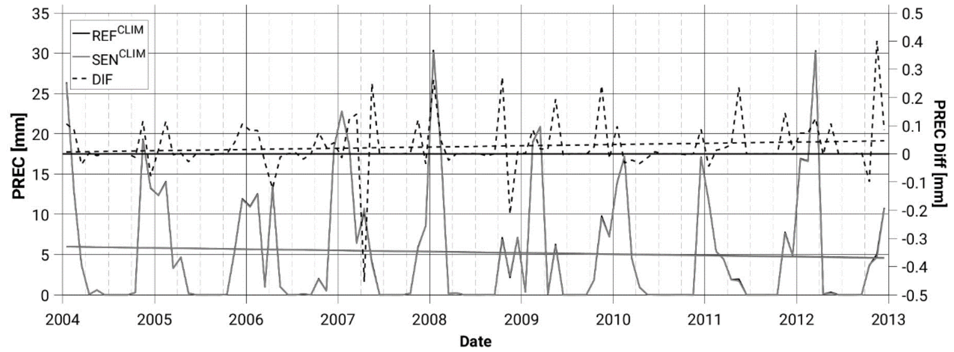
REF^CLIM
SEN^CLIM
DIF
PREC [mm]
PREC Diff [mm]
Date

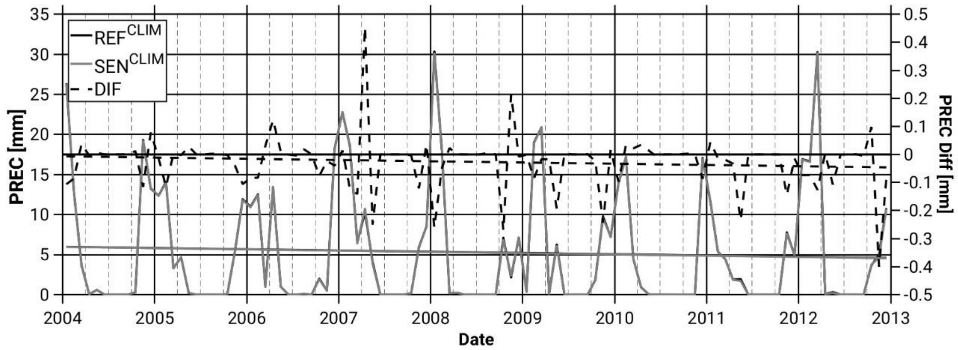
REF^CLIM
SEN^CLIM
DIF
PREC [mm]
PREC Diff [mm]
Date

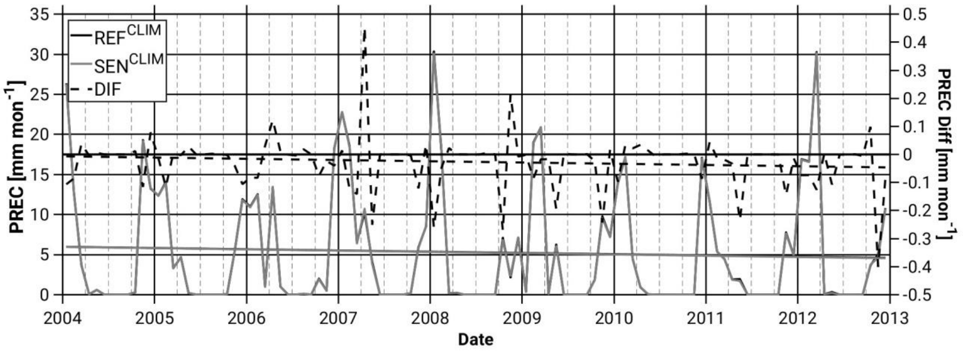

~~-~~(c)

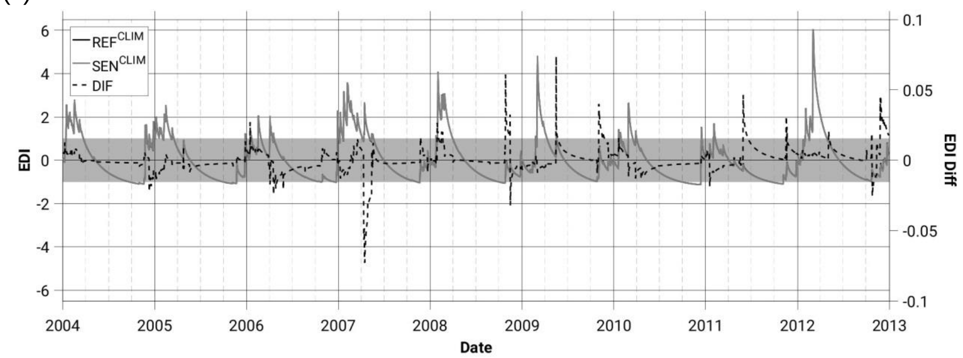

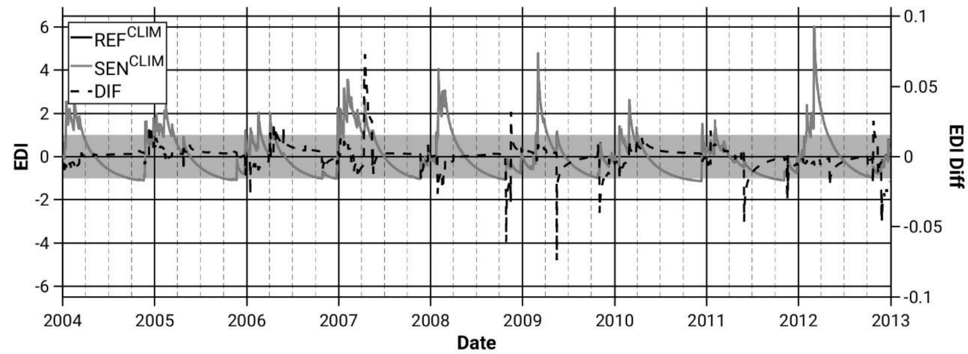

Figure 4: Temporal evolution of the monthly-daily accumulated areal mean values of (a) Evaporation, (b) Precipitation, (c) Effective Drought Index (EDI), from the REF^{CLIM} (full black line) and the SEN^{CLIM} (full grey line) simulations and~~.~~ d~~D~~ifferences~~ are~~ depicted with black dashed lines. The light grey band in (c) indicates the common soil state (-1<EDI<+1). All grid points in the ~~investigation domain~~study area (Figure 1) and the period 2004 to 2013 are considered.

(a)

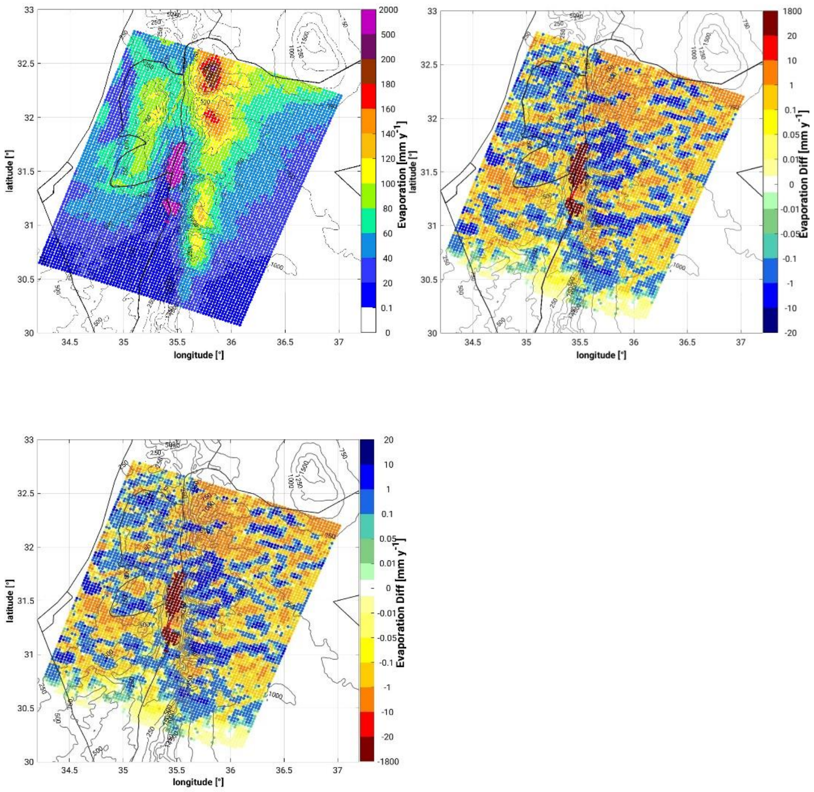
latitude [°]
longitude [°]
Evaporation [mm y-1]
Evaporation Diff [mm y-1]

(b)

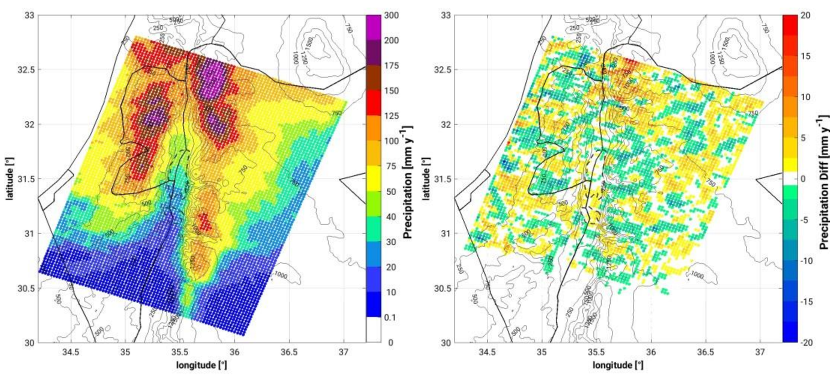
latitude [°]
longitude [°]
Precipitation [mm y-1]
Precipitation Diff [mm y-1]

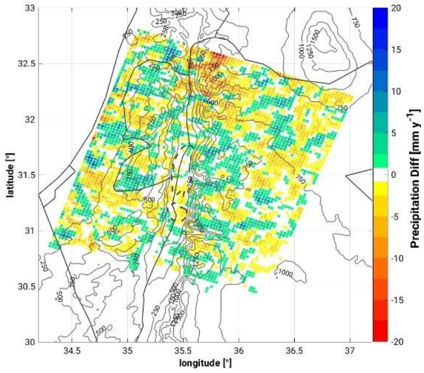

Figure 5: Spatial distribution of (a) evaporation in the REF^{CLIM} simulation (left) and the difference between the ~~REF^{CLIM} and~~ SEN^{CLIM} and the REF^{CLIM} simulations (right), and (b) precipitation in the REF^{CLIM} simulation (left) and the difference between the SEN^{CLIM} and the REF^{CLIM} ~~REF^{CLIM} and SEN^{CLIM}~~ simulations (right). The period 2004 to 2013 is considered.

(a) (b)

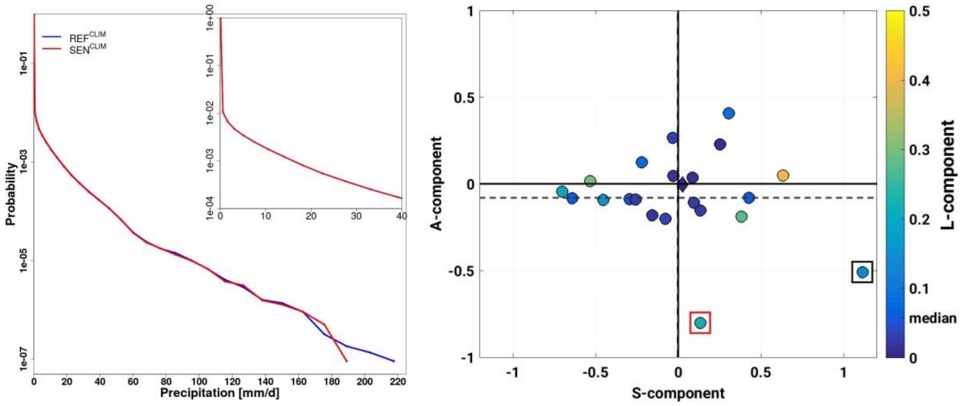

Figure 6: (a) Probability density function of daily precipitation intensities. All grid points in the investigation domain (Figure 1) and the period 2004 to 2013 are considered. (b) SAL diagram between REF^{CLIM} and SEN^{CLIM} simulations. Every circle corresponds to a simulated heavy precipitation event (listed in Table 1). The diamond (close to the zero-zero) illustrates the mean of all events. A-component (amplitude), S-component (structure), L-component (location). The inner colour indicates the L-component. ~~Squares~~ Boxes point out the two events examined in this study, CASE1 and CASE2 (see section 3.2).

(a)

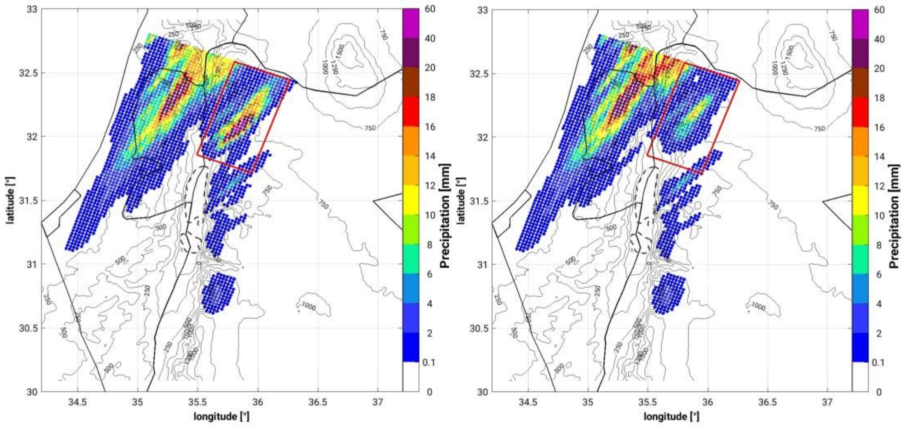
latitude [°]
longitude [°]
Precipitation [mm]
latitude [°]
longitude [°]
Precipitation [mm]

(b)

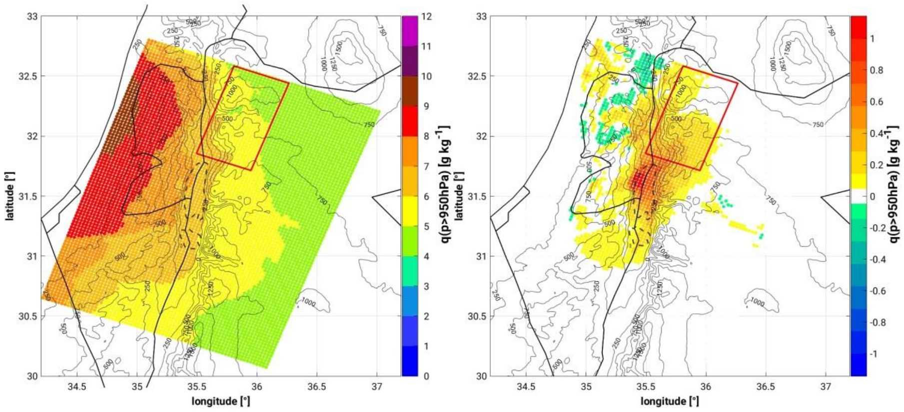
latitude [°]
longitude [°]
q(p>950hPa) [g kg^{-1}]
latitude [°]
longitude [°]
q(p>950hPa) [g kg^{-1}]

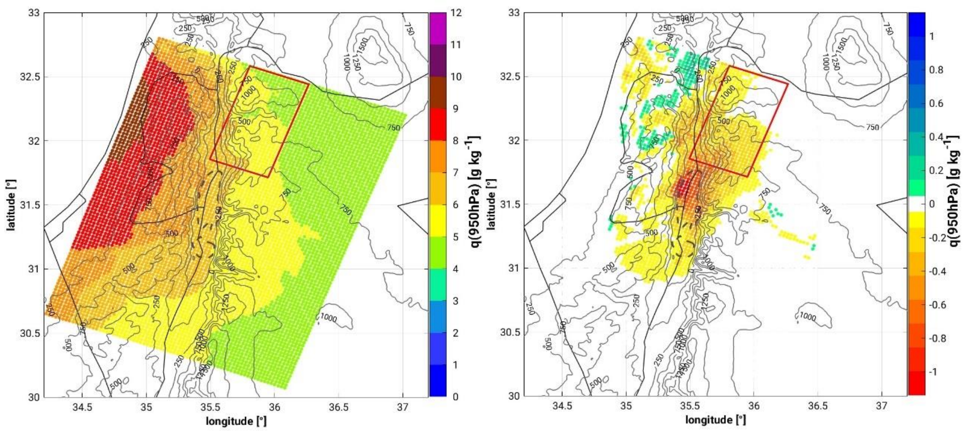
latitude [°]
longitude [°]
q(950hPa) [g kg^{-1}]

(c)

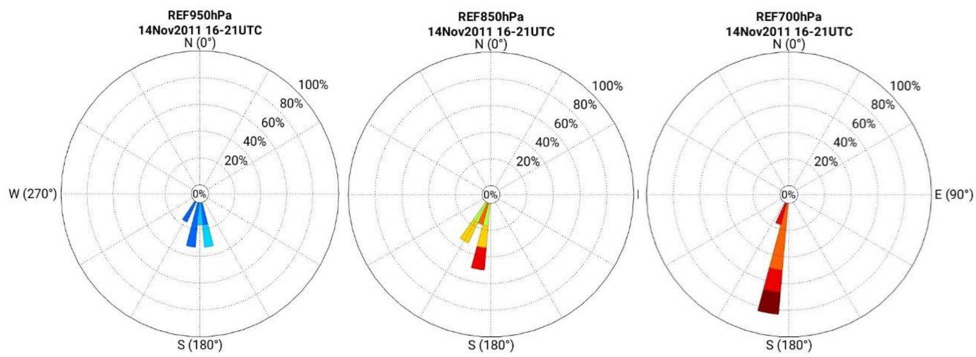
REF950hPa
14Nov2011 16-21UTC
REF850hPa
14Nov2011 16-21UTC
REF700hPa
14Nov2011 16-21UTC
N (0°)
S (180°)
W (270°)
E (90°)

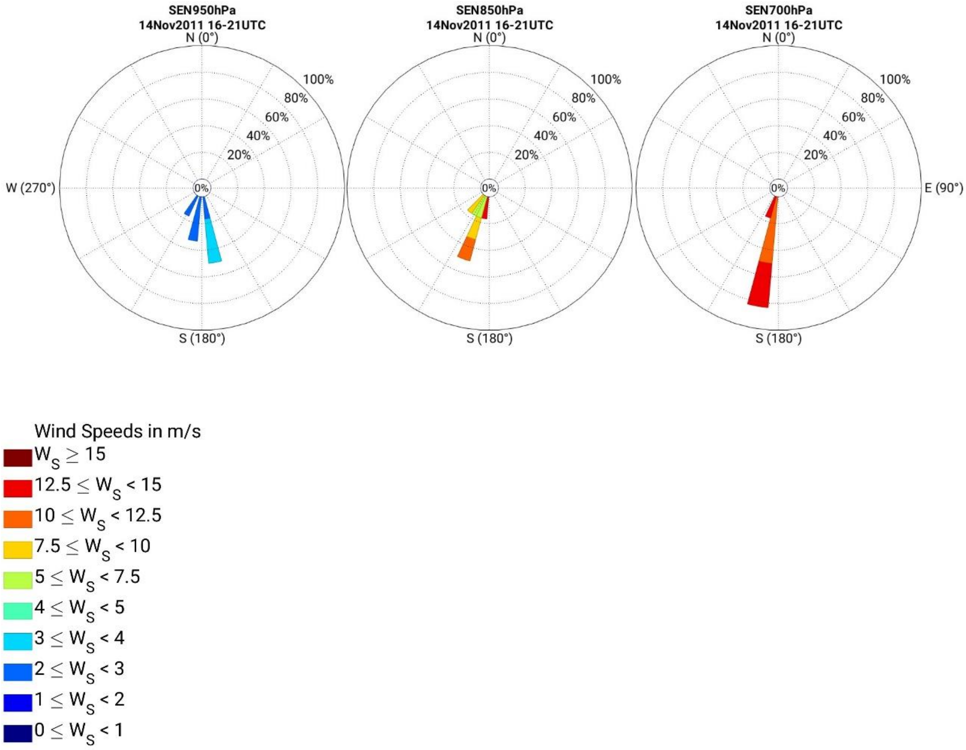

Figure 7: Spatial distribution of (a) 24-h ~~mean~~ accumulated precipitation from 14.11 09 UTC to 15.11 08 UTC ~~of, (a) precipitation~~ from the REF$^{14.11}$ simulation (left) and the SEN$^{14.11}$ simulation (right) and (b) specific humidity below 950 hPa, from the REF$^{14.11}$ simulation (left) and the difference between the REF$^{14.11}$ and SEN$^{14.11}$ simulations, as a mean for the 6-h period prior to convection initiation in the target area (14 November 16 UTC to 21 UTC), and (c) wind conditions at 700 hPa, 850 hPa, and 950 hPa (no relevant differences with respect to the 10-m field) for the same time period. Wind roses are centred at about 35.82°E-32.07°N in our target area.

(a)

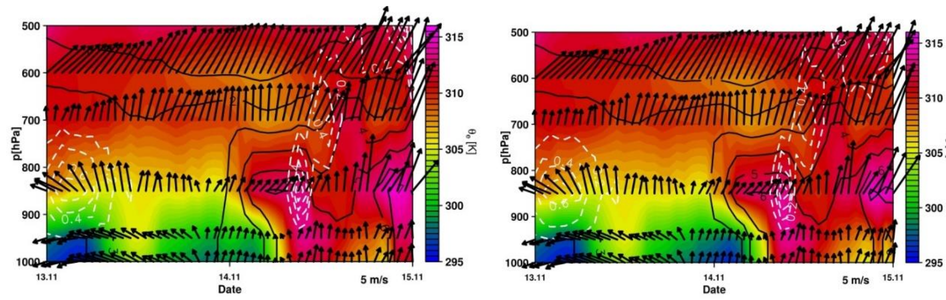

(b)

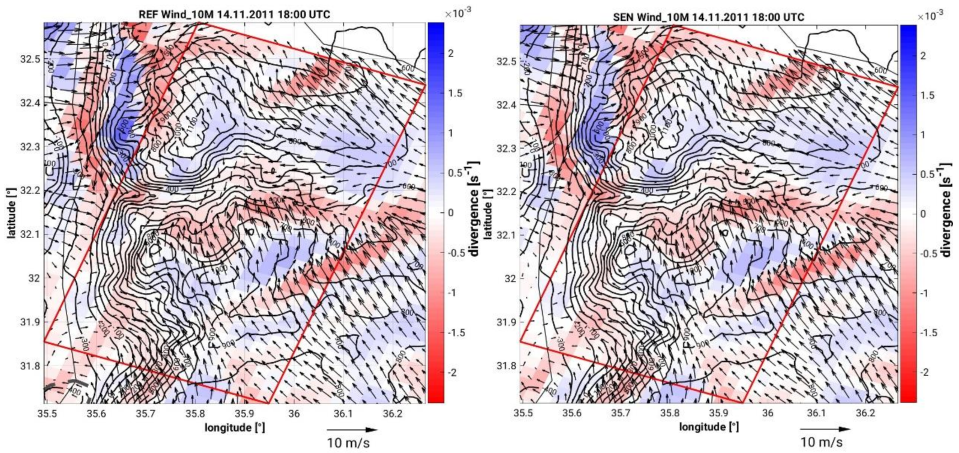

Figure 8: (a) Vertical-temporal cross-section of equivalent potential temperature (colour scale; K), specific humidity (black isolines; g/kg), horizontal wind vectors (north-pointing upwards, m/s) and vertical velocity (white dashed contours with 0.1 m/s increments) of the REF$^{14.11}$ (left) and SEN$^{14.11}$ (right) simulations, over a representative grid point in the sub-study region, 32.05°N 35.79°E. (b) Spatial distribution of 10-m horizontal wind (wind vectors; m/s) and corresponding divergence/convergence field (colour scale; s^{-1}) at 18 UTC on the 14 November 2011 from the REF$^{14.11}$ (left) and SEN$^{14.11}$ (right) simulations.

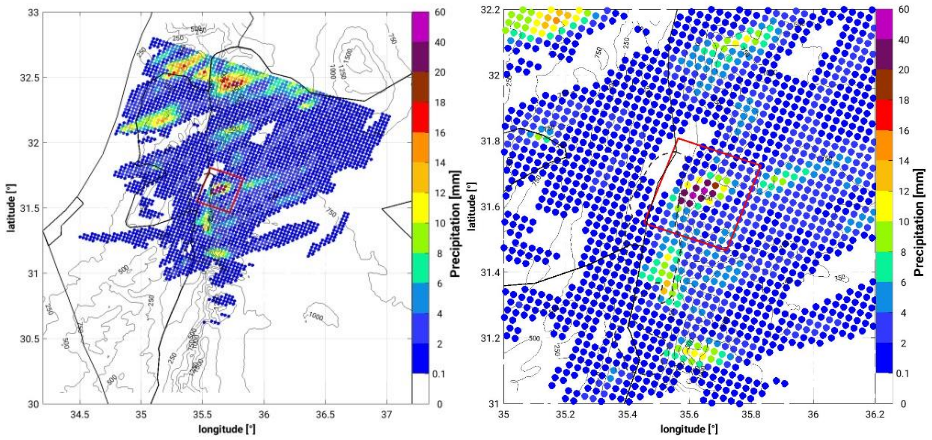
latitude [°]
longitude [°]
Precipitation [mm]

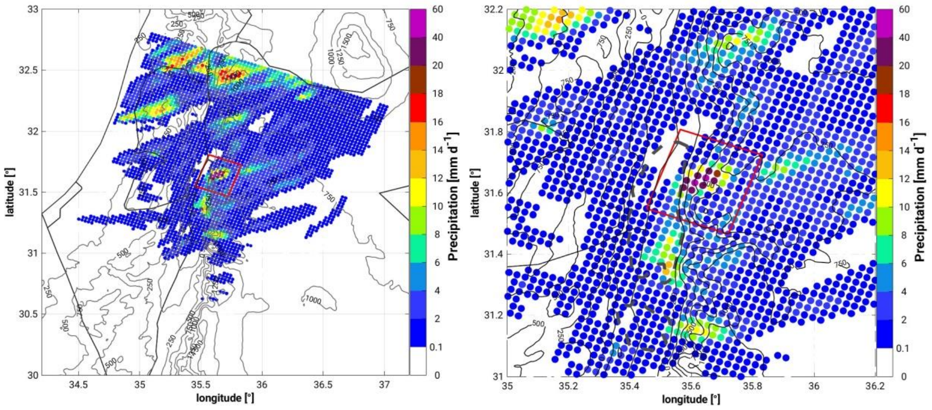
latitude [°]
longitude [°]
Precipitation [mm d^{-1}]

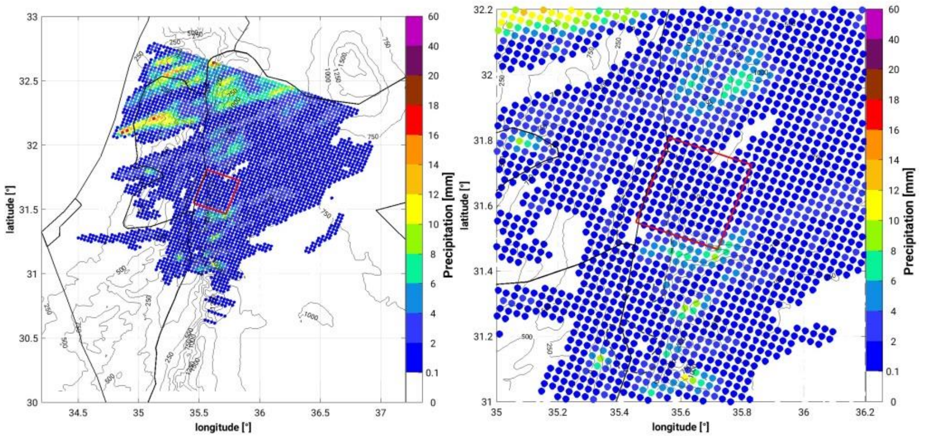
latitude [°]
longitude [°]
Precipitation [mm]

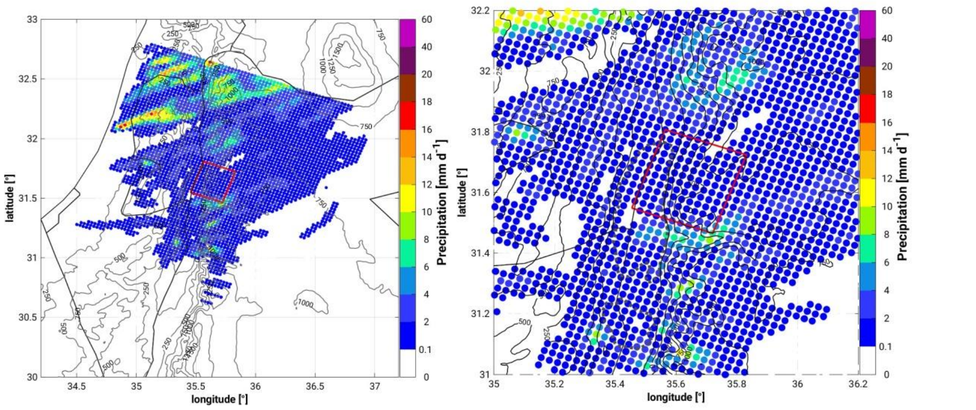

Figure 9: 24-h mean spatial distribution of precipitation from the REF$^{19.11}$ simulation (top-left; zoom top-right) and the SEN$^{14.11}$ simulation (bottom-left; zoom bottom-right) for the period 18 November 2011 11 UTC to 19 November 2011 10 UTC.

(a)

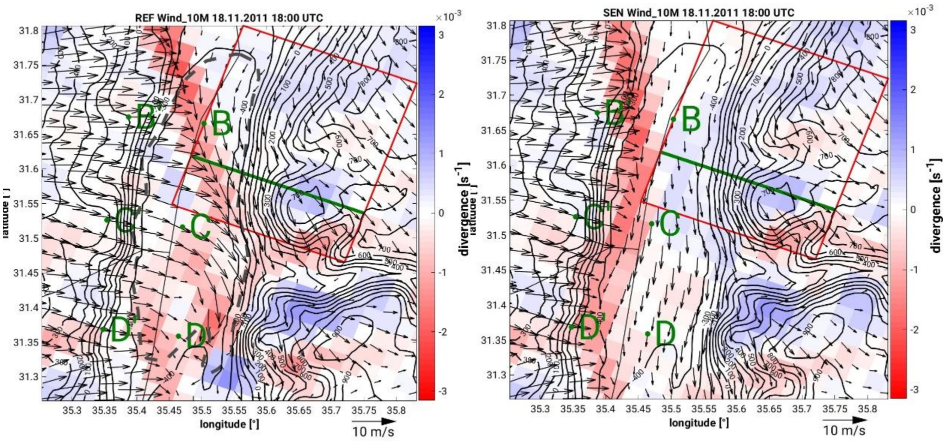
REF Wind_10M 18.11.2011 18:00 UTC
SEN Wind_10M 18.11.2011 18:00 UTC
longitude [°]
latitude [°]
divergence [s-1]
10 m/s
B
B'
C
C'
D
D'

(b)

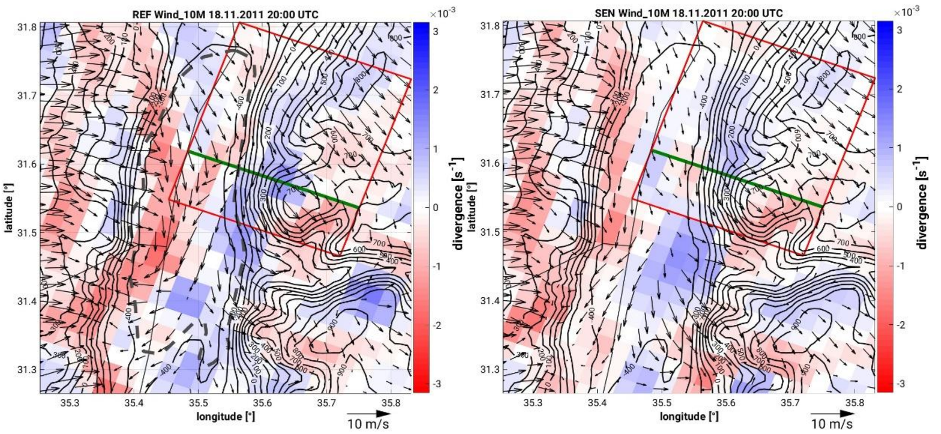
REF Wind_10M 18.11.2011 20:00 UTC
SEN Wind_10M 18.11.2011 20:00 UTC
longitude [°]
latitude [°]
divergence [s-1]
10 m/s

(c)

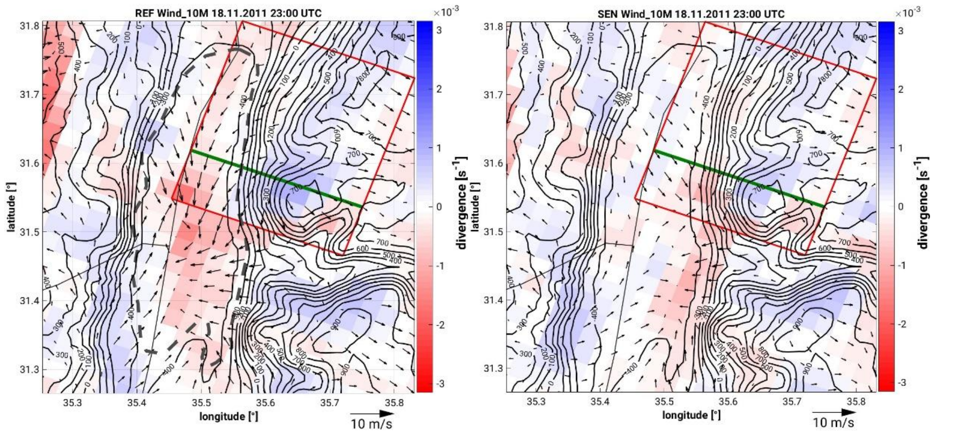

(d)

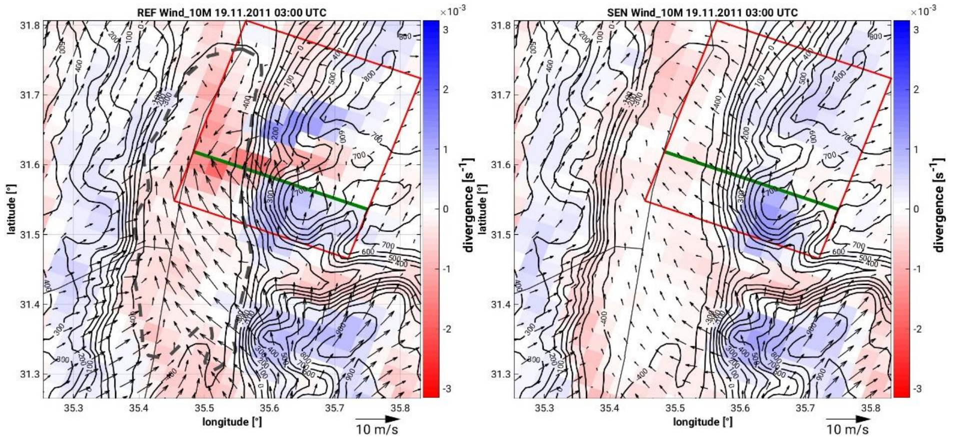

Figure 10: Spatial distribution of 10-m horizontal wind (wind vectors; m/s) and corresponding divergence/convergence field (colour scale; s^{-1}) at 18 UTC, 20 UTC, 23 UTC on the 19 November, and 03 UTC on the 20 November 2011 from the $REF^{14.11}$ (left) and $SEN^{14.11}$ (right) simulations. The topography is indicated by the black full isolines. The transects (B-C-D and B'-C'-D') corresponding to the locations in which temperature comparisons are made are indicated in Figure 10a. The green line indicates the position of the vertical cross-section in Figure 11.

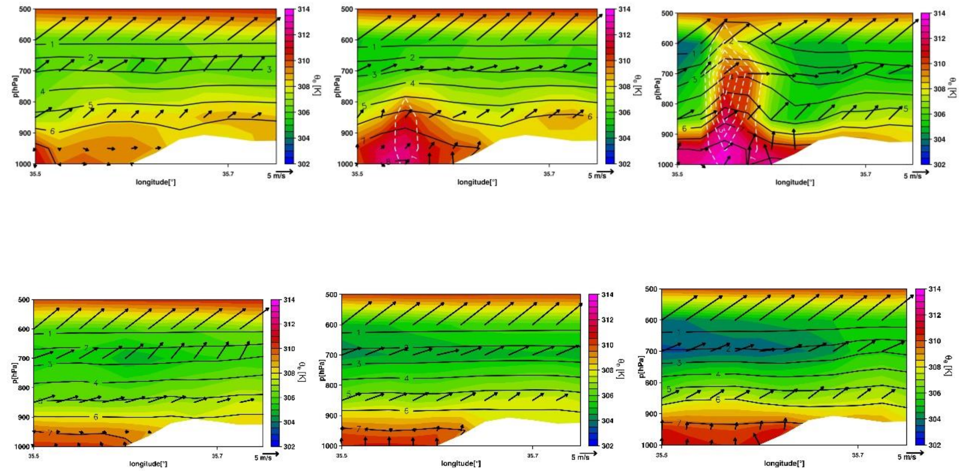

Figure 11: Vertical cross-section of equivalent potential temperature (colour scale; K), specific humidity (black isolines; g/kg), horizontal wind vectors (north-pointing upwards, m/s) and vertical velocity (white dashed contours with 1 m/s increments) of the $REF^{14.11}$ (top) and $SEN^{14.11}$ (bottom) simulations at 01 UTC (left), 02 UTC (middle) and 03 UTC (right). The location of the cross-section is indicated in Figure 10.

Near East Desertification: impact of Dead Sea drying on the local conditions leading to convection

Samiro Khodayar[1,2] and Johannes Hoerner[2]

[1]Institute of Meteorology and Climate Research (IMK-TRO), Karlsruhe Institute of Technology (KIT), Karlsruhe, Germany

[2]Mediterranean Centre for Environmental Studies (CEAM), Valencia, Spain

Submitted to Atmospheric Chemistry and Physics

(HyMeX Inter-journal SI)

* Corresponding author. E-mail address: Khodayar_sam@gva.es (S. Khodayar)

Mediterranean Centre for Environmental Studies (CEAM),

Technological Park, Charles R. Darwin Street, 14 46980 - Paterna - Valencia - Spain

Abstract

The Dead Sea desertification-threatened region is affected by continual lake level decline and occasional, but life-endangering flash-floods. Climate change has aggravated such issues in the past decades. In this study, the impact of the Dead Sea drying on the severe convection generating heavy precipitation in the region is investigated. Sensitivity simulations with the high-resolution convection-permitting regional climate model COSMO-CLM and several numerical weather prediction (NWP) runs on an event time scale are performed over the Dead Sea area. A reference simulation covering the 2003 to 2013 period and a twin sensitivity experiment, in which the Dead Sea is dried out and set to bare soil, are compared. NWP simulations focus on heavy precipitation events exhibiting relevant differences between the reference and the sensitivity decadal realization to assess the impact on the underlying convection-related processes.

The drying of the Dead Sea is seen to affect the atmospheric conditions leading to convection in two ways: (a) the local decrease in evaporation reduces moisture availability in the lower boundary layer locally and in the neighbouring, directly affecting atmospheric stability. Weaker updrafts characterize the drier and more stable atmosphere of the simulations where the Dead Sea has been dried out. (b) Thermally driven wind system circulations and resulting divergence/convergence fields are altered preventing in many occasions convection initiation because of the omission of convergence lines. On a decadal scale, the difference between the simulations suggests that in future regional climate, under ongoing lake level decline, a decrease in evaporation, higher air temperatures and less precipitation may be expected.

Key Words: Dead Sea drying, climate change, convection, heavy precipitation, boundary layer, wind systems, *high-resolution modelling*

1. Introduction

The Eastern Mediterranean and the Middle East is a sensitive climate change area (Smiatek et al. 2011). The anticipated warming in the 21st century combined with the general drying tendency, suggest important regional impacts of climate change, which should be investigated to assess and mitigate local effects on society and ecosystems. The Dead Sea basin is dominated by semi-arid and arid climates except by the north-western part that is governed by Mediterranean climate (Greenbaum et al. 2006). It is an ideal area to study climate variation in the Near East. It was already discussed by Ashbel (1939) the influence of the Dead Sea on the climate of its neighbouring regions. The change in the climate of the Dead Sea basin caused by the drying of the Dead Sea has also been evidenced in the last decades (Alpert et al. 1997; Cohen and Stanhill 1996; Stanhill 1994). The Dead Sea is the lowest body of water in the world (~ -430 m) surrounded by the Judean Mountains (up to ~ 1 km amsl) to the west and to the east by the Maob Mountains (up to ~ 3 km amsl). The area in between is rocky desert. The complex topography of the area favours the combined occurrence of several wind regimes in addition to the general synoptic systems, namely valley and slope winds, Mediterranean breezes and local lake breezes (e.g. Shafir and Alpert 2011). These wind systems are of great importance for the living conditions in the region since they influence the visibility and the air quality (e.g. Kalthoff et al. 2000; Corsmeier et al. 2005) as well as the atmospheric temperature and humidity. Since the Dead Sea is a terminal lake of the Dead Sea Valley, no natural outflow exists, being evaporation the main loss of water, being the wind velocity and vapour pressure deficit identified as the main governing factors of evaporation throughout the year (Metzger et al. 2017). Through the high evaporation the lake level declines and results in a desertification of the shoreline and a changing fraction of water and land surface in the valley. The documented Dead Sea water level drop of about 1 m/y in the last decades (Gavrieli et al. 2005) is mainly due to the massive water consumption at its upstream having climate changes a small contribution to the lake level decrease (Lensky and Dente 2015). This situationseverely affects agriculture, industry and the environmental conditions in the area, thus, leading to substantial economic losses (Arkin and Gilat 2000).

The Jordan River catchment and Dead Sea exhibit in the north, annual precipitation in the order of 600-800 mm, whereas in the south, there is an all year arid climate with an annual precipitation of <150 mm (Schaedler and Sasse 2006). Rain occurs between October and May and can be localized or widespread (Dayan and Sharon 1980) (Sharon and Kutiel 1986). Rainfall varies seasonally and annually, and it is often concentrated in intense showers (Greenbaum et al. 2006) caused mainly by severe convection (Dayan and Morin 2006). Flash floods are among the most dangerous meteorological hazards affecting the Mediterranean countries (Llasat et al 2010), thus, knowledge about the processes shaping these events is of high value. This is particularly relevant in arid climates, where rainfall is scarce, and often, local and highly variable. In flood-producing rainstorms, atmospheric processes often act in concert at several scales. Synoptic-scale processes transport and redistribute the excess sensible and latent heat accumulated over the region and subsynoptic scale processes determine initiation of severe convection and the resulting spatio-temporal rainfall characteristics. The main responsible synoptic weather patterns leading to heavy rainfall in the region are in general well known and described in previous publications (e.g. Belachsen et al. 2017; Dayan and Morin 2006). Belachsen et al. (2017) pointed out that three main synoptic patterns are associated to these heavy rain events: Cyprus low accounting for 30% of the events, Low to the east of the study region for 44%, and Active Read Sea Trough for 26%. The first two originate from the Mediterranean Sea, while the third is an extension of the Africa monsoon. Houze (2012) showed that orographic effects lead to enhanced rainfall generation; rain cells are larger where topography is higher. Sub-synoptic scale processes play a decisive role in deep convection generation in the region. Convection generated by static instability seems to play a more important role than synoptic-scale vertical motions (Dayan and Morin 2006). The moisture for developing intensive convection over the Dead Sea region can be originated from the adjacent Mediterranean Sea (Alpert und Shay-EL 1994) and from distant upwind sources (Dayan and Morin 2006).

In this study, the drying of the Dead Sea is investigated focusing on the impact on atmospheric conditions leading to heavy precipitating convection in the region. The relevance of the Dead Sea as a local source of moisture for precipitating convection as well as the impact of the energy balance partitioning changes and related processes caused by the drying of the Dead Sea are investigated. With this purpose, a sensitivity experiment with the high-resolution regional climate model COSMO-CLM [Consortium for Small scale Modelling model (COSMO)-in Climate Mode (CLM); Böhm et al. 2006] is conducted. The high horizontal grid spacing used (~ 2.8 km) resolves relevant orographic and small-scale features of the Dead Sea basin, which is not the case when coarser resolution simulations are performed. Moreover, at this resolution convection is explicitly resolved instead of being parametrized, which has been already extensively demonstrated to be highly beneficial for the simulation of heavy precipitation and convection-related processes. The benefit of employing high-resolution convection permitting simulations is mainly in sub-daily time-scales, (e.g., Prein et al., 2013; Fosser et al., 2014; Ban et al., 2014), however, daily precipitation is also positively affected, particularly in winter time (Fosser et al., 2014). Previous studies in the area applying high-resolution modelling agree with the benefitial impact of finer resolution against coarser ones (e.g. *Rostkier-Edelstein et al. 2014; Hochman et al. 2018; Kunin et al. 2019*).

The impact of completely drying the Dead Sea on the regional atmospheric conditions and precipitating convection is discussed. A decadal simulation and several event-based Numerical Weather Prediction (NWP) runs covering the eastern Mediterranean are carried out. A process understanding methodology is applied to improve our knowledge about how sub-synoptic scale processes leading to severe convection are affected by the drying of the Dead Sea. The article is organized as follows. Section 2 provides an overview of the data and the methodology used. Then, in section 3, the climatology of the region based on the high-resolution convection-permitting decadal simulation is presented and the impact of drying the Dead Sea is examined across scales. Finally, conclusions are discussed in section 4.

2. Data and methodology

2.1 The COSMO-CLM model

In this investigation, the regional climate model (RCM) of the non-hydrostatic COSMO model, COSMO-CLM (CCLM), is used (Version 5.0.1). It has been developed by the Consortium for Small-scale modeling (COSMO) and the Climate Limited-area Modeling Community (CLM) (Böhm et al., 2006). It uses a rotated geographical grid and a terrain-following vertical coordinate. The model domain covers the southern half of the Levant, centred around the Dead Sea, with a horizontal resolution of 7 km and 2.8 km, 60 vertical levels and a time step of 60 and 20 seconds, respectively. Using IFS (Integrated Forecasting System) analysis, the spectral weather model of ECMWF (European Centre for Medium-Range Weather Forecast) as driving data for the simulations, a double nesting procedure was employed. The coarsest nest at 0.0625º resolution (about 7 km) covers 250 grid points in x direction and 250 grid points in y direction. The size and location of the 7 km domain has been considered large enough to have into consideration all possible synoptic situations relevant for the development of extreme phenomena in the study area as well as the influence of the Mediterranean Sea. The finest nest at 0.025º (circa 2.8 km) covers 150 x 150 grid points, thus a total area of 22500 grid points and includes the study area (72 grid point in x direction and 92 in y direction) centred around the Dead Sea.

A Tiedtke (1989) mass-flux scheme is used for moist convection in the 7 km, and reduced Tiedke mass-flux scheme for shallow convection. Contrary to the CCLM-7 km simulation, where convection is parameterized, in the CCLM-2.8 km convection is explicitly resolved (Doms and Baldauf, 2015), so only the reduced Tiedke mass-flux scheme is used for shallow convection. The model physics includes a cloud physics parameterization with 5 types of hydrometeors (water vapor, cloud water, precipitation water, cloud ice, precipitation ice), a radiative transfer scheme based on a delta-two-stream solution (Ritter and Geleyn, 1992) and a roughness-length dependent surface flux formulation based on modified Businger relations (Businger et al., 1971).

Orography data from GLOBE (Global Land One-km Base Elevation Project) of NOAA (National Oceanic and Atmospheric Administration) and soil data from HWSD (Harmonized Worlds Soil Database) TERRA is used. HWSD is a global harmonization of multiple regional soil data sets with a spatial resolution of 0.008° (FAO, 2009), resulting in 9 different soil types in the model, namely ‘ice and glacier', 'rock / lithosols', 'sand', 'sandy loam', 'loam', 'loamy clay', 'clay', 'histosols', and 'water'.

Multiple model runs have been performed. A 7 km run from 2003 to 2013 with dailyoutput is used as nesting for two 2.8 km runs over the same time span. The Dead Sea is dried out and replaced with soil types from the surrounding area in one of them (SEN), the other one is used as reference (CLIM). For the detailed investigation of convective events on 14.11.2011 and 19.11.2011, sub-seasonal simulations have been performed with the same settings as the decadal simulation, but with hourly outputs due to the limitations imposed by the daily output.

2.2 Methodology

In order to assess the impact of the drying of the Dead Sea on the atmospheric conditions leading to severe convection in the region, a set of sensitivity experiments was performed. A decadal simulation covering the 2003 to 2013 time period was carried out with the convection permitting 2.8 km COSMO-CLM model. Lateral boundary conditions and initial conditions are derived from the European Centre for Medium-Range Weather Forecasts (ECMWF) data. The COSMO-CLM 7 km is used as nesting step in between the forcing data and the 2.8 km run. This reference simulation will be hereafter referred to as REF^{CLIM} simulation. Parallel to this, a sensitivity experiment (hereafter SEN^{CLIM}) is carried out in which the Dead Sea is dried out and set to bare soil on -405 m level (depth of the Dead Sea in the external data set, GLOBE (Hastings and Dunbar, 1999)). After examination of the results, the first year of simulations is considered spin-up time, thus, our analysis covers the 2004-2013 period.

The precipitation field has been validated using the EOBS dataset (Haylock et al. 2008) with a resolution of 0.1° and available for the period 1980-2011, and the APHRODITE's (Asian Precipitation - Highly-Resolved Observational Data Integration Towards Evaluation: Yatagai et al. 2008, 2012) daily gridded precipitation which is the only long-term continental-scale daily product that contains a dense network of daily rain-gauge data for Asia. It has a resolution of 0.25º and is available for 1980-2007. The APHRODITE data shows generalized lower precipitation values than EOBS, but still higher than our simulation particularly close to the northern Mediterranean shoreline, over coastal-flat terrain, whereas the best agreement is at areas dominated by complex terrain. This agrees with previous high-resolution modelling activities in the region such as Rostkier-Edelstein et al. (2014) using WRF at 2 km. They suggest in this publication that inaccuracies in the gridded SST dataset used in the simulations could be responsible for the observed bias highlighting the strong sensitivity of precipitation in the Mediterranean basin to very small differences in the SST (Miglietta et al. 2011). Despite these biases the comparison of the temporal areal-mean of the model simulations at 7 km and 2.8 km and the APHRODITE dataset demonstrates that in general the model quiete well captures the precipitation events. An improvement is seen at the finer resolution.

Regional dry and wet periods are identified and quantified in the simulations by means of the Effective Drought Index (EDI; Byun and Wilhite 1999; Byun and Kim 2010). The EDI is an intensive measure that considers daily water accumulations with a weighting function for time passage normalizing accumulated precipitation. The values are accumulated at different time scales and converted to standard deviations with respect to the average values. Here we use an accumulation period of 365 days. EDI dry and wet periods are categorized as follows: moderate dry periods $-1.5 < EDI < -1$, severe dry periods $-2 < EDI < -1.5$, and extreme dry periods $EDI < -2$. Normal periods are revealed by $-1 < EDI < 1$ values.

Based on daily mean values, precipitation and evapotranspiration distribution and possible tendencies in the 10-year period are assessed. To further asses the most affected areas in our study area, this is divided in four subdomains surrounding the Dead Sea and trying to respect the orographic pattern in the area (Figure 3). Annual cycles are thus separately investigated to take into consideration the relevant differences in orography, soil types, and distance to the coast among others (Figure1), which are known to have a significant impact in the precipitation distribution in the region (e.g. Belachsen 2017; Houze 2012). . Differences in the annual cycle and temporal evolution of precipitation and evapotranspiration between the REF^{CLIM} and SEN^{CLIM} are discussed. Also, differences in the near-surface and boundary layer conditions and geopotential height patterns are examined. Geographical patterns of mean evapotranspiration and precipitation and differences with respect to the reference simulation are assessed. Probability distribution functions (PDFs), and the Structure, Amplitude and Location (SAL: Wernli et al. 2008) analysis methodologies are used to illustrate differences in the mean and extreme precipitation between the reference and the sensitivity experiments. The SAL is an object-based rainfall verification method. This index provides a quality measure for the verification of quantitative precipitation forecasts considering three relevant aspects of precipitation pattern: the structure (S), the amplitude (A), and the location (L). The A component measures the relative deviation of the domain-averaged rainfall; positive values indicate an overestimation of total precipitation, negative values an underestimation. The component L measures the distance of the center of mass of precipitation from the modelled one, and the average distance of each object from the center of mass. The component S is constructed in such a way that positive values occur if precipitation objects are too large and/or too flat and negative values if the objects are too small and/or too peaked, quantifying the physical distance between the centres of mass of the two rainfall fields to be compared. Perfect agreement between prediction and reference are characterized by zero values for all components of SAL. Values for the amplitude and structure are in the range (−2, 2), where ±0.66 represents a factor of 2 error. The location component ranges from 0 to 2, where larger values indicate a greater separation between centres of mass of the two rainfall fields. This is done by selecting a threshold value of 1/15 of the maximum rainfall accumulation in the domain (following Wernli et al. 2008). The structure and location components are thus independent of the total rainfall in the domain.

Differences in the temporal evolution of precipitation between the REF^{CLIM} and SEN^{CLIM} are identified. In Table 1, those events in which an area-mean (study area, Figure 1) difference between both simulations higher than ±0.1 mm/d exists are selected as potential heavy precipitation events and classified attending to their synoptic scale environment, and atmospheric stability conditions (Table 1).

Although Dayan and Morin (2006) discuss that in general large-scale vertical motions do not provide the sufficient lifting necessary to initiate convection, it was demonstrated by Dayan and Sharon (1980) that a relationship exists between the synoptic-scale weather systems and deep moist convection, being those systems responsible for the moisturizing and destabilization of the atmosphere prior to convective initiation. They pointed out that indices of instability proved the most efficient determinants of the environment characterizing each rainfall type in the region. Thus, two indicators of the atmospheric degree of stability/instability, namely the Convective Available Potential Energy (CAPE; Moncrieff and Miller 1976) and the KO-index (Andersson et al. 1989), are examined in this study. The CAPE is a widely known index indicating the degree of conditional instability. Whereas, the KO-index, which is estimated based on the equivalent potential temperature at 500, 700, 850 and 1000 hPa (following the recommendations by Bolton 1980), describes the potential of deep convection to occur as a consequence of large-scale forcing (Andersson et al. 1989; Khodayar et al. 2013). Generally, regions with KO-index < 2 K and large-scale lifting are identified as favourable for deep convection. Parcel theory (50 hPa ML (Mixed Layer) parcel) and virtual temperature correction (Doswell and Rasmussen 1994) are applied to these calculations.

Based on the above criteria, a separation was made between events with widespread rainfall and those more localized. Among the latter, we selected two events to illustrate the local impacts on the boundary layer conducive to deep moist convection. Particularly, differences in the amount, structure and location of precipitation are assessed by examining the spatial patterns and the SAL verification method. The two selected events for detail analysis in this study are those showing the larger SAL deviations. Those two cases occur close in time. Carefull inspection of the atmospheric conditions after the first event shows no significant differences between simulations suggesting no connetion between both events.Even though a more detail analysis is provided for the two selected cases, all convective-events listed in Table 1 have been examined to assess the main impacts on the mechanisms leading to convection. High-resolution simulations with the NWP COSMO 2.8 km model are performed with hourly output temporal resolution and covering a 3-day period (including 48-h prior to the day of the event, from 00 UTC) to capture atmospheric pre-conditions conducive to deep moist convection. For this, a reference simulation, REF^{NWP}, and a sensitivity experiment, SEN^{NWP}, are carried out for each event.

3. Results and discussion

3.1 Climatology of the Dead Sea region

Annual cycle

To assess the climatology of the study region (Figure 1) the annual evaporation and precipitation cycles based on daily means of the respective quantities are investigated (Figure 2). Additionally, we examine the evolution of specific humidity (Qv_{2m}) and temperature at 2 m (T_{2m}) as well as total column integrated water vapour (IWV) and low-boundary layer (< 900 hPa) equivalent potential temperature (Θ_e). Possible changes in the atmospheric stability conditions are evaluated by examination of the CAPE and KO-index. In Figure 2, all grid points over the study region (Figure 1) and the time period 2004-2013 are considered. Differences between the REF^{CLIM} and the SEN^{CLIM} simulations are also discussed.

The annual cycle of evaporation shows minimum values in the autumn season (around October, ~ 0.1 mm/d) and maximum evaporation in spring (around March, ~ 0.4 mm/d). The dependency with the precipitation cycle is clear with maximum values of the latter around March and rain occurring between October and May (Figure 2a) in agreement with observations in the area (Dayan and Sharon 1980). The difference between the evaporation in the REF^{CLIM} and the SEN^{CLIM} simulations indicates a mean decrease in the order of 0.02 (February) to ~ 0.1 (August) mm/d in the absence of the Dead Sea water (SEN^{CLIM}). The largest difference is in the dry period (May to October) when water availability is less dependent on precipitation, and evaporation is higher over the Dead Sea in contrast to the minimum values over land (Metzger et al. 2017). In general, there is a decrease of about 0.5 % in precipitation in the SEN^{CLIM} simulation. In contrast to the differences in evaporation, precipitation differences between the reference and the sensitivity experiment occur in both directions during the rain period, from October to May. Examining the total number over the whole decadal simulation it is seen that the number of dry or wet days (> 0.1 mm/d) or heavy precipitation events is not largely affected in the sensitivity experiment. In general, the number of dry days increases (fewer wet days) in the SEN^{CLIM} simulation, whereas the number of high intensity events show almost no variation. For each simulation, the difference between precipitation and evaporation is negative mainly in spring and summer contributing to the dryness in the region. Furthermore, the negative difference between the REF^{CLIM} and SEN^{CLIM} simulations indicates that the PREC-EVAP difference is higher in the SEN^{CLIM} simulation probably in relation to the reduced evaporation over the dry sea area and the general decrease in the precipitation amount in the region.

In addition to the reduced evaporation and precipitation (about 0.5 %) in the whole domain in the SEN^{CLIM} simulation a drier and warmer lower-troposphere is identified

(Figure 2b) in agreement with the observational assessment by Metzger et al. (2017) of the cooling effect of evaporation on air temperature in the region. The annual cycle of IWV and $\Theta_{e<900hPa}$ in Figure 2c show that the impact of the dry Dead Sea resulting evaporation is less pronounced when a deeper atmospheric layer is considered. Indeed, $\Theta_{e<900hPa}$ evolution evidences that the warming effect due to the decreased evaporation in the SEN^{CLIM} simulation is restricted to the near surface.

In Figure 2d, the annual cycle of areal mean CAPE displays larger values in the period from August to November, being this the period more favourable for convection. Positive CAPE differences between the REF^{CLIM} and the SEN^{CLIM} simulations are presumably in relation to the identified distinct lower-atmospheric conditions, being these more favourable and consequently CAPE values higher in the REF^{CLIM} simulation. In the same period, the KO-index indicates a more potentially unstable atmosphere, i.e. prone to deep convection because of large-scale forcing, and larger differences between simulations.

In agreement with the well-known precipitation distribution in the region most of the events occur in A1 (north-west) and A2 (north-east). Also, in these subdomains larger differences between the REF^{CLIM} and SEN^{CLIM} simulations are identified pointing out the relevance of the Dead Sea evaporation in the pre-convective environment for rainfall episodes over the study area (Figure3a). Considering only land grid points almost no difference between simulations is found in the evaporation annual cycle of A1 and A2 (Figure3b) suggesting the distinct amount of moisture advected towards A1 and A2 from the Dead Sea in REF^{CLIM} and SEN^{CLIM} as responsible for the differences in the boundary layer conditions conducive to convection. Also, in these subdomains the dryer and warmer lower boundary layer and the reduced instability in the SEN^{CLIM} are recognized

Inter-annual variability

In Figures 4 we discuss the inter-annual variability (based on monthly-daily areal mean values) of evaporation, precipitation as well as drought evolution.

The reduced evaporation in the annual cycle of the SEN^{CLIM} simulation for the whole investigation domain, resulting from the drying of the Dead Sea and affected evaporation, remains from year to year (Figure 4a). Larger differences between the simulations occur in the May to November months in agreement with the annual cycle in Figure 2a. This, and the time period of the maximum/minimum is constant over the years. A tendency towards lower evaporation at each simulation and higher differences between both at the end of the period are identified. An inter-annual fluctuation is observed in both REF^{CLIM} and SEN^{CLIM} simulations. The yearly rate of evaporation shows, for example, in REF^{CLIM} maximum values of about 7 mm in 2011 and around 17 mm in 2012. This is in agreement with the positive correlation expected between precipitation and evaporation, a trend towards decreased precipitation and a correspondence between drier years such as the 2011-2012 period and lower annual evaporation are seen in Figure 4b. Year to year EDI calculations in Figure 4c help us identify the regional extreme dry and wet periods. The EDI range of variation from about -1 to 2 for the whole period of simulation indicates that the dry condition is the common environment in the area, while the wet periods, EDI up to 6, could be identified as extreme wet periods (relative to the area), in this case in the form of heavy precipitation events. Maximum positive EDI values are in the first months of the year in agreement with the precipitation annual cycle in Figure 2, whereas minimal EDI values occur in summer and autumn indicative of the dry conditions in these periods. Differences in the EDI calculations from both simulations reveal distinct precipitation evolutions and denote timing differences in the occurrence of the precipitation events. When the regional climate evolution is examined in combination with the impact on the number of heavy precipitation events (Table 1) the impact is stronger in the dry period of 2011 (Figure 4a). About six events show relevant differences in this period, contrary to the average 3 episodes per year.

Spatial distribution

The geographical patterns of evaporation and precipitation are presented in Figure 5. Over the Dead Sea, the simulated average annual evaporation for the period under consideration is in the order of 1500-1800 mm/y, in contrast to the values in the deserts east and south, where the evaporation is less than 20 mm/y. Observed annual evaporation of this lake is known to be about 1500 mm and to vary with the salinity at the surface of the lake and freshening by the water inflow (Dayan and Morin 2006; Hamdani et al. 2018). Over land, higher evaporation is seen over the Judean Mountains and the Jordanian Highlands. High correlation with the orography and soil types is seen (Figure 1). Evaporation is probably correlated with rainfall which in turn is correlated with topography. Particularly, in the Jordanian Highlands where maximum evaporation is around 200 mm/y, the complex topography coincides with sandy loam soils, whereas most of the soil in study region is defined as loamy clay or clay (Figure 1). The evaporative difference field between simulations in Figure 5a shows a highly inhomogeneous patchiness not evidencing any relationship with orography or soil type, but rather with changes in the precipitation pattern in the SEN^{CLIM} simulation as seen in Figure 5b.

In agreement with the temporal series of areal mean precipitation in Figure 3 higher annual precipitation are in the north-west and -east, with respect to the southern regions. Topographic features exert a large impact on precipitation distribution with maxima of about 175 to 300 mm/y over the Judean Mountains and the Jordanian Highlands. To the northern end of the Dead Sea valley, the largest precipitation difference between the REF^{CLIM} and the SEN^{CLIM} simulations is identified, rather than directly over the Dead Sea area noting the importance of advected moisture from the Dead Sea evaporative flux upslope and along the Dead Sea valley as well as the indirect effects of a different spatial distribution of low-tropospheric water vapour in the occurrence of precipitating convection.

Regarding the impact on the large-scale conditions, differences in the spatial pattern and strength of the 500 hPa geopotential height field are identified over the Dead Sea (not shown). In the 10-year mean, differences up to 0.002gpdm higher in SEN than in REF are observed. Around the Dead Sea area, the differences are smaller and more irregular. Generally, the differences are higher in the east of the Dead Sea than in the west.

Precipitation probability distribution function

While the probability for lower intensity precipitation is very similar in the REF^{CLIM} and the SEN^{CLIM} simulations differences are recognized in the higher precipitation intensities, from about 150 mm/d (Figure 6a). Particularly, above 180 mm/d extreme precipitation values occur less frequent at the SEN^{CLIM} simulation where a drier, warmer and more stable atmosphere is identified (Figure 2).

SAL

The use of the SAL method in this study differs from the approach frequently presented in literature since it is here not our purpose to examine differences between the simulated field and observations (adequate observations for this comparison are not available in the area), but to compare changes regarding the structure, amount and location of the precipitation field between our reference and sensitivity experiments. Figure 6b shows that when the mean precipitation over the whole simulation period is considered all three SAL components are close to zero, meaning that very small differences are found. However, when single precipitation events in the REF^{CLIM} simulation are compared with the same period at the SEN^{CLIM} simulation, larger differences regarding structure, amount and location of rainfall events are found. For further examination of this issue two exemplary heavy precipitation events (indicated by boxes in Figure 6b) are analysed in detail. In both cases, a negative A-component is recognized, that is, less precipitation falls in the SEN^{CLIM} simulation. The S-component also evidences the change in the structure of the convective cells. The L-component is low meaning that the convective location does not change significantly in the SEN^{CLIM} simulation, in contrast to the intensity and structure of the cells.

3.2 Sensitivity of atmospheric conditions to the Dead Sea drying: episodic investigation

Among those events exhibiting differences in the precipitation field between both simulations (Table 1 and Figure 6b) two situations occurring in the time period of the 14 to 19 November 2011 are investigated in the following.

In this term, the synoptic situation is characterized by a Cyprus low and its frontal system located over the Dead Sea at about 00 UTC on the 15 November 2011 and at 12 UTC on the 18 November 2011. The low-pressure system and its frontal system induced strong south-westerly to westerly winds with mean wind velocities up to 15 m/s.

In the first situation (hereafter CASE1), in association with the western movement of the cold front a convective system develops over the Jordanian Highlands with precipitation starting at about 21 UTC on the 14 November 2011. This convective system is of high interest because of the large difference in its development between the $REF^{14.11}$ and the $SEN^{14.11}$ simulations.

In Figure 7a the 24-h accumulated precipitation, from 14.11 09 UTC to 15.11 08 UTC, in the investigation area is shown for the $REF^{14.11}$ and the $SEN^{14.11}$ simulations. Two precipitation areas are seen, on the north-western and north-eastern of the Dead Sea. Larger difference between models is on the north-eastern region (24-h accumulated precipitation > 100 mm/d in $REF^{14.11}$, while < 50 mm/d in $SEN^{14.11}$), which is the focus of our analysis.

The $REF^{14.11}$ simulation shows that in the 6 hours period prior to the initiation of convection the pre-convective atmosphere and more specifically the lower boundary layer exhibit a moist (IWV ~ 24-30 mm, qvPBLmax ~ 7-10 g/kg) and unstable (CAPE ~ 1100 J/kg; KO-index ~ -8 K; not shown) air mass on the western side of the investigation area, particularly close to the western Mediterranean coast, and drier (IWV~ 8-16; qvPBLmax ~ 4-6 g/kg) and more stable conditions (CAPE< 200 J/kg; KO-index ~ 0-2 K) on the eastern side of the domain (Figure 7b). A maximum difference of about 5 g/kg from west to east is established in the lower boundary layer.

Main differences between both simulations are over the Dead Sea (IWV difference up to 2 mm and qvPBL up to 1.5 g/kg) and north and north-east of it, but almost similar conditions everywhere else. In our target area (subdomain of investigation where the convection episode takes place (red box in Figure 7)), north-east of the Dead Sea, a drier and a more stable atmosphere is identified at the $SEN^{14.11}$ simulation.

The evolution of the wind circulation systems in the area is similar in both simulations (Figure 7c). The 700 hPa, 850 and 950 hPa winds dominantly blow from the south south-west during the pre-convective environment advecting the moist unstable air mass towards the Dead Sea valley and north-east of it, directly affecting the atmospheric conditions at the target area (for a comparison with a climatology of the wind conditions in the region please see Metzger et al. 2017). In both simulations, the passage of the cold front over the Dead Sea establishes a strong southerly wind from about 10 UTC on the 14 November 2011.

Prior to this time, dry air was advected below about 850 hPa towards the target area from the east. The turning of the low-level winds and the resulting moistening of the atmosphere is well and equally captured by both simulations (Figure 8a). Furthermore, at the near-surface, from about 16 UTC, ~ 5 h prior to convection initiation in the target area, a near-surface convergence line forms at the foothills of the northern part of the Jordanian Highlands, which is also well and equally captured by both simulations (Figure 8b). The lifting provided by the convergence line triggers convection in the area. However, the drier and more stable atmosphere in the $SEN^{14.11}$simulation results in less intense convection, weaker updrafts, and reduced precipitation at the eastern slope of the valley.

In the second case, CASE2, we address an episode of localized convection taking place on the north-western edge of the Dead Sea in the REF simulation, whereas no convection develops in the SEN simulation. The isolated convection in the REF simulation left about 50 mm rain in 3 h starting at about 03 UTC on the 19 November 2011 (Figure 9).

In contrast to CASE1, the modification of the pre-convective environment relevant for convective initiation is in this case dominated by dynamical changes in the mesoscale circulations. Differences in the evolution and strength of the Mediterranean Sea Breeze

(MSB), the Dead Sea breeze and orographic winds influence atmospheric conditions in the target area leading to the assistance to or to the absence of convection. The most significant difference observed between the simulations is in the development of a strong near-surface convergence line in the REF simulation (which is not present in the SEN simulation hindering convection in the area), which forms about 2 h before convective initiation (Figure 10).

Even in the first hours of the 18 November 2011 differences in the speed and direction of the near-surface winds over the Dead Sea and on the eastern flank of the Jordanian Highlands could be identified. A fundamental difference between simulations occurs from about 17 UTC when strong westerly winds indicating the arrival of the MSB reach the western shore of the Dead Sea. One hour later, in the REF$^{19.11}$ run the MSB strongly penetrates the Dead Sea valley reaching as far as the eastern coast in the centre to south areas. However, in the SEN$^{19.11}$ simulation the MSB does not penetrate downward, instead strong northerly winds flow along the valley (Figure 10a). Numerous observational and numerical studies carried out to investigate the dynamics of the MSB (e.g. Naor et al. 2017; Vuellers et al. 2018) showed that the downward penetration of the MSB results from temperature differences between the valley air mass, which is warmer than the maritime air mass. An examination of temperature differences along a near-surface north-south valley transect (positions in Figure 10a) indicates a decrease of about 4 ºC at the near-surface over the dried Dead Sea area in contrast to negligible changes on a parallel transect inland, on the western coast of the Dead Sea. These evidences the notorious impact of the absence of water in the valley temperature, thus, gradients in the region. The colder valley temperatures do not favour the downward penetration of the MSB, which strongly affects the atmospheric conditions in the valley. Moreover, a north-easterly land breeze is visible from about 20 UTC on the eastern shore of the Dead Sea in the REF$^{19.11}$ simulation, but not in the SEN$^{19.11}$ simulation (Figure 10b). This situation reflects an interesting case different from the ones generally presented in former investigations in the area (e.g. Alpert et al. 1997 ; and Alpert et al. 2006b) in which due to the recent weakening of the Dead-Sea breeze, mainly because of the drying and shrinking of the Sea, the Mediterranean breeze penetrates stronger and earlier into the Dead-Sea Valley increasing the evaporation because of the strong, hot and dry wind.

Mountain downslope winds develop in both simulations from about 22 UTC. One hour later, strong northerly valley flow in the northern part of the Dead Sea contrasts with the westerly flow in the SEN$^{19.11}$ simulation (Figure 10c). As the valley cools down during night time in the SEN simulation, T2m decreases about 1 K from 20 UTC to 03 UTC in contrast with the 0.1 K decrease of the Dead Sea in the REF simulation, the temperature gradient weakens and the northerly valley flow present in the REF simulation is absent in the SEN simulation. During the night, the synoptic conditions gain more influence than the local wind systems governing the conditions in the valley during day time. South-easterly winds prevail in the valley in both simulations. Much stronger wind velocities are reached in the REF simulation, confirming the sensitivity of large-scale dynamics to near-surface climate change-induced impacts.

The encounter of the north north-westerly and south south-easterly winds over the Dead Sea area in the $REF^{19.11}$ simulation induces the formation of a convergence zone, which intensifies and extends offshore over the next hours and determines the location of convective initiation. Meanwhile, homogeneous south-easterly winds are observed in the SEN simulation (Figure 10d).

The differences in the wind circulations contribute to a different distribution of the atmospheric conditions in the target area, particularly, low-tropospheric water vapour as seen in the vertical cross sections in Figure 11. The evolution of the atmospheric conditions in the 3-h period prior to convective initiation evidences the deeper and wetter boundary layer in the $REF^{19.11}$ simulation at the north-western foothills of the ridge at the Jordanian Highlands. Differences of IWV up to 2 mm, and of instability (CAPE) close to 200 J/kg are found in this area (not shown). This is the location of the convergence line where convective updrafts, which start close to the ground, are triggered reaching a maximum vertical velocity of about 5 m/s above the convergence zone in the $REF^{19.11}$ simulation.

4. Conclusions

The drying and shrinking of the Dead Sea has been extensively investigated in the last decades from different points of view. This process has been related to significant local climate changes which affect the Dead Sea valley and neighboring regions. The climate of the Dead Sea is very hot and dry. But occasionally the Dead Sea basin is affected by severe convection generating heavy precipitation, which could lead to devastating flash floods.

In this study, high-resolution COSMO model simulations are used to assess the impact of the Dead Sea on the occurrence of convective precipitation in the region. A set of high-resolution, ~ 2.8 km, climate simulations covering the period 2003 to 2013, and several numerical weather prediction (NWP) runs on an event time scale (~ 48-36 h) are performed over the Dead Sea area. On a decadal time scale, two simulations are carried out. The first “reference” run with the Dead Sea area, and a second run “sensitivity” in which the Dead Sea is dried out and set to bare soil. The NWP simulations focus on two heavy precipitation events exhibiting relevant differences between the reference and the sensitivity decadal runs. A total of four simulations are performed in this case.

As the energy balance partitioning of the Earth’s surface changes due to the drying of the Dead Sea, relevant impacts could be identified in the region. From a climatological point of view, in a future regional climate under ongoing Dead Sea level decline, less evaporation, higher air temperatures and less precipitation is to expect. Reduced evaporation over the Dead Sea occurs from May to October. The cooling effect of evaporation in the neighboring areas results in an increase of T-2m in the absence of the Dead Sea. Atmospheric conditions, such as air temperature and humidity, are mostly affected in the lower-tropospheric levels, which in turn influence atmospheric stability conditions, hence, precipitating convection. In general, the number of dry/wet days is not largely affected by the drying of the Dead Sea, although these differences could be larger for hourly precipitation; rather the structure and intensity of the heavier precipitation events is changed. While a general and homogeneous decrease in evaporation is seen at the SEN^{CLIM} simulation, precipitation deviations occur in both directions, which could suggest and impact on the timing of the events. A relevant year to year variability is observed in evaporation-precipitation which indicates the need of long time series of observations to understand local conditions and to validate model simulations.

The detailed analysis of two heavy precipitation events allowed us to further assess the possible causes and the processes involved regarding the decrease in precipitation intensity or the total omission of convection with respect to the reference simulation in the absence of the Dead Sea water. Two main components, strongly affected by the drying of the Dead Sea, are found to be highly relevant for the understanding of the environmental processes in the Dead Sea region.

(a) First, the lower-atmospheric boundary layer conditions. Changes in the energy balance affect the atmosphere through the heat exchange and moisture supply. The drying of the Dead Sea in the SEN simulations and the resulting decrease in local evaporation, impact the Dead Sea Basin conditions and the neighbouring areas. A reduction in boundary layer humidity and an increase in temperature result in a general decrease of atmospheric instability and weaker updrafts indicating reduced deep-convective activity. Main differences on the atmospheric conditions are directly over the Dead Sea, but these conditions are frequently advected to neighbouring areas by the thermally driven wind systems in the region which play a key role for the redistribution of these conditions and the initiation of convection.

(b) Secondly, wind systems in the valley. In the arid region of the Dead Sea Basin with varied topography, thermally and dynamically driven wind systems are key features of the local climate. Three different scales of climatic phenomena coexist: The Mediterranean Sea Breeze (MSB), the Dead Sea breeze and the orographic winds, valley-, and slope-winds, which are known to temper the climate in the Dead Sea valley (Shafir and Alpert, 2011). The drying of the Dead Sea in the SEN simulation disturbs the Dead Sea thermally driven wind circulations. The Dead Sea breezes are missing, weaker wind speeds characterize the region and along valley winds are consequently affected. Furthermore, the dynamics of the Mediterranean breeze penetration into the Jordan Valley are affected.

Consequently, the impacts on convection initiation and development are twofold:
(i) Distinct redistribution of atmospheric conditions, locally or remotely, which yields to different atmospheric conditions that in the absence of the Dead Sea result in a reduced moisture availability in the lower atmospheric levels and increased stability hindering convection or reducing the intensity of the events.
(ii) Modification of the divergence/convergence field. The absence of the Dead Sea substantially modifies the wind circulation systems over the Dead Sea valley, which leads to the omission of convergence lines which act as triggering mechanism for convection.

We can conclude that in general the lack of sufficient low-atmospheric moisture in relation to the drying of the Dead Sea, the increase of atmospheric stability in addition to an absence or reduction in the intensity of the convergence zones, works against initiation or intensification of precipitating convection in the area. The relevance of the small-scale variability of moisture and the correct definition and location of convergence lines for an accurate representation of convective initiation illustrates the limitation and the lack of adequate observational networks in the area and the need for high-resolution model simulations of boundary layer processes to predict intense and localised convection in the region.

These results contribute to gain a better understanding of expected conditions in the Dead Sea valley and neighbouring areas under continual lake level decline. Energy balance partitioning and wind circulation systems are determinant for local climatic conditions, e.g. temperature and humidity fields as well as aerosol redistribution, therefore, any change should be well understood and properly represented in model simulations of the region. Our results point out, in agreement with past modelling activities in the region, the need to further improve the representation of precipitation fields in the area, particularly close to the Mediterranean coastline. More accurate Mediterranean SST input fields have been suggested as relevant to reduce the model inaccuracies. Furthermore, a more realistic representation of the lake shape, water salinity and temperature, as well as Dead Sea abundance must be addressed to accurately describe the impact on the simulation results. In a further step, the authors will investigate some of these issues performing sensitivity experiments, and will assess the impact of model grid resolution on the horizontal and vertical flow field in the region across scales, including the impact on large-scale dynamics. We will also put emphasis in trying to better understand the dynamics of the MSB under lake level decline using high-resolution modelling, especially the contrasting behaviour pointed out in this study. Fine resolution simulations up to 100 m will be performed for this purpose. Furthermore, we will provide a verification of the complex chain of processes in the area using unique measurements in the framework of the interdisciplinary virtual institute Dead Sea Research VEnue (DESERVE; Kottmeier et al., 2016).

Author contribution

SK wrote the manuscript, analysed the data, interpreted the results and supervised the work. JH carried out data analysis, interpretation of results and prepared all the figures.

Acknowledgements

The first author's research was supported by the Bundesministerium für Bildung und Forschung (BMBF; German Federal Ministry of Education and Research). The authors acknowledge the colleagues at the Karlsruhe Institute of Technology (KIT) involved in the interdisciplinary virtual institute Dead Sea Research VEnue (DESERVE) for their support and interesting discussions. We acknowledge Sebastian Helgert and Alberto Caldas Alvarez for their assistance in the preparation of the simulations. This article is a contribution to the HyMeX program.

References

Alpert, P., and Shay-EL, Y.,: The Moisture Source for the Winter Cyclones in the Eastern Mediterranean. Israel Meteorological Research Papers, 5, 20-27, 1994.

Alpert, P., and Coauthors: Relations between climate variability in the Mediterranean region and the tropics: ENSO, South Asian and African monsoons, hurricanes and Saharan dust. Developments in Earth and Environmental Sciences, 4, 149-177, https://doi.org/10.1016/S1571-9197(06)80005-4, 2006.

Alpert, P., Shafir, H., and Issahary, D.,: Recent Changes in the Climate At the Dead Sea – a Preliminary Study. Climatic Change, 37(3), 513-537, https://doi.org/10.1023/A:1005330908974, 1997.

Andersson, T., Andersson, M., Jacobsson, C., Nilsson, S.: Thermodynamic indices for forecasting thunderstorms in southern Sweden. Meteorol. Mag. 116, 141-146, 1989.

Arkin, Y., and Gilat, A.: Dead Sea sinkholes - an ever-developing hazard. Environmental Geology, 39(7), 711-722, https://doi.org/10.1007/s002540050485, 2000.

Ashbel, D., and Brooks, C.: The influence of the dead sea on the climate of its neighbourhood. Quarterly Journal of the Royal Meteorological Society, 65(280), 185-194, https://doi.org/10.1002/qj.49706528005, 1939.

Ban, N., Schmidli, J., and Schär, C.: Evaluation of the convection-resolving regional climate modeling approach in decade-long simulations, J. Geophys. Res. Atmos., 119, 7889– 7907, https://doi.org/10.1002/2014JD021478, 2014.

Belachsen, I., Marra, F., Peleg, N., and Morin, E.: Convective rainfall in dry climate: relations with synoptic systems and flash-flood generation in the Dead Sea region. Hydrology and Earth System Sciences Discussions, 21, 5165-5180, https://doi.org/10.5194/hess-21-5165-2017, 2017.

Böhm, U., and Coauthors: The Climate Version of LM: Brief Description and Long-Term Applications. COSMO Newsletter, 6, 225-235, 2006.

Businger, J., Wyngaard, J., Izumi, Y., and Bradley, E.: Flux-Profile Relationships in the Atmospheric Surface Layer. Journal of the Atmospheric Sciences, 28(2), 181-189, https://doi.org/10.1175/1520-0469(1971)028<0181:FPRITA>2.0.CO;2, 1971.

Byun, H., and Kim, D.: Comparing the Effective Drought Index and the Standardized Precipitation Index. Options Méditerranéennes. Séries A. Mediterranean Seminars, 95, 85-89, 2010.

Byun, H., and Wilhite, D.: Objective quantification of drought severity and duration. J. Climate, 12(9), 2747-2756, https://doi.org/10.1175/1520-0442(1999)012<2747:OQODSA>2.0.CO;2, 1999.

Cohen, S., and Stanhill, G.: Contemporary Climate Change in the Jordan Valley. J. Appl. Meteor., 35(7), 1051-1058, https://doi.org/10.1175/1520-0450(1996)035<1051:CCCITJ>2.0.CO;2, 1996.

Corsmeier, U., Behrendt, R., Drobinski, P., Kottmeier, C.: The mistral and its effect on air pollution transport and vertical mixing, Atmos. Res., 74, 275–302, https://doi.org/https://doi.org/10.1016/j.atmosres.2004.04.010, 2005.

Dayan, U., and Morin, E.: Flash flood – producing rainstorms over the Dead Sea: A review. Geological Society of America, 401(4), 53-62, https://doi.org/10.1130/2006.2401(04) , 2006.

Dayan, U., and Sharon, D.: Meteorological parameters for discriminating between widespread and spotty storms in the Negev. Israel Journal of Earth Sciences, 29(4), 253-256, 1980.

Dayan, U., Ziv, B., Margalit, A., Morin, E., and Sharon, D.: A severe autumn storm over the middle-east: synoptic and mesoscale convection analysis. Theoretical and Applied Climatology, 69(1-2), 103-122, https://doi.org/10.1007/s007040170038, 2001.

Doms, G., and Baldauf, M.: A Description of the Nonhydrostatic Regional COSMO-Model. Part I: Dynamics and Numerics. Deutscher Wetterdienst, 2015.

Doswell, C., and Rasmussen, E.: The Effect of Neglecting the Virtual Temperature Correction on CAPE Calculations. Weather and Forecasting, 9(4), 625-629, https://doi.org/10.1175/1520-0434(1994)009<0625:TEONTV>2.0.CO;2, 1994.

FAO/IIASA/ISRIC/ISSCAS/JRC.: Harmonized World Soil Database (version 1.2). FAO, Rome, Italy and IIASA, Laxenburg, Austria, (accessed 01.02.2017) , 2009.

Fosser, G., Khodayar, S., and Berg, P., 2014: Benefit of convection permitting climate model simulations in the representation of convective precipitation, Clim. Dyn., 44(1– 2), 45– 60.

Gavrieli, I., Bein, A., and Oren, A., 2005: The expected impact of the “Peace Conduit” project (the Red Sea - Dead Sea pipeline) on the Dead Sea. Mitigation and Adaptation Strategies for Global Change, 10(4), 759-777, https://doi.org/10.1007/s11027-005-5144-z.

European Commission, Joint Research Centre, 2003: Global Land Cover 2000 database, (accessed 01.02.2017).

GLOBE National Geophysical Data Center, 1999: Global Land One-kilometer Base Elevation (GLOBE) v.1. Hastings, D. and P.K. Dunbar. National Geophysical Data Center, NOAA, (accessed 01.02.2017).

Greenbaum, N., Ben-Zvi, A., Haviv, I., and Enzel, Y., 2006: The hydrology and paleohydrology of the Dead Sea tributaries. Geological Society of America, 401(4), 63-93, https://doi.org/10.1130/2006.2401(05).

Haylock, M.R., Hofstra, N., Klein Tank, A.M.G., Klok, E.J., Jones, P.D. and New, M. 2008, A European daily high-resolution gridded dataset of surface temperature and precipitation. Journal of Geophysical Research: Atmospheres, 113, D20119. https://doi.org/10.1029/2008JD10201.

Hochman, A., Mercogliano, P., Alpert, P., Saaroni, H. and Bucchignani, E., 2018. High-resolution projection of climate change and extremity over Israel using COSMO-CLM. International Journal of Climatology, 38(14), pp.5095-5106.

Houze, R., 2012: Orographic effects on precipitating clouds. Reviews of Geophysics, 50(1), https://doi.org/10.1029/2011RG000365.

Kalthoff, N., Horlacher, V., Corsmeier, U., Volz-Thomas, A., Kolahgar, B., Geiß, H., Möllmann-Coers, M., and Knaps, A. 2000: Influence of valley winds on transport and dispersion of airborne pollutants in the Freiburg-Schauinsland area, J. Geophys. Res. Atmos, 105, 1585–1597, https://doi.org/10.1029/1999jd900999.

Khodayar, S., Kalthoff, N., and Schaedler, G., 2013: The impact of soil moisture variability on seasonal convective precipitation simulations. Part I: validation, feedbacks, and realistic initialisation. Meteorologische Zeitschrift, 22(4), 489-505, https://doi.org/10.1127/0941-2948/2013/0403.

Kunin, P., Alpert, P. and Rostkier-Edelstein, D., 2019. Investigation of sea-breeze/foehn in the Dead Sea valley employing high resolution WRF and observations. Atmospheric Research.

Lensky, N. and Dente, E., 2015. The hydrological proecesses driving the accelerated Dead Sea level decline in the past decades. Geological Survey of Israel Report.

Llasat, M., and Coauthors, 2010: High-impact floods and flash floods in Mediterranean countries: the FLASH preliminary database. Advances in Geosciences, 23, 47-55, https://doi.org/10.5194/adgeo-23-47-2010.

Metzger, J., Nied, M., Corsmeier, U., Kleffmann, J., and Kottmeier, C., 2017: Dead Sea evaporation by eddy covariance measurements versus aerodynamic, energy budget, Priestley-Taylor, and Penman estimates. Hydrology and Earth System Sciences Discussions, 22(2), 1135-1155, https://doi.org/10.5194/hess-2017-187.

Miglietta MM, Conte D, Mannarini G, Lacorata G, Rotunno R. 2011. Numerical analysis of a Mediterranean 'hurricane' over south-eastern Italy: sensitivity experiments to sea surface temperature. *Atmos. Res.* **101**: 412–426.

Moncrieff, M., and Miller, M., 1976: The dynamics and simulation of tropical cumulonimbus and squall lines. Quarterly Journal of the Royal Meteorological Society, 102(432), 373-394, https://doi.org/10.1002/qj.49710243208, 2014.

Naor, R., Potchter, O., Shafir, H., and Alpert, P.: An observational study of the summer Mediterranean Sea breeze front penetration into the complex topography of the Jordan Rift Valley, Theor. Appl. Climatol., 127, 275–284, https://doi.org/10.1007/s00704-015-1635-3, 2017.

Prein, A., Gobiet, A., Suklitsch, M., Truhetz, H., Awan, N., Keuler, K., and Georgievski, G. : Added value of convection permitting seasonal simulations, Clim. Dyn., 41(9– 10), 2655– 2677, 2013.

Ritter, B., and J.-F. Geleyn, 1992. A comprehensive radiation scheme for numerical weather prediction models with potential applications in climate simulations. Mon. Wea. Rev., 120, 303–325.

Rostkier-Edelstein, D., Liu, Y., Wu, W., Kunin, P., Givati, A. and Ge, M., 2014. Towards a high-resolution climatography of seasonal precipitation over Israel. International Journal of Climatology, 34(6), pp.1964-1979.

Schaedler, G., and Sasse, R.: Analysis of the connection between precipitation and synoptic scale processes in the Eastern Mediterranean using self-organizing maps. Meteorologische Zeitschrift, 15(3), 273-278, https://doi.org/10.1127/0941-2948/2006/0105, 2006.

Shafir, H., and Alpert, P.: Regional and local climatic effects on the Dead-Sea evaporation. Climatic Change, 105(3-4), 455-468, https://doi.org/10.1007/s10584-010-9892-8, 2011.

Sharon, D., and Kutiel, H.: The distribution of rainfall intensity in Israel, its regional and seasonal variations and its climatological evaluation. International Journal of Climatology, 6(3), 277-291, https://doi.org/10.1002/joc.3370060304, 1986.

Smiatek, G., Kunstmann, H., and Heckl, A.: High-resolution climate change simulations for the Jordan River area. Journal of Geophysical Research, 116(D16), https://doi.org/10.1029/2010JD015313, 2011.

Stanhill, G.: Changes in the rate of evaporation from the dead sea. International Journal of Climatology, 14(4), 465-471, https://doi.org/10.1002/joc.3370140409,1994.

Vicente-Serrano, S., Beguería, S., López-Moreno, J.: A Multiscalar Drought Index Sensitive to Global Warming: The Standardized Precipitation Evapotranspiration Index. J. Climate, 23(7), 1696-1718, https://doi.org/10.1175/2009JCLI2909.1, 2010.

Vüllers, J., Mayr, G. J., Corsmeier, U., and Kottmeier, C.: Characteristics and evolution of diurnal foehn events in the Dead Sea valley. Atmos. Chem. Phys., 18, 18169-18186, https://doi.org/10.5194/acp-18-18169-2018, 20, 2018.

Wernli H, Paulat M, Hagen M, Frei C. SAL – a novel quality measure for the verification of quantitative precipitation forecasts. Mon. Weather Rev. 136: 4470–4487, 2008.

Yatagai, A., Alpert, P. and Xie, P. (2008) Development of a daily gridded precipitation data set for the Middle East. Advances in Geosciences, 12, 1–6.

Yatagai, A., Kamiguchi, K., Arakawa, O., Hamada, A., Yasutomi, N. and Kitoh, A., 2012: APHRODITE: constructing a long-term daily gridded precipitation dataset for Asia based on a dense network of rain gauges. Bulletin of the American Meteorological Society, 93, 1401–1415.

Tables

	PREC $_{diffmn}$	REF $_{PMX}$	SEN $_{PMX}$	PREC relative diff [%]	Synoptic Situation	REF $_{CAPEmx}$	SEN $_{CAPEmx}$	REF $_{KOmn}$	SEN $_{KOmn}$	Localised/ Widespread (Subarea affected)
08.12.2004	0,10	30,09	31,31	2,76	ARST	1	1	4,85	4,85	W (A1, A2)
13.01.2006	-0,11	45,64	54,64	-4,26	Cyprus Low	239	225	6,57	6,54	L/W (A1, A3)
16.04.2006	0,11	57,41	56,09	4,89	Syrian Low	43	47	1,97	1,94	L (A1, A4)
10.04.2007	0,29	42,61	70,20	30,78	Cyprus Low	686	679	-4,77	-4,70	L (A2, A4)
13.04.2007	0,12	134,36	127,79	1,62	Cyprus Low	573	576	-1,95	-1,92	L (A1, A2, A3, A4)
12.05.2007	-0,16	41,82	47,90	-8,24	Syrian Low	436	81	-5,30	-5,29	L (A1, A2)
27.01.2008	-0,14	23,11	17,24	-17,25	Syrian Low	7	7	5,12	5,12	W (A1, A3)
25.10.2008	-0,23	139,01	125,73	-16,52	ARST	1274	1361	-5,50	-4,08	L (A3)
13.11.2008	0,30	40,83	45,55	25,68	ARST	25	7	1,37	1,38	L (A2, A4)
14.05.2009	-0,39	59,28	68,84	-8,49	Syrian Low	433	429	-3,90	-3,91	L (A1, A2, A3, A4)
15.05.2009	0,20	49,23	42,28	13,50	Syrian Low	208	203	-2,30	-2,36	L (A1, A2, A3)
31.10.2009	-0,19	166,21	111,79	-7,65	Cyprus Low	435	445	-5,03	-4,46	L (A1, A2)
15.01.2011	0,11	73,02	72,03	3,74	Syrian Low	49	37	7,82	7,83	L/W (A1, A4)
28.05.2011	-0,24	44,51	32,73	-14,33	Cyprus Low	158	170	-10,27	-10,26	W (A2)
15.11.2011	-0,11	42,65	9,34	-65,90	Cyprus Low	2	0	-7,14	-7,12	L (A1, A2)
17.11.2011	0,11	90,07	93,04	4,76	Cyprus Low	386	304	-9,14	-9,16	L (A1)
18.11.2011	-0,11	28,68	34,69	-8,67	Cyprus Low	356	378	-8,61	-8,65	L (A1)
19.11.2011	0,03	58,11	12,36	4,09	Cyprus Low	133	81	-7,60	-7,46	L (A2, A4)
22.10.2012	0,20	29,88	41,64	51,21	ARST	2068	2097	-5,83	-5,59	L (A1, A2)
09.11.2012	-0,11	27,20	22,56	-18,29	Cyprus Low	218	215	3,97	3,98	W (A1)
23.11.2012	-0,21	155,77	117,81	-10,17	ARST	189	286	-2,18	-1,95	L (A1, A2, A3)
25.11.2012	-0,11	41,48	54,33	-7,87	ARST	354	332	4,19	4,37	L (A3, A4)

Table 1: Classification of heavy precipitation cases in the decadal simulation covering the period 2004 to 2013. The areal-mean (study area, Figure 1) difference (PREC$_{diffmn}$) and maximum grid precipitation in the reference (REF$_{PMX}$) and sensitivity (SEN$_{PMX}$) realizations, the precipitation relative difference in %, the synoptic situation, and the stability conditions illustrated by maximum grid point CAPE (CAPEmx) and minimum grid point KO-index (KOmn) are summarized. Additionally, the nature of the precipitation, localized (L) or widespread (W) and the main subarea affected (following division in Figure 1; A1, A2, A3, A4) are listed.

Figures

(a)

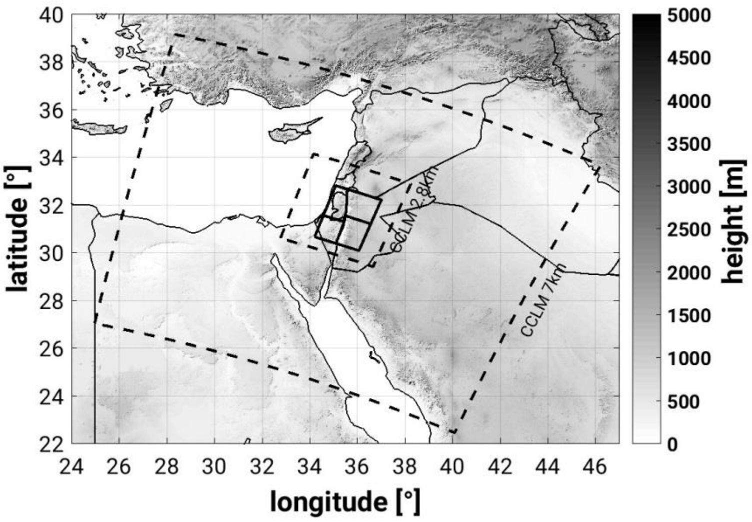

(b)

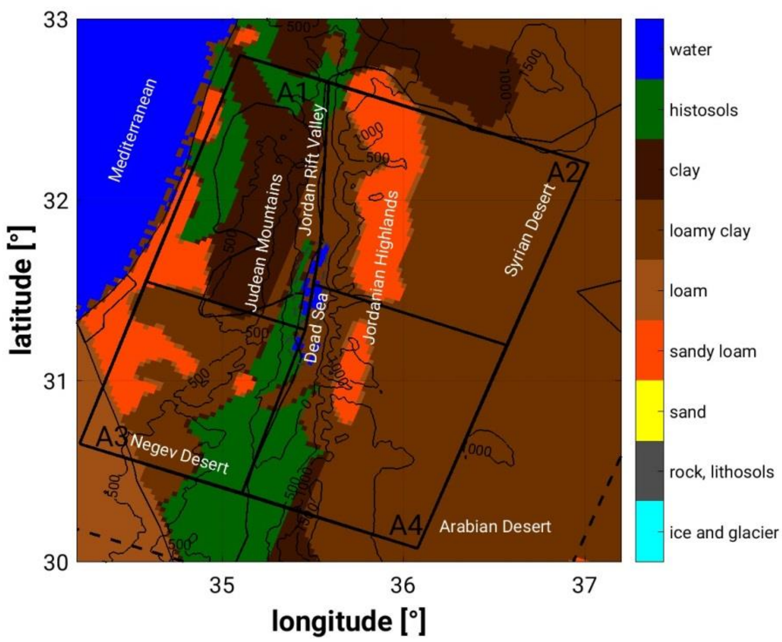

Figure 1: (a) Topography (m above msl), simulation domains (dashed lines, CCLM7km and CCLM2.8km) and study area (bold line). (b) Model soil types (colour scale), topography (black isolines) and study area (black bold line) including the 4 subdomains to be examined, A1-4 (Area 1-4).

(a)

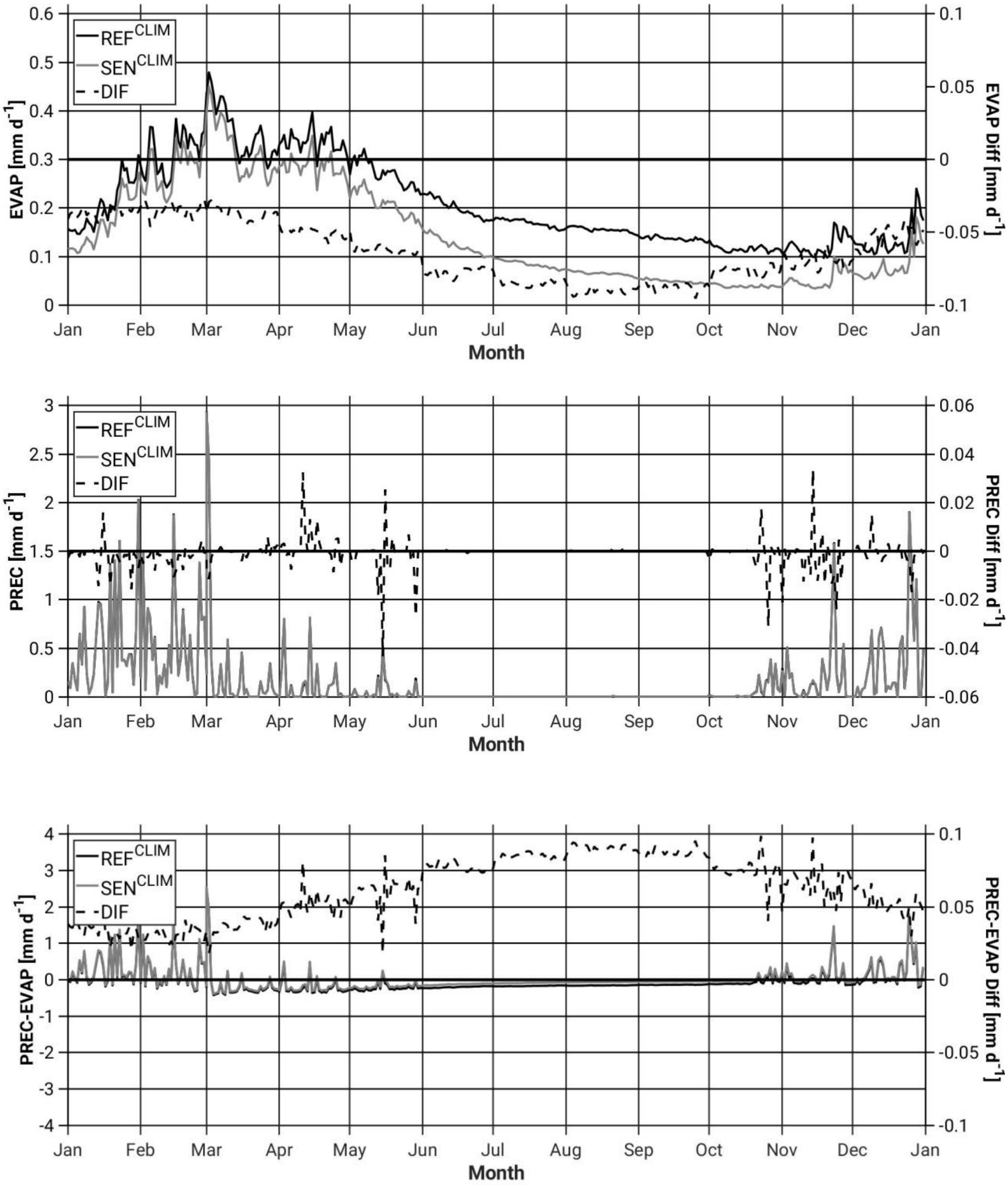
REF^CLIM
SEN^CLIM
DIF
EVAP [mm d^-1]
EVAP Diff [mm d^-1]
PREC [mm d^-1]
PREC Diff [mm d^-1]
PREC-EVAP [mm d^-1]
PREC-EVAP Diff [mm d^-1]
Jan Feb Mar Apr May Jun Jul Aug Sep Oct Nov Dec Jan
Month

(b)

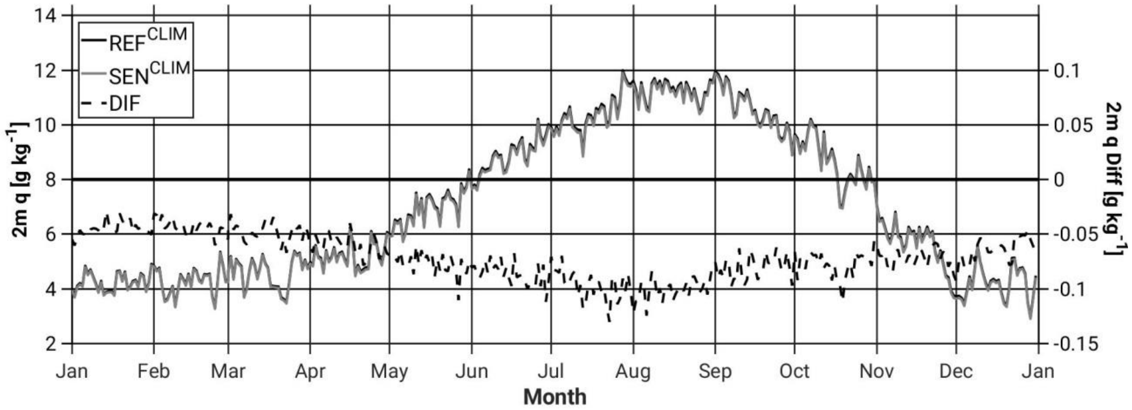
REF^CLIM
SEN^CLIM
DIF
2m q [g kg^-1]
2m q Diff [g kg^-1]
14
12
10
8
6
4
2
0.1
0.05
0
-0.05
-0.1
-0.15
Jan Feb Mar Apr May Jun Jul Aug Sep Oct Nov Dec Jan
Month

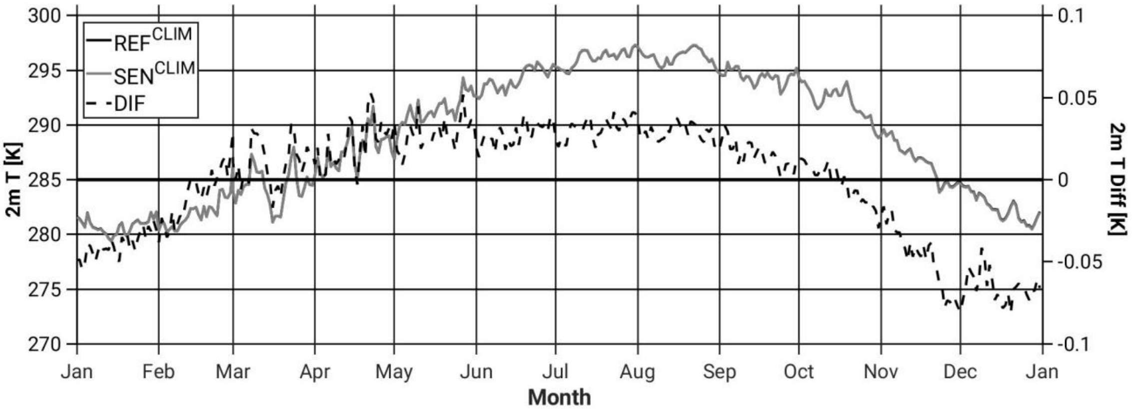
REF^CLIM
SEN^CLIM
DIF
2m T [K]
2m T Diff [K]
300
295
290
285
280
275
270
0.1
0.05
0
-0.05
-0.1
Jan Feb Mar Apr May Jun Jul Aug Sep Oct Nov Dec Jan
Month

(c)

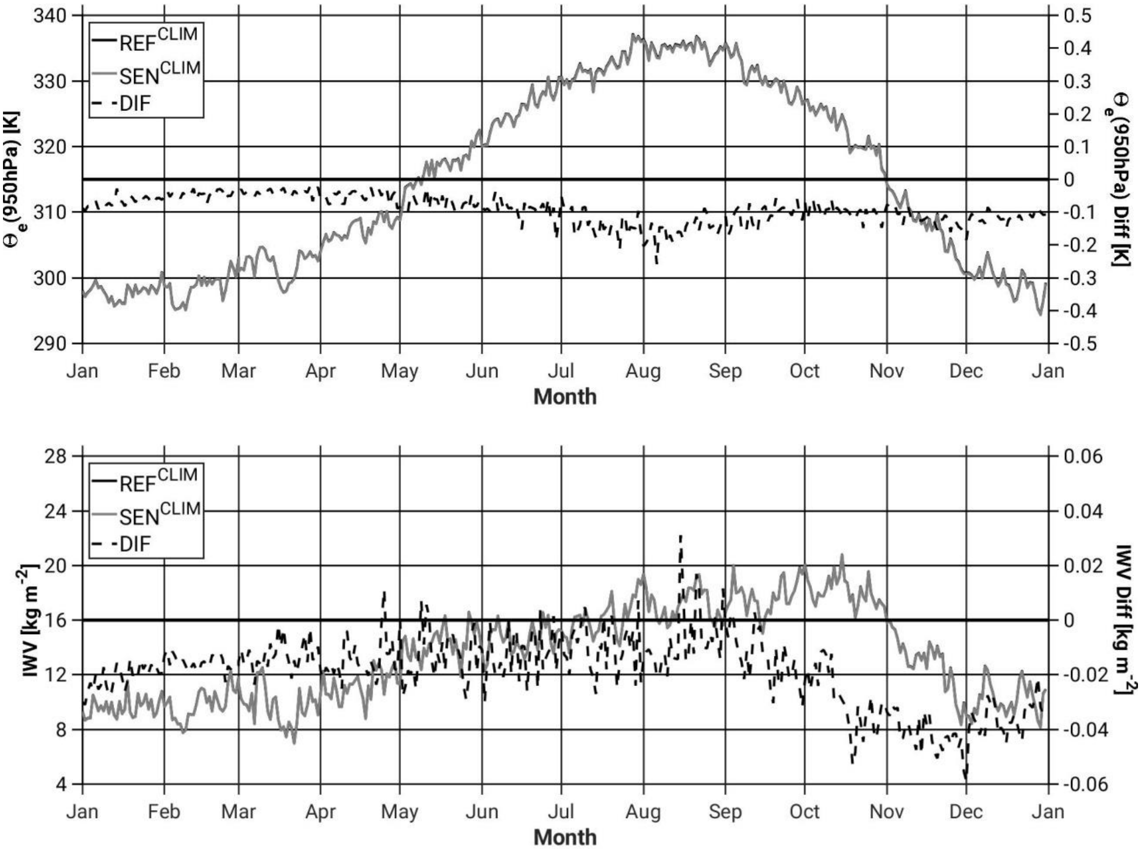
REF^CLIM
SEN^CLIM
DIF
Θe(950hPa) [K]
Θe(950hPa) Diff [K]
340
330
320
310
300
290
0.5
0.4
0.3
0.2
0.1
0
-0.1
-0.2
-0.3
-0.4
-0.5
Jan Feb Mar Apr May Jun Jul Aug Sep Oct Nov Dec Jan
Month
REF^CLIM
SEN^CLIM
DIF
IWV [kg m^-2]
IWV Diff [kg m^-2]
28
24
20
16
12
8
4
0.06
0.04
0.02
0
-0.02
-0.04
-0.06
Jan Feb Mar Apr May Jun Jul Aug Sep Oct Nov Dec Jan
Month

(d)

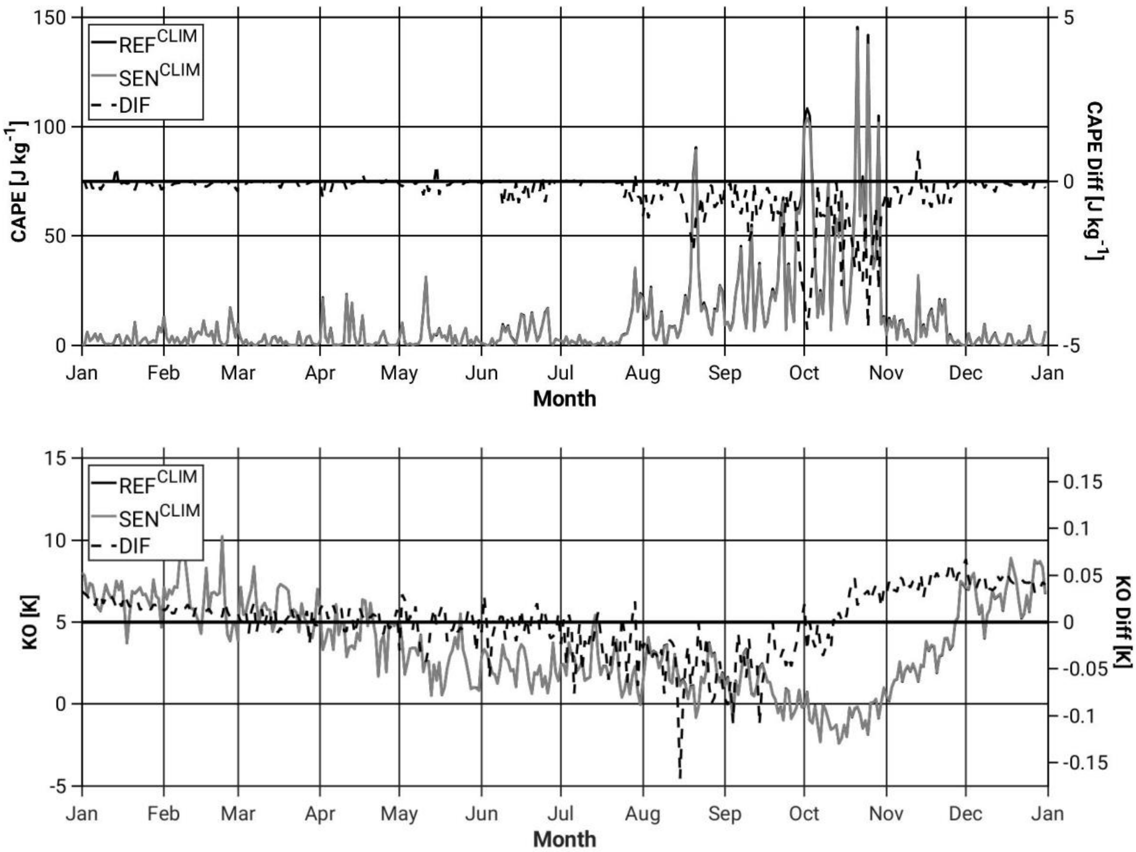

Figure 2: Annual cycle of the areal-daily averaged (and differences (black dashed line; SEN-REF)) of (a) evaporation, precipitation, and precipitation minus evaporation (b) specific humidity and temperature at 2-m, and (c) Θ_e below 950 hPa and IWV, and (d) CAPE and KO-index, from the REF^{CLIM} (full black line) and the SEN^{CLIM} (full grey line) simulations. All grid points in the study area (Figure 1) and the period 2004 to 2013 are considered.

(a)

Area1 (NW)

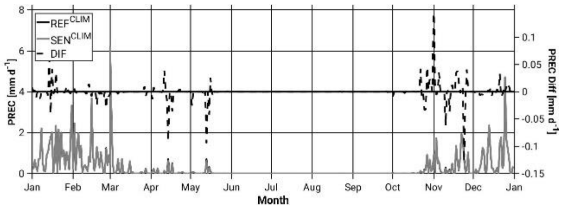

Area2 (NE)

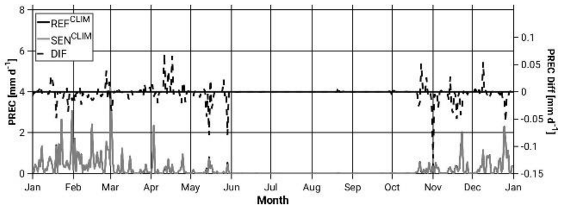

Area3 (SW)

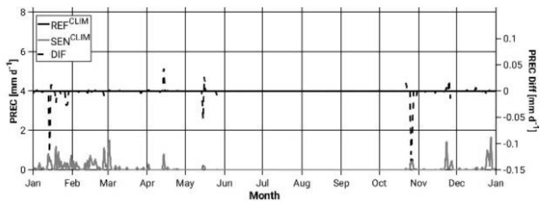

Area4 (SE)

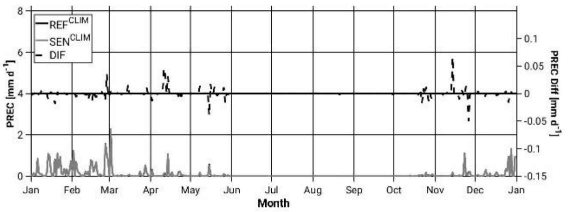

(b)

Area1 (NW)

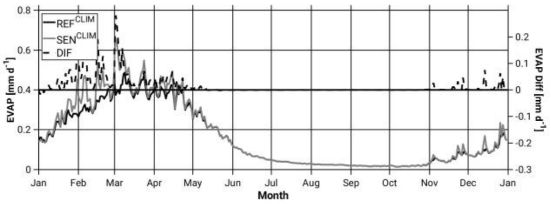

Area2 (NE)

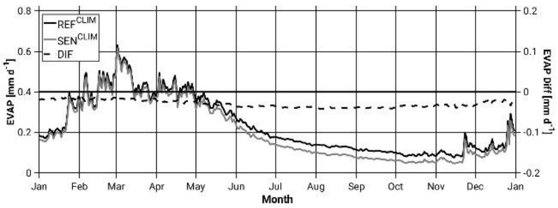

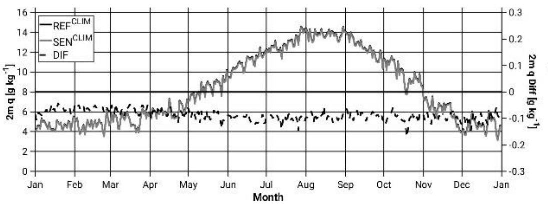

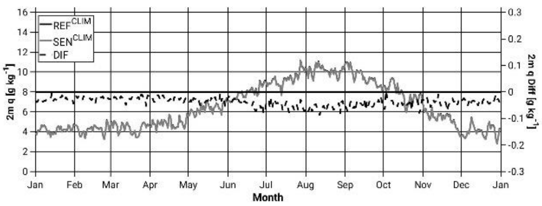

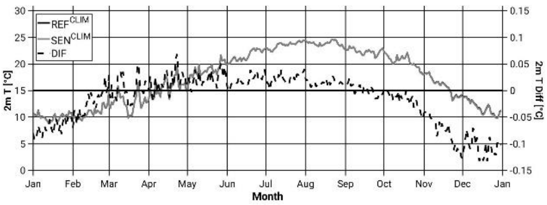

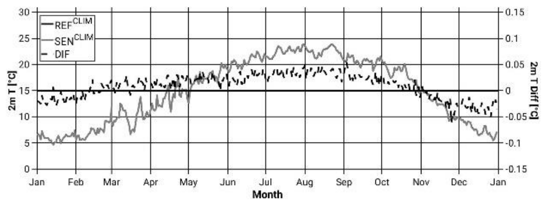

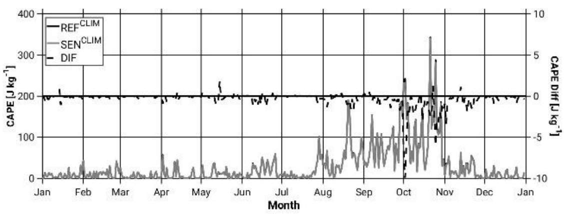

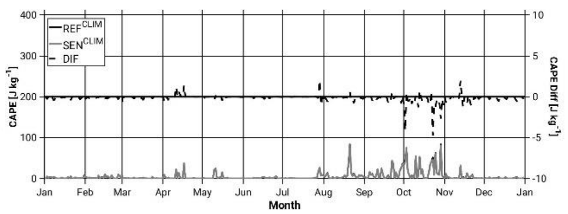

Figure 3: Annual cycle of the areal-daily averaged (and differences (black dashed line; SEN-REF)) of (a) precipitation for areas A1, A2, A3, A4 (see Figure 1b), and (b) evaporation, specific humidity and temperature at 2-m, and CAPE for areas A1 and A2, from the REF^{CLIM} (full black line) and the SEN^{CLIM} (full grey line) simulations. Only land points in the study area (Figure 1) for evaporation, and all grid points for the rest of variables and the period 2004 to 2013 are considered.

(a)

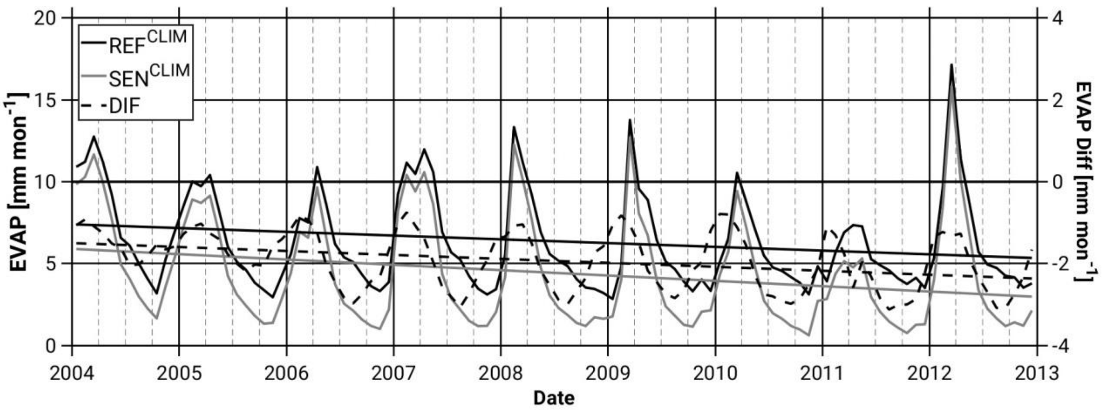

(b)

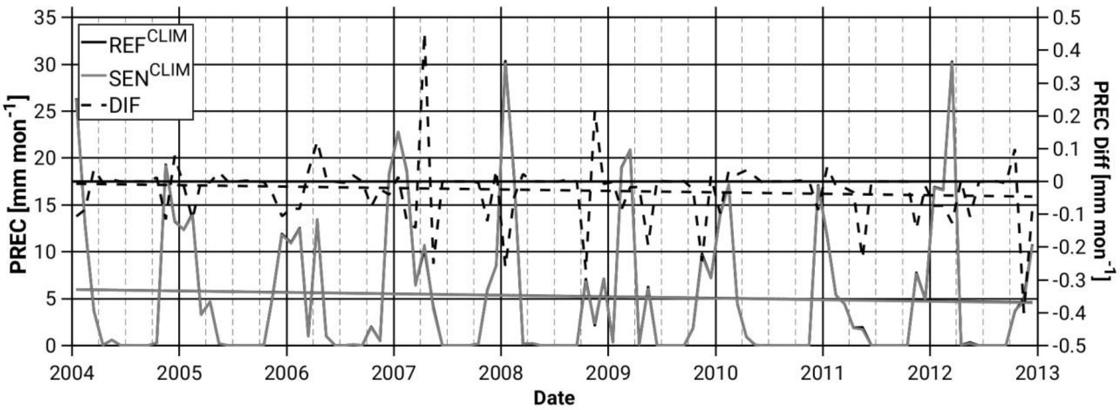

(c)

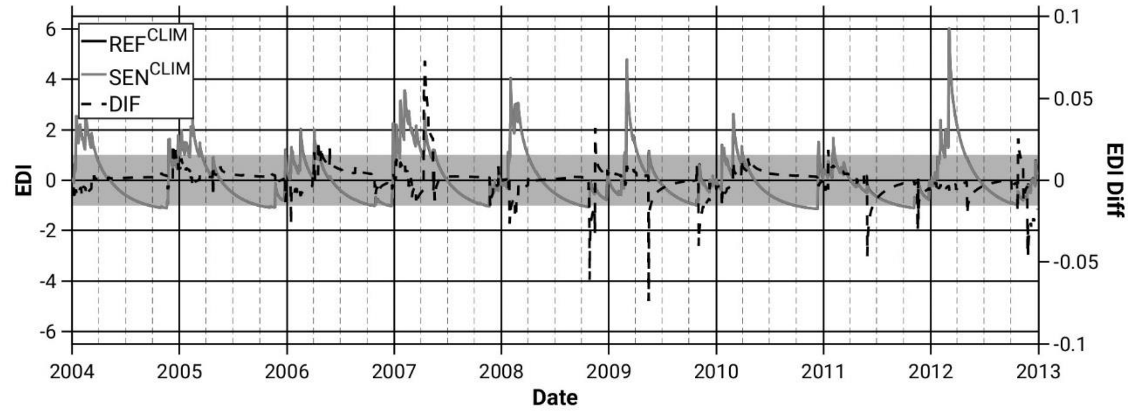

Figure 4: Temporal evolution of the monthly-daily accumulated areal mean values of (a) Evaporation, (b) Precipitation, (c) Effective Drought Index (EDI), from the REF^{CLIM} (full black line) and the SEN^{CLIM} (full grey line) simulations and differences depicted with black dashed lines. The light grey band in (c) indicates the common soil state (-1<EDI<+1). All grid points in the study area (Figure 1) and the period 2004 to 2013 are considered.

(a)

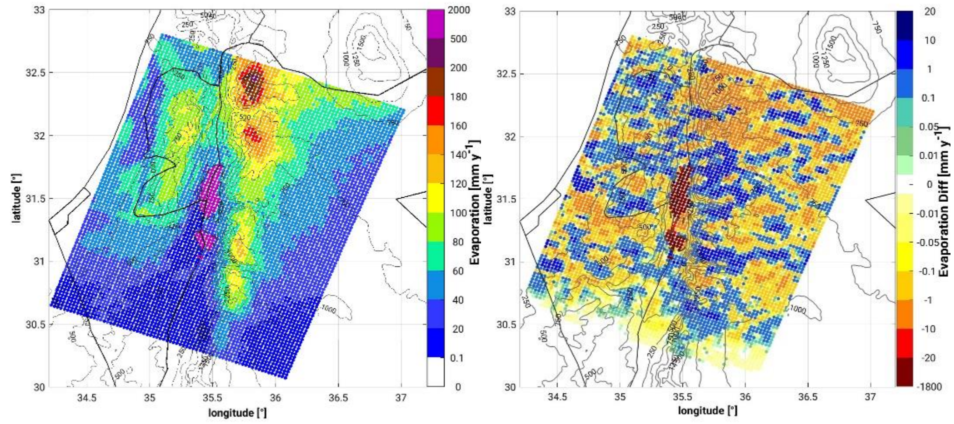

(b)

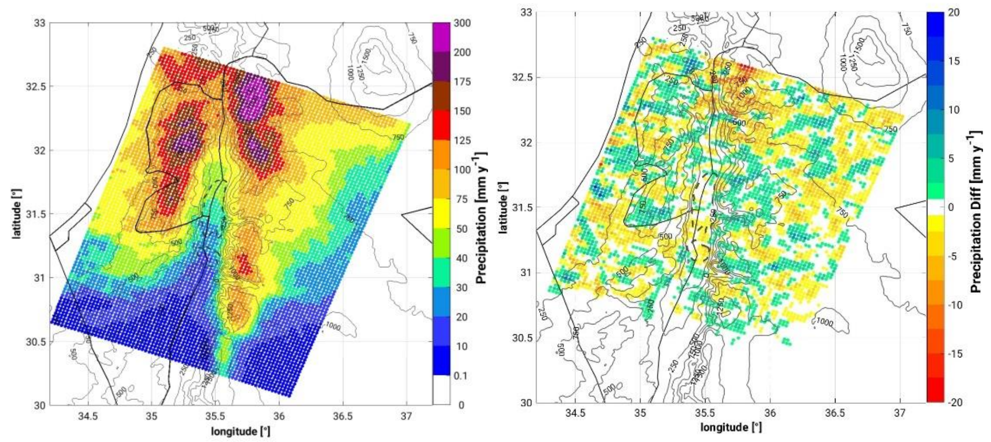

Figure 5: Spatial distribution of (a) evaporation in the REF^{CLIM} simulation (left) and the difference between the SEN^{CLIM} and the REF^{CLIM} simulations (right), and (b) precipitation in the REF^{CLIM} simulation (left) and the difference between the SEN^{CLIM} and the REF^{CLIM} simulations (right). The period 2004 to 2013 is considered.

(a) (b)

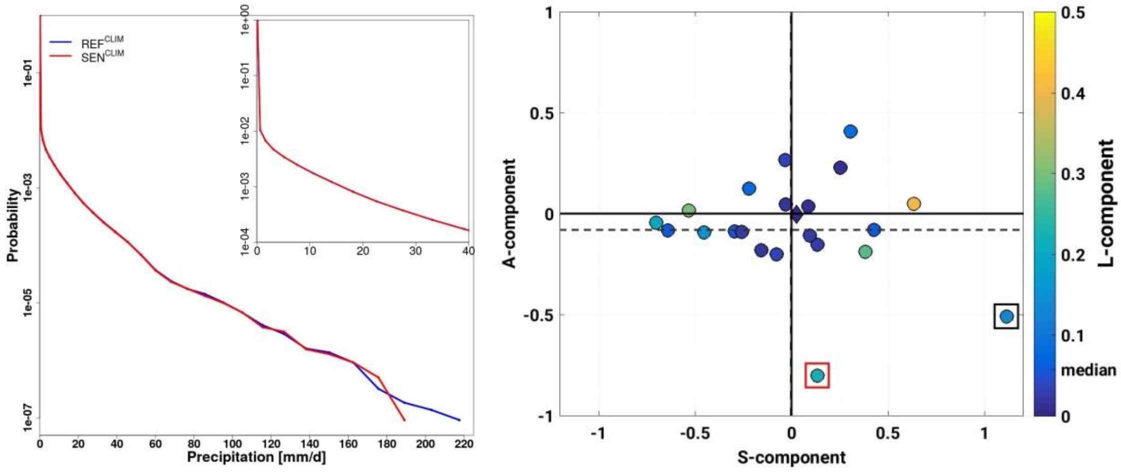

Figure 6: (a) Probability density function of daily precipitation intensities. All grid points in the investigation domain (Figure 1) and the period 2004 to 2013 are considered. (b) SAL diagram between REF^{CLIM} and SEN^{CLIM} simulations. Every circle corresponds to a simulated heavy precipitation event (listed in Table 1). The diamond (close to the zero-zero) illustrates the mean of all events. A-component (amplitude), S-component (structure), L-component (location). The inner colour indicates the L-component. Boxes point out the two events examined in this study, CASE1 and CASE2 (see section 3.2).

(a)

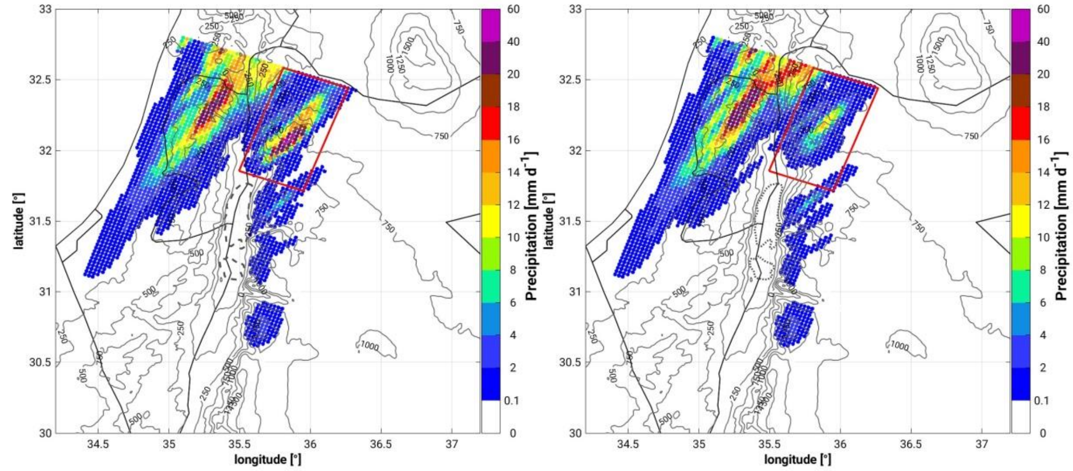
latitude [°]
longitude [°]
Precipitation [mm d^{-1}]

(b)

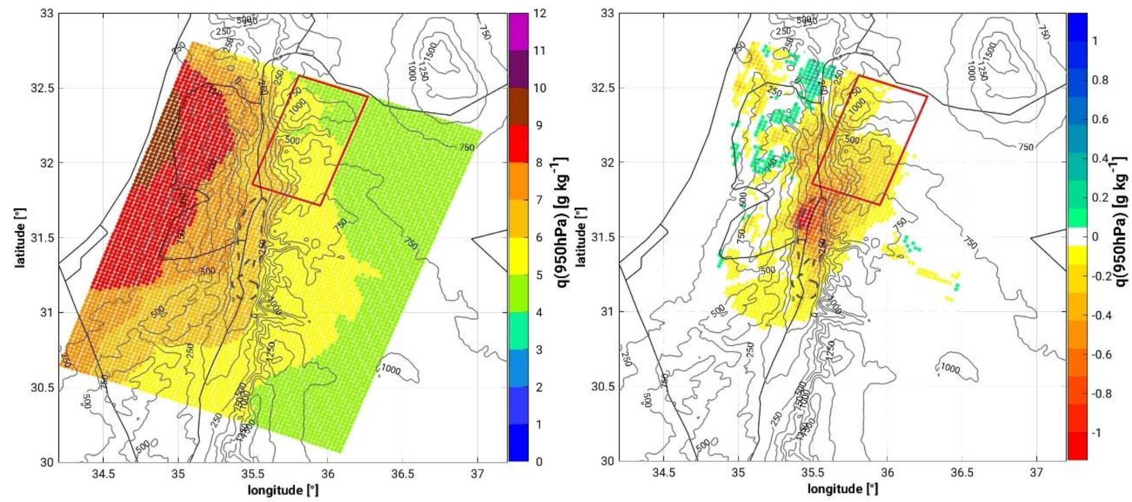
latitude [°]
longitude [°]
q(950hPa) [g kg^{-1}]

(c)

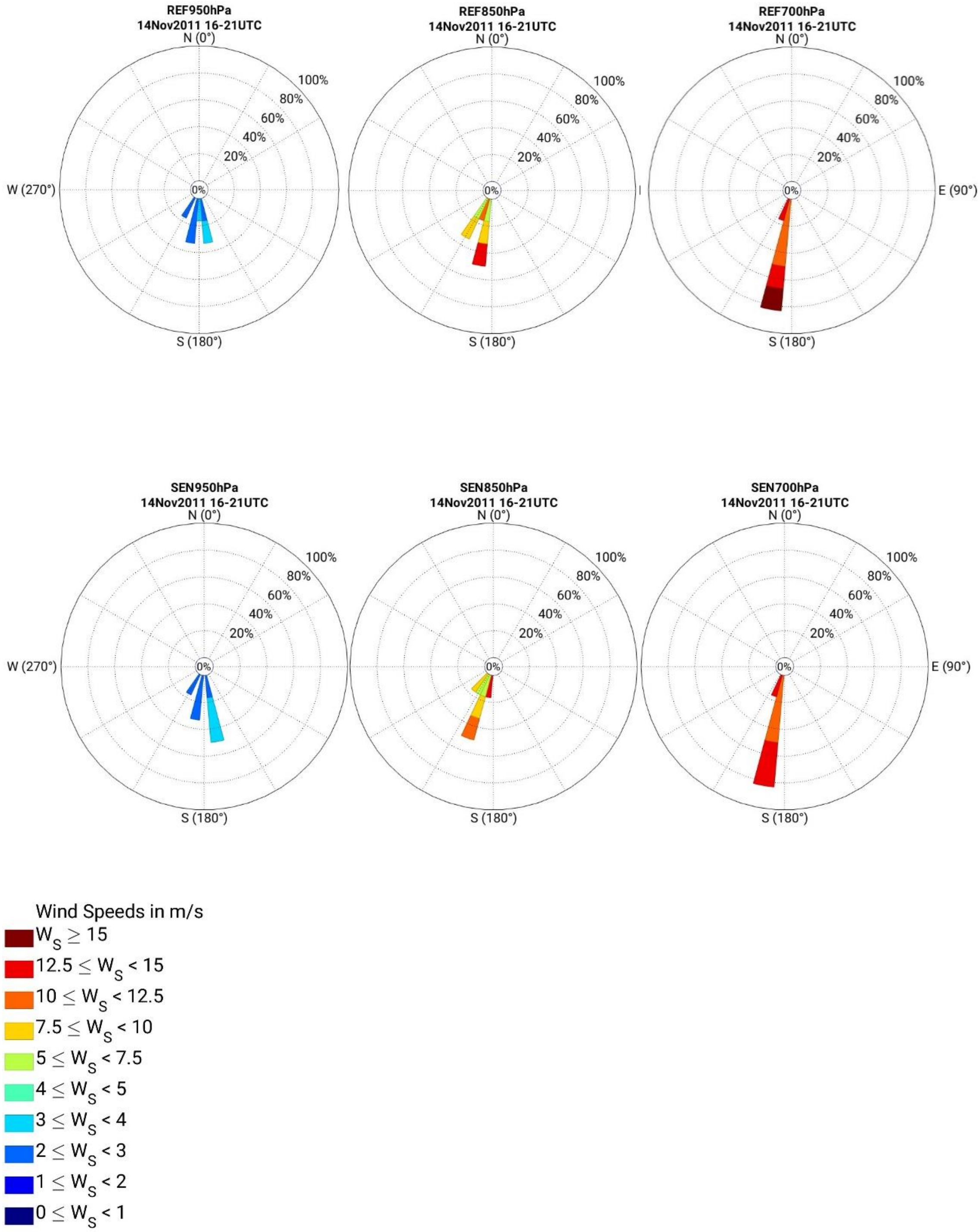
REF950hPa
14Nov2011 16-21UTC
REF850hPa
14Nov2011 16-21UTC
REF700hPa
14Nov2011 16-21UTC
SEN950hPa
14Nov2011 16-21UTC
SEN850hPa
14Nov2011 16-21UTC
SEN700hPa
14Nov2011 16-21UTC
N (0°)
E (90°)
S (180°)
W (270°)
0%
20%
40%
60%
80%
100%
Wind Speeds in m/s
$W_S \geq 15$
$12.5 \leq W_S < 15$
$10 \leq W_S < 12.5$
$7.5 \leq W_S < 10$
$5 \leq W_S < 7.5$
$4 \leq W_S < 5$
$3 \leq W_S < 4$
$2 \leq W_S < 3$
$1 \leq W_S < 2$
$0 \leq W_S < 1$

Figure 7: Spatial distribution of (a) 24-h accumulated precipitation from 14.11 09 UTC to 15.11 08 UTC from the $REF^{14.11}$ simulation (left) and the $SEN^{14.11}$ simulation (right) and (b) specific humidity below 950 hPa, from the $REF^{14.11}$ simulation (left) and the difference between the $REF^{14.11}$ and $SEN^{14.11}$ simulations, as a mean for the 6-h period prior to convection initiation in the target area (14 November 16 UTC to 21 UTC), and (c) wind conditions at 700 hPa, 850 hPa, and 950 hPa (no relevant differences with respect to the 10-m field) for the same time period. Wind roses are centred at about 35.82°E-32.07°N in our target area.

(a)

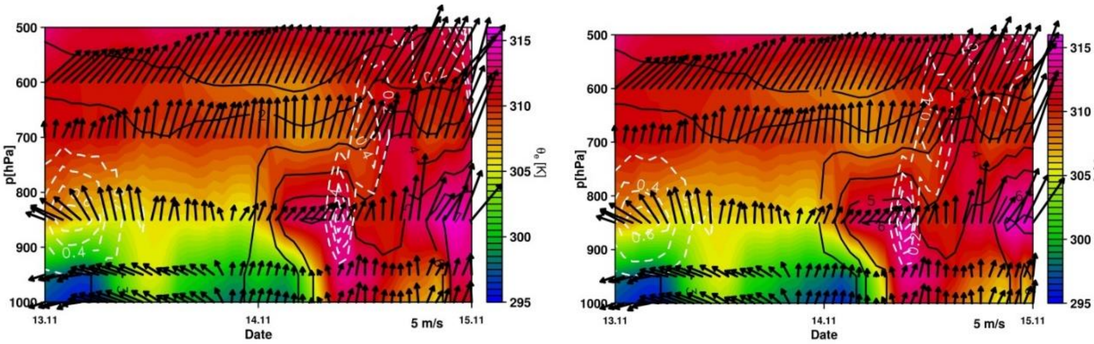

(b)

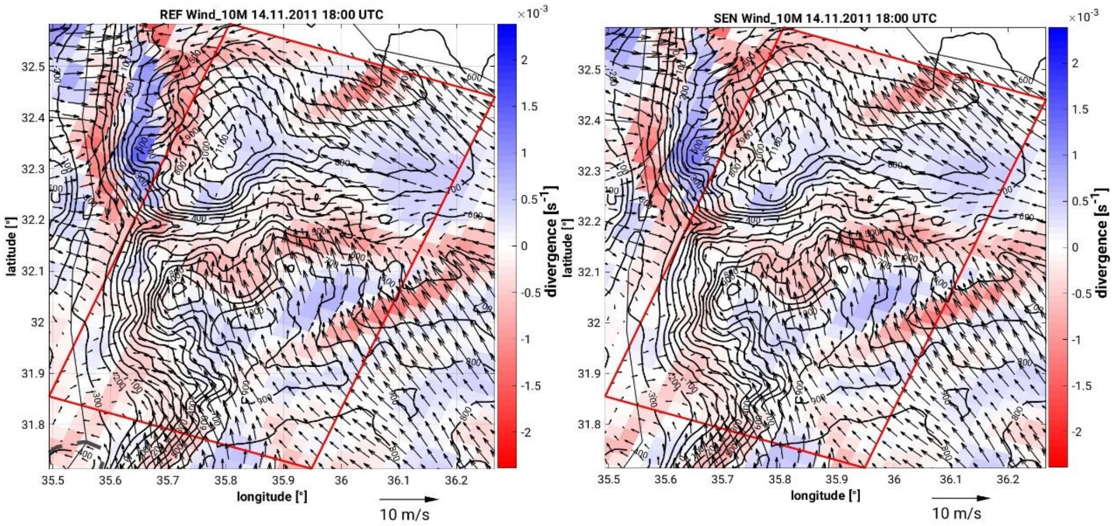

Figure 8: (a) Vertical-temporal cross-section of equivalent potential temperature (colour scale; K), specific humidity (black isolines; g/kg), horizontal wind vectors (north-pointing upwards, m/s) and vertical velocity (white dashed contours with 0.1 m/s increments) of the REF$^{14.11}$ (left) and SEN$^{14.11}$ (right) simulations, over a representative grid point in the sub-study region, 32.05°N 35.79°E. (b) Spatial distribution of 10-m horizontal wind (wind vectors; m/s) and corresponding divergence/convergence field (colour scale; s^{-1}) at 18 UTC on the 14 November 2011 from the REF$^{14.11}$ (left) and SEN$^{14.11}$ (right) simulations.

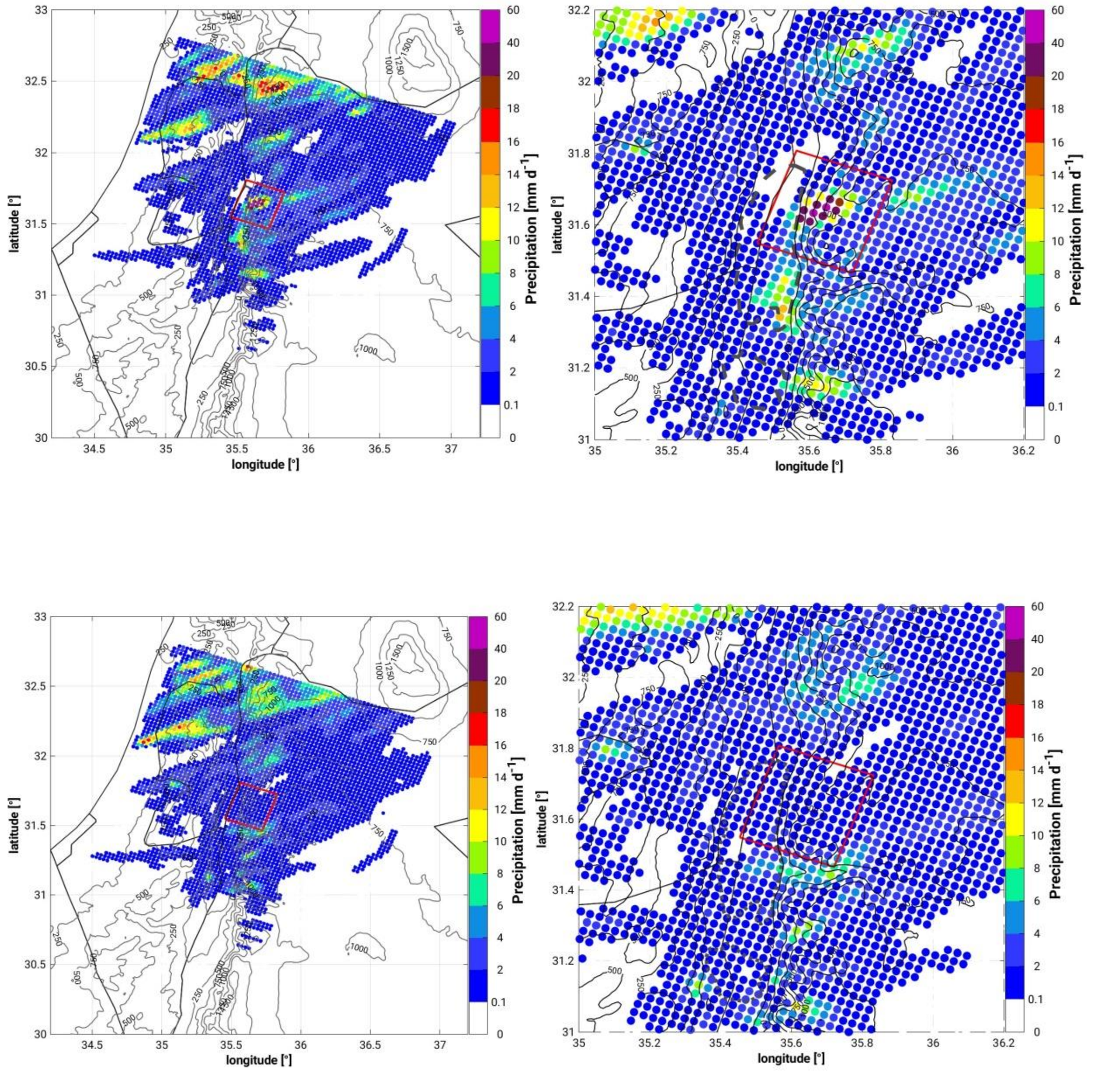

Figure 9: 24-h mean spatial distribution of precipitation from the REF$^{19.11}$ simulation (top-left; zoom top-right) and the SEN$^{14.11}$ simulation (bottom-left; zoom bottom-right) for the period 18 November 2011 11 UTC to 19 November 2011 10 UTC.

(a)

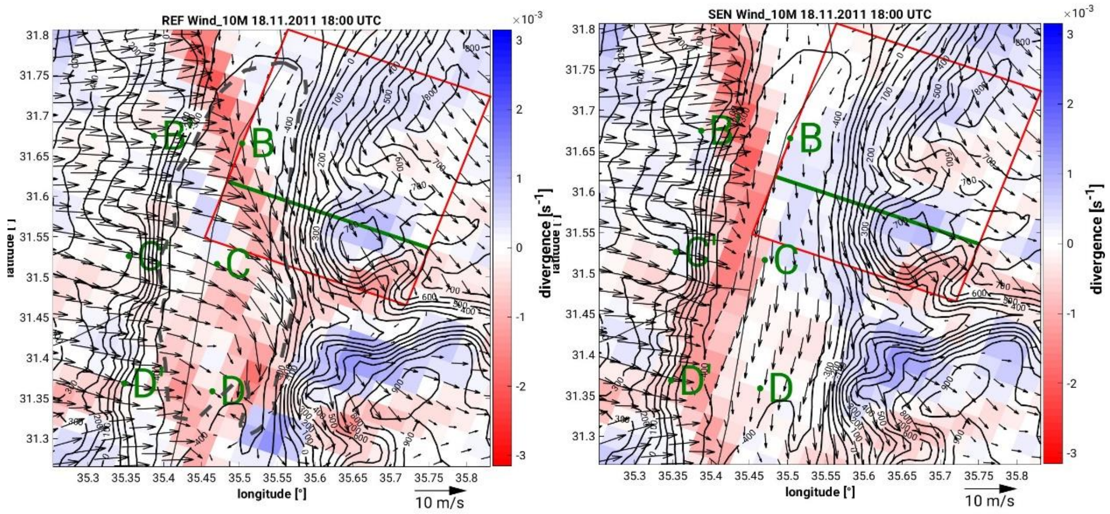
REF Wind_10M 18.11.2011 18:00 UTC
SEN Wind_10M 18.11.2011 18:00 UTC
latitude [°]
longitude [°]
divergence [s⁻¹]
×10⁻³
10 m/s
B
C
D

(b)

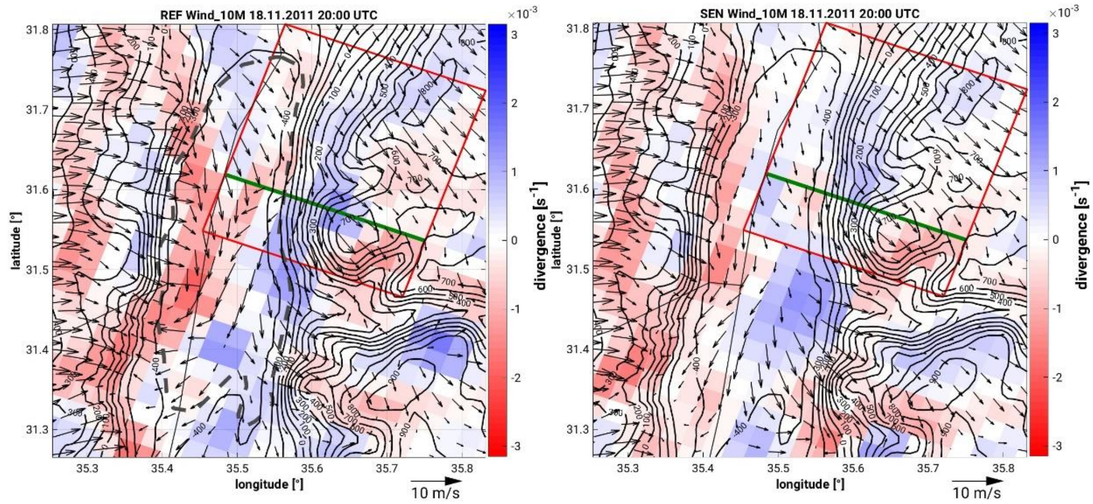
REF Wind_10M 18.11.2011 20:00 UTC
SEN Wind_10M 18.11.2011 20:00 UTC
latitude [°]
longitude [°]
divergence [s⁻¹]
×10⁻³
10 m/s

(c)

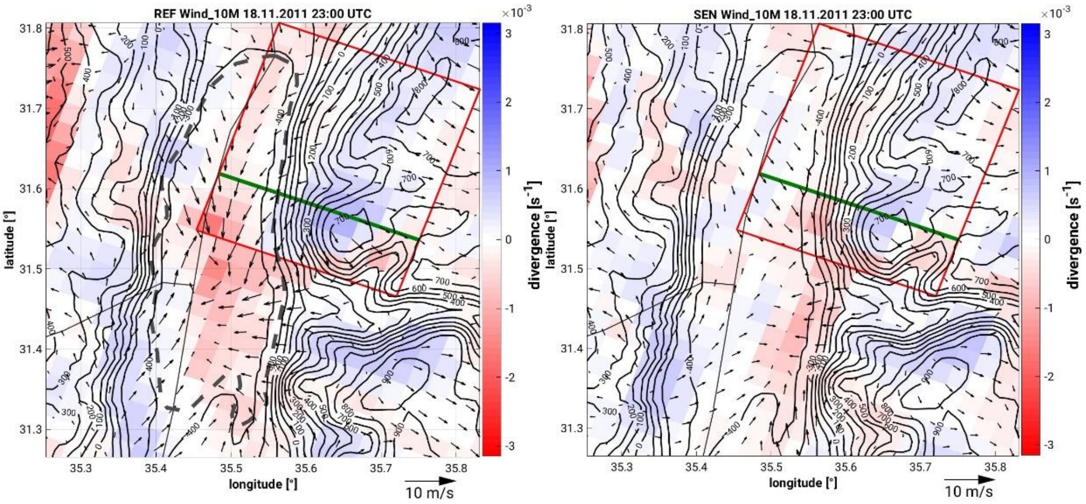

(d)

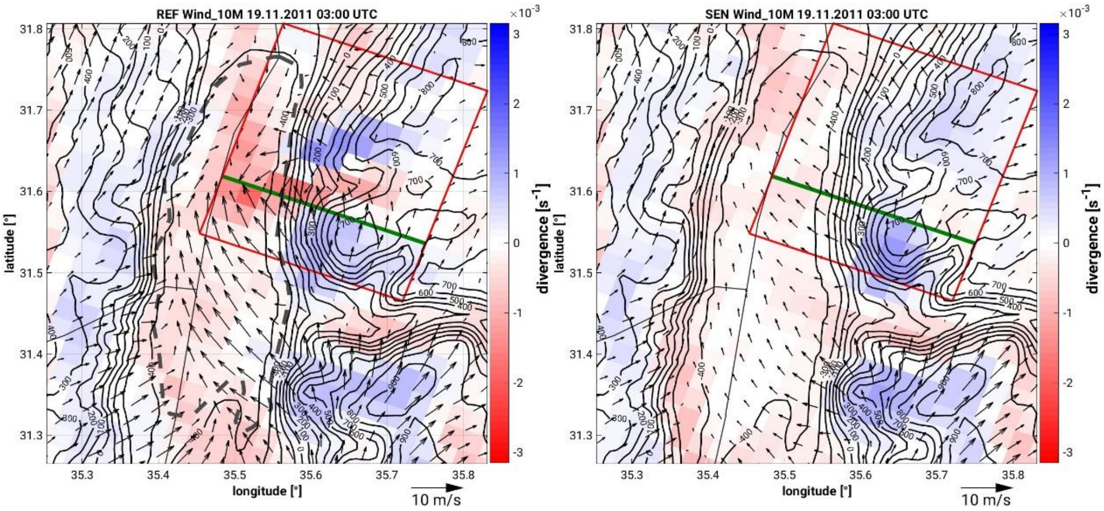

Figure 10: Spatial distribution of 10-m horizontal wind (wind vectors; m/s) and corresponding divergence/convergence field (colour scale; s^{-1}) at 18 UTC, 20 UTC, 23 UTC on the 19 November, and 03 UTC on the 20 November 2011 from the $REF^{14.11}$ (left) and $SEN^{14.11}$ (right) simulations. The topography is indicated by the black full isolines. The transects (B-C-D and B'-C'-D') corresponding to the locations in which temperature comparisons are made are indicated in Figure 10a. The green line indicates the position of the vertical cross-section in Figure 11.

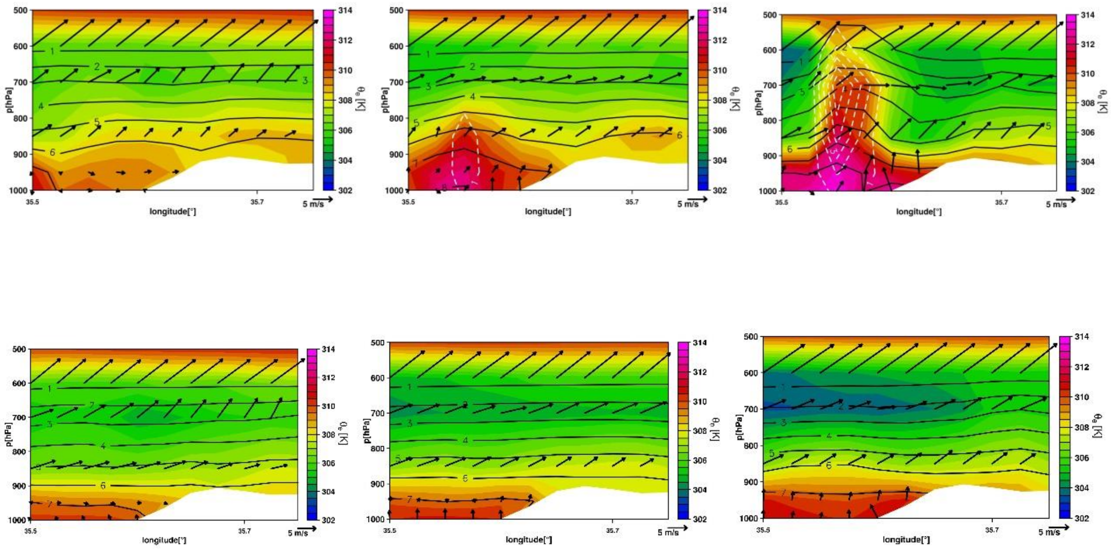

Figure 11: Vertical cross-section of equivalent potential temperature (colour scale; K), specific humidity (black isolines; g/kg), horizontal wind vectors (north-pointing upwards, m/s) and vertical velocity (white dashed contours with 1 m/s increments) of the REF[14.11] (top) and SEN[14.11] (bottom) simulations at 01 UTC (left), 02 UTC (middle) and 03 UTC (right). The location of the cross-section is indicated in Figure 10.